

CP VIOLATION, MASS HIERARCHY AND OCTANT DEGENERACY IN TERRESTRIAL NEUTRINO OSCILLATION EXPERIMENTS

A thesis submitted in partial fulfilment of the requirements for the degree of
Doctor of Philosophy

ANKUR NATH

Enrollment No. PHP17004

Registration No. TZ189838 of 2018



DEPARTMENT OF PHYSICS

SCHOOL OF SCIENCES

TEZPUR UNIVERSITY, SONITPUR - 784028

ASSAM, INDIA

July, 2022

In Accompanied with the thoughts of my parents

Manju Devi and Kusheshwar Nath.

Abstract

The Standard Model (SM) is an ensemble of electromagnetic, weak, and strong forces in particle physics. Neutrinos, in the SM, are chargeless, spin-half particles, called fermions, that come in three flavours: electron neutrino (ν_e), muon neutrino (ν_μ), and tau neutrino (ν_τ). In SM, neutrinos are massless. The Super-Kamiokande (SK) experiment from Japan discovered the experimental proof of neutrinos' mass in 1998, and the Sudbury Neutrino Observatory (SNO) from Canada confirmed it in 2002. The observation of non-zero neutrino mass is explained by the neutrino oscillation phenomenon. Neutrino Oscillation is described by a 3×3 unitary matrix, widely known as Pontecorvo-Maki-Nakagawa-Sakata (PMNS) matrix. PMNS matrix connects the three flavors with three mass eigenstates ν_1 , ν_2 and ν_3 of masses m_1 , m_2 and m_3 respectively. The matrix is commonly parameterized by three mixing angles (θ_{12} , θ_{13} and θ_{23}), one CP-violating phase δ_{CP} and two Majorana phases (ρ_1 and ρ_2). However, the Majorana phases have no effect in neutrino oscillations. Neutrino oscillation is measured by comparing the flux of neutrinos of one flavour produced to that of neutrinos of another flavour observed in a detector separated by a distance (called the baseline) from the source. The probability of oscillation of neutrino from one flavour to another is dependent on mass-squared differences (Δm_{21}^2 and Δm_{31}^2), the neutrino energy, the baseline and the density of the matter passed through by the neutrino, besides the four parameters of the PMNS matrix.

Although a few percent precision measurements of three mixing angles and two mass-squared differences have been achieved, a complete picture of neutrino oscillation is yet to be understood. There are at least three unknowns, which the ongoing and upcoming neutrino oscillation experiments plan to address in the next decades. The *first* unknown is CP violation (CPV) in the leptonic sector. Despite a recent hint of maximal CPV from the δ_{CP} measurement by the T2K experiment, it requires higher statistics to establish whether CP is violated or not. The *second*

unknown is the neutrino mass hierarchy (MH), which refers to the order of the three mass eigenvalues of neutrino mass eigenstates. Whether the MH is normal ($m_1 < m_2 < m_3$) or inverted ($m_3 < m_1 < m_2$) is still a question. While the recent measurements from individual experiments mildly favor the former, the efforts for fitting jointly multiple neutrino data samples show that the preference to the normal MH becomes less significant. Thus, more neutrino data is essential to shed light on the neutrino MH. The *third* unknown on the list is the octant of mixing angle θ_{23} . Whether θ_{23} is exactly equal to 45° , in the lower octant (LO, $\theta_{23} < 45^\circ$) or in the higher octant (HO, $\theta_{23} > 45^\circ$) is of interest to pursue. Moreover, besides resolving these unknowns, the precision measurements of the oscillation parameters for a unitary test of the leptonic mixing matrix are among the major targets of the ongoing and future neutrino oscillation experiments.

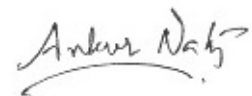
In this thesis, we explore the prospects of achieving these unknowns in light of three terrestrial neutrino oscillation experiments: the extended run of Tokai-To-Kamioka (T2K-II) and NuMI Off-axis ν_e Appearance (NO ν A-II), as well as the reactor-based medium baseline (R-MBL) experiment Jiangmen Underground Neutrino Observatory (JUNO). The work explores the physics reach for the targets by around 2027, when the 3rd generation of the neutrino experiments starts operation, with a combined sensitivity of the three experiments. It is shown that a joint analysis of these three experiments can conclusively determine the neutrino mass hierarchy. Also, at certain values of δ_{CP} , it provides closely around a 5σ confidence level (C.L.) to exclude CP conserving values and more than 50% fractional region of *true* δ_{CP} values can be explored with a statistical significance of at least a 3σ C.L. Besides, the joint analysis can provide unprecedented precision measurements of the atmospheric neutrino oscillation parameters and a great offer to solve the θ_{23} octant degeneracy in the case of non-maximal mixing.

Keywords: Neutrino oscillations; mass hierarchy; leptonic CP violation; octant degeneracy; maximal mixing; terrestrial experiments.

Declaration

I certify that

- The work contained in the dissertation is original and has been done by myself under the general supervision of my supervisors.
- The work has not been submitted to any other Institute for any degree or diploma.
- I have followed the guidelines provided by Tezpur University in writing the thesis.
- I have conformed to the norms and guidelines given in the Ethical Code of Conduct of the university.
- Whenever I have used materials (data, theoretical analysis, and text) from other sources, I have given due credit to them by citing them in the text of the dissertation and giving their details in the references.



Ankur Nath



Department of Physics
Tezpur University

Napaam, Tezpur- 784028, Assam, India.

Dr. Ng. K. Francis
Associate Professor

Phone: 03712-275559
Fax: 03712-267005, 267006
E-Mail : francis@tezu.ernet.in

CERTIFICATE

This is to certify that the thesis entitled “**CP Violation, Mass Hierarchy and Octant Degeneracy in Terrestrial Neutrino Oscillation Experiments**” submitted to Tezpur University in the Department of Physics under the School of Sciences in partial fulfillment of the requirements for the award of the degree of **Doctor of Philosophy in Physics** is a record of original research work carried out by **Mr. Ankur Nath** under my supervision and guidance.

All helps received by him from various sources have been duly acknowledged. No part of this thesis has been submitted elsewhere for award of any other degree.

Signature of Supervisor
(Ng. K. Francis)
Associate Professor
Department of Physics
Tezpur University
Assam, India-784028



Certificate

This is to certify that the thesis entitled “**CP Violation, Mass Hierarchy and Octant Degeneracy in Terrestrial Neutrino Oscillation Experiments**” submitted to Tezpur University in the Department of Physics under the School of Sciences in partial fulfillment of the requirements for the award of the degree of **Doctor of Philosophy in Physics** has been examined by us on and found to be satisfactory.

The Committee recommends for award of the degree of Doctor of Philosophy.

Signature of Principal Supervisor

Signature of External Examiner

Acknowledgment

“Kindness is the language the deaf can hear, and the blind can see.”

- Mark Twain

I want to applaud and express my gratitude to the few people who were kind to me and helped me get through these trying times. At the outset, I would like to express my sincere thanking to my supervisor, Dr. Ng. K. Francis, for his insightful advice and on occasion, his motivation. He provided suggestions, which helped me finally develop the thesis. It would not be possible to complete this uphill journey without his unwavering support.

I am grateful to Dr. Cao Van Son, my collaborator at Institute For Interdisciplinary Research in Science and Education (IFIRSE), Quy Nhon, Binh Dinh, Vietnam for providing me with technical assistance in GLOBES to help me address the thesis’ objectives. I’d also like to thank Dr. N. T. Hong Van, Mr. Tran Van Ngoc, and Ms. Phan To Quyen for our fruitful conversations. I will always be grateful to Prof. Jean Trân Thanh Vân, the President of the Rencontres du Vietnam, and the International Centre for Interdisciplinary Science and Education (ICISE), Vietnam, for taking the time to consider my request and funding my trip to Vietnam in the middle of 2019 to conduct the preliminary phase of the research.

I would like to extend my gratitude toward my doctoral committee: Prof. Jayanta Kumar Sarma and Dr. Moon Moon Devi for their critical comments throughout the tenure of my work. I also would like to acknowledge all the faculty members of Department of Physics, Tezpur University for their encouragements. The acknowledgment section would be incomplete without thanking Narayan Sarma Da, the heart and soul of all the department, in helping the research scholars with every required formalities.

I appreciate Prof. Joachim Kopp, Dr. Ananya Mukherjee, Dr. Samiran Roy, Dr. Monojit Ghosh, Dr. Mehedi Masud, and Dr. Debajyoti Dutta for answering my

emails whenever I had questions, both in theoretical and technical aspects.

I value the interactions I have with each of my physics department peers and the memorable moments we have had together on campus. For their love and support, I will always hold Mr. Animesh Barman and Mr. Bikash Thapa close to my heart. I treasure the times I spent with my senior, the late Biswa Kumar Das, the then Senior technical Assistant of the department. I'd also like to look back on my experiences at the university's Saraighat CV Raman Men Hostel (SCVRMH). One of my absolute favourite days of my life happened to occur here.

Last but not least, I want to express my gratitude to my parents, Mr. Kusheshwar Nath and Mrs. Manju Devi, my brothers, my maternal uncles, Mr. Ranjit Kumar Nath and Mr. Ratna Nath, my cousin Mr. Tarun Kumar Nath, and my extended family member Saswati Chutia for their unconditional love and willingness to share the difficult times. In times of need, my close friends Aakash, Amit, Gogo Da, Dickshit Da, and Bichita have helped me beyond expectations.

At the conclusion, I would like to express my gratitude to everyone who contributed to the thesis in some way, both inside and outside the Tezpur University fraternity. I'll end by asking the unseen power to preserve our energy so that we can devote ourselves to completing the difficult tasks ahead.

Ankur Nath

Glossary of Terms

LEP	Large E lectron P ositron
VEV	Vacuum E xpectation V alue
PMNS	P ontecorvo- M aki- N akagawa- S akata
CP	C harge- P arity
T2K	T okai- T o- K amioka
NO ν A	Nu MI O ff-axis N eutrino A ppearance
A-LBL	A ccelerator-based L ong B ase L ine
POT	<i>protons-on-target</i>
MH	M ass H ierarchy
PVC	P oly v inyl C hloride
JUNO	J iangmen U nderground N eutrino O bservatory
NPP	N uclear P ower P lant
GW	G iga- W att
R-SBL	R eactor-based S hort B aseline
R-MBL	R eactor-based M edium B aseline
A-LBL	A ccelerator-based L ong B aseline
RENO	R eactor E xperiment for N eutrino O scillation
KamLAND	K amioka L iquid scintillator A nti N eutrino D etector
GLOBES	G eneral L ong B aseline E xperiment S imulator
PSE	P ost S mearing E fficiency
CCQE	C harged C urrent Q uasi- E lastic
NC	N eutral C urrent
MINOS	M ain I njector N eutrino O scillation S earch
SK	S uper- K amiokande

Contents

1	Introduction	1
1.1	β Decay and the Neutrino	1
1.2	Neutrinos in the Standard Model	3
1.3	Neutrino Oscillation	5
1.4	Sources of Neutrinos	7
1.4.1	Natural Sources	8
1.4.2	Terrestrial Neutrino Sources	12
1.5	Knowns and Unknowns in Neutrino Physics	22
1.5.1	Questions within standard 3ν oscillation framework	24
1.5.2	Beyond standard 3ν neutrino oscillation	27
1.6	Scope of the Thesis	30
	Bibliography	30
2	Neutrino Oscillation Phenomenology at Terrestrial Neutrino Experiments	43
2.1	PMNS matrix parametrization	43
2.1.1	Majorana phase in neutrino oscillation	47
2.2	Three Neutrino Flavour Oscillation in Vacuum	49

2.3	Three Neutrino Flavour Oscillation in Matter	58
2.3.1	Neutrino Oscillation Probability in Matter	62
2.4	Oscillation Parameter Degeneracy	71
2.5	Summary	74
	Bibliography	74
3	Experiment Specifications and Event Spectra	79
3.1	Specifications of the Terrestrial Neutrino Oscillation Experiments .	80
3.1.1	T2K-II	80
3.1.2	NO ν A-II	83
3.1.3	JUNO	86
3.2	Simulation Technique	88
3.2.1	GLOBES package	89
3.2.2	Neutrino Flux for T2K-II and NO ν A-II	91
3.3	Event Spectra	97
3.3.1	T2K-II and NO ν A	97
3.3.2	JUNO	104
3.4	Discussion	105
	Bibliography	105
4	Leptonic CP Violation and Mass-Hierarchy in T2K-II, NOνA-II and JUNO	110
4.1	Introduction	110
4.1.1	Importance of JUNO	113
4.2	Method of χ^2 analysis	114

4.3	Mass Hierarchy	116
4.4	CP Violation	120
4.5	Effect of varying exposure of T2K-II on mass hierarchy and CP Violation	123
4.6	Discussion	124
	Bibliography	125
5	Octant Degeneracy and Precision Measurements of Oscillation Parameters in T2K-II, NOνA-II and JUNO	127
5.1	Introduction	127
5.2	Allowed regions of θ_{13} mixing angle and δ_{CP}	129
5.3	Allowed regions of θ_{23} mixing angle and Δm_{31}^2	130
5.4	Resolving the octant of the θ_{23} mixing angle:	131
5.5	Discussion	132
	Bibliography	133
6	Conclusion and Future Scopes	134
	Publications based on the Thesis Works	137

List of Figures

1-1	Measurements of the hadron production cross-section around the Z^0 resonance. The curves indicate the predicted cross-section for two, three and four neutrino species with SM couplings and negligible mass [13].	4
1-2	Natural and artificial sources of neutrino in a nutshell[20].	7
1-3	The pp (CNO) chain of the solar thermonuclear reaction is shown in the left (right) figure. The produced neutrinos are depicted in bold fonts [21]	8
1-4	An observable electron anti-neutrino ($\bar{\nu}_e$) spectrum in reactor neutrino experiment [57].	13
1-5	Allowed regions of $\sin^2 \theta_{12} - \Delta m_{21}^2$ for fixed $\theta_{13} = 8.6^\circ$ for solar and KamLAND data, with and without Super Kamiokande results. The updated allowed regions are showed at 1σ , 90%, 2σ , 99% and 3σ C.L for 2 d.o.f.. The analysis for KamLAND is given by solid green contours with best fit marked by a green star [75].	14
1-6	Process of neutrino production, propagation and detection in accelerator neutrino oscillation experiments. The left portion of the image is the NuMI beamline [79] which are employed in the MINOS [80], MINOS+ [81] and NO ν A [82] experiments.	16
1-7	Neutrino energy as a function of the parent π -energy for different off-axis angles(<i>left</i>) and the overall predicted flux per given exposure(<i>right</i>). The figure is a description of the NO ν A experiment [83].	19

1-8	Feynman diagrams for different types of neutrinos interactions at the detector. The image is taken from https://www.phys.ksu.edu/reu/2018/song.html	20
1-9	The neutrino and antineutrino per nucleon CC cross sections (for an isoscalar target) divided by neutrino energy as a function of energy [103].	21
1-10	Illustration of normal and inverted neutrino mass hierarchies.	25
2-1	Feynman diagrams of the coherent forward elastic scattering processes experienced by neutrinos on the particles in matter.	59
2-2	$P(\nu_\mu \rightarrow \nu_e)$ for $L=295$ (<i>top</i>) and $L=810$ km (<i>bottom</i>) for $\delta_{CP} = -\pi/2$	68
2-3	$P(\bar{\nu}_\mu \rightarrow \bar{\nu}_e)$ for $L=295$ (<i>top</i>) and $L=810$ km (<i>bottom</i>) for $\delta_{CP} = -\pi/2$	69
2-4	$P(\nu_\mu \rightarrow \nu_e)$ and $P(\bar{\nu}_\mu \rightarrow \bar{\nu}_e)$ for $L=295$ (<i>top</i>) and $L=810$ km (<i>bottom</i>) for $\delta_{CP} = 0, -\pi/2$	70
2-5	The Eight-fold degeneracy in $\nu_\mu \rightarrow \nu_e$ appearance channel for $\text{NO}\nu\text{A}$ baseline. Courtesy: Son Cao [23].	73
2-6	$P_{\mu e}(\theta_{23}, \delta_{CP}) = P_{\mu e}(\theta'_{23}, \delta'_{CP})$ Degeneracy at $E_\nu = 0.6$ GeV (T2K).	73
2-7	$P_{\mu e}(\theta_{23}, \delta_{CP}) = P_{\mu e}(\theta'_{23}, \delta'_{CP})$ Degeneracy at $E_\nu = 2.0$ GeV ($\text{NO}\nu\text{A}$).	74
2-8	$P_{\mu\mu}(\theta_{23}) = P_{\mu\mu}(\pi/2 - \theta_{23})$ Degeneracy at $E_\nu = 0.6$ GeV for T2K(<i>left</i>) and 2.0 GeV for $\text{NO}\nu\text{A}$ (<i>right</i>).	74
3-1	A Schematic diagram of J-PARC, Tokai to Super-K detector, Kamioka. Images taken from Mishima K, et al. 9th International Workshop on Accelerator Alignment, September 26-29, 2006.	80
3-2	Schematic of T2K far neutrino detector: Super Kamiokande [8].	81

3-3	A graphic representation of one of the first neutrino interactions captured at the NOvA far detector in northern Minnesota. The dotted red line represents the neutrino beam, generated at Fermilab in Illinois and sent through 500 miles of earth to the far detector. The image on the left is a simplified 3-D view of the detector, the top right view shows the interaction from the top of the detector, and the bottom right view shows the interaction from the side of the detector. The information is reproduced from https://vms.fnal.gov/asset	84
3-4	Interaction topologies for $CC\nu_\mu$ (<i>top</i>), $CC\nu_e$ (<i>middle</i>) and NC (<i>bottom</i>) neutrino interactions [18]	85
3-5	Location of JUNO site [22].	86
3-6	A schematic view of the JUNO detector [22]	88
3-7	Recent results of T2K experiment. The <i>top</i> figures show the reconstructed energy distribution for ν_e appearance and the <i>bottom</i> figures represent the ν_μ disappearance events. The left (right) plot shows the events in neutrino (antineutrino) mode [31]	91
3-8	Reconstructed neutrino energy spectra for the NOvA FD. The <i>left</i> figures show the reconstructed energy distribution for $\nu_{\mu\mu}$ disappearance and the <i>right</i> figures represent the ν_e appearance events. The top (bottom) plot shows the events in neutrino (antineutrino) mode. The appearance events are classified in three bins from lowest to highest purity: “Peripheral”, “Low PID”, and “High PID” [32]	92
3-9	T2K flux at far detector for antineutrino mode (left panel) and neutrino mode (right panel), updated in 2016.	94
3-10	NOvA Near Detector Flux.	95
3-11	NOvA Far Detector Flux normalized to 10^{20} POTs per year.	96
3-12	Expected event spectra of the signal and background as a function of reconstructed neutrino energy for T2K-II for appearance sample. The spectra are for ν -mode. Same oscillation parameters as Ref. [38] are used.	98

3-13	Same as Figure 3-12, but for $\bar{\nu}$ -mode.	99
3-14	Expected event spectra of the signal and background as a function of reconstructed neutrino energy for T2K-II disappearance sample. The spectra are for ν -mode. Same oscillation parameters as Ref. [38] are used.	100
3-15	Same as Figure 3-14, but for $\bar{\nu}$ -mode.	101
3-16	Expected event spectra of the signal and background as a function of reconstructed neutrino energy for NO ν A-II for the appearance channel. The spectra are for ν -mode. <i>Normal</i> MH, $\delta_{CP} = 0$, and other oscillation parameters given in Tab. 2.1 are assumed.	102
3-17	Same as Figure 3-16, but for $\bar{\nu}$ -mode.	102
3-18	Expected event spectra of the signal and background as a function of reconstructed neutrino energy for NO ν A-II for disappearance channel. The spectra are for ν -mode. <i>Normal</i> MH, $\delta_{CP} = 0$, and other oscillation parameters given in Tab. 2.1 are assumed.	103
3-19	Same as Figure 3-18, but for $\bar{\nu}$ -mode.	103
3-20	JUNO event rate calculated at same oscillation parameters as Ref. [22]	105
4-1	Baseline dependence on A_{CP} . The thin vertical lines show the ambiguity from the θ_{23} octant degeneracy. The positions of the intercept at $L = 0$ for $\sin \delta_{CP} = 0, \pm 1$ are shown [1].	111
4-2	Electron antineutrino disappearance probability for JUNO.	113
4-3	MH sensitivities as a function of <i>true</i> δ_{CP} calculated for various experimental setups. $\sin^2 \theta_{23} = 0.5$ is assumed to be true.	118
4-4	MH sensitivities as a function of <i>true</i> δ_{CP} calculated for the joint analyses of all considered experiments but at different $\sin^2 \theta_{23}$ values.	118
4-5	MH sensitivities as a function of <i>true</i> δ_{CP} calculated for all considered experiments for comparing two possible MH hypotheses. $\sin^2 \theta_{23} = 0.5$ is assumed to be true.	119

4-6	Dependence of the neutrino MH sensitivity on the θ_{13} true values: $\sin^2 \theta_{13} = 0.02241$ is the best fit obtained with NuFIT 4.1 [5], $\sin^2 \theta_{13} = 0.02221$ is with NuFIT 5.0 [6], and $\sin^2 \theta_{13} = 0.02034$ is 3σ C.L. lower limit. <i>Normal</i> MH and $\sin^2 \theta_{23} = 0.5$ are assumed to be true.	119
4-7	CPV sensitivity as a function of the <i>true</i> value of δ_{CP} obtained with different analyses. <i>Normal</i> MH and $\sin^2 \theta_{23} = 0.5$ are assumed to be <i>true</i> . Top (bottom) plot is with the MH assumed to be <i>unknown</i> (<i>known</i>) in the analysis respectively.	121
4-8	CPV sensitivity as a function of the <i>true</i> value of δ_{CP} obtained with a joint analysis of all considered experiments at different <i>true</i> $\sin^2 \theta_{23}$ values (0.43, 0.5, 0.6). Top (bottom) plot is with the <i>normal</i> (<i>inverted</i>) MH respectively assumed to be true.	122
4-9	Dependence of the combined sensitivity on T2K-II POT exposure on MH sensitivities as a function of <i>true</i> δ_{CP} obtained with a joint analysis of all considered experiments. <i>Normal</i> MH and $\sin^2 \theta_{23} = 0.5$ are assumed to be true.	123
4-10	Dependence of the combined sensitivity on T2K-II POT exposure on CPV sensitivity as a function of the <i>true</i> value of δ_{CP} obtained with a joint analysis of all considered experiments. <i>Normal</i> MH and $\sin^2 \theta_{23} = 0.5$ are assumed to be true.	124
5-1	Allowed region of $\sin^2 \theta_{13}$ - δ_{CP} at the 3σ C.L. compared between a joint analysis of T2K-II and NO ν A-II and the present constraint from the global data [4].	130
5-2	Allowed region in the $\sin^2 \theta_{23}$ - Δm_{31}^2 space at 90% C.L. with various experimental setups. <i>Normal</i> MH and $\sin^2 \theta_{23} = 0.5$ are assumed to be true.	130
5-3	Allowed region of <i>test</i> $\sin^2 \theta_{23}$ at 3σ C.L as a function of <i>true</i> $\sin^2 \theta_{23}$. <i>Normal</i> MH and $\delta_{\text{CP}} = -\frac{\pi}{2}$ are assumed to be true.	131
5-4	Statistical significance to exclude the <i>wrong</i> octant as a function of $\sin^2 \theta_{23}$. <i>Normal</i> MH and $\delta_{\text{CP}} = -\frac{\pi}{2}$ are assumed to be true.	132

List of Tables

1.1	The structure of quarks and leptons in the SM. ‘L’ and ‘R’ stand for left and right-handed particles.	3
1.2	Classification of neutrino oscillation experiments with their source-detector distance (L), energy (E) and sensitivity to Δm_{ij}^2	12
1.3	The neutrino oscillation parameters, according to two different global fits- Global Fit 1[75] & Global Fit 2[76].	23
2.1	Global constraint of oscillation parameters with <i>normal</i> mass hierarchy assumed [18].	67
3.1	Summary of the thermal power and baseline to the JUNO detector for the Yangjiang (YJ) reactor cores	87
3.2	Summary of the thermal power and baseline to the JUNO detector for the Taishan (TS) reactor cores.	87
3.3	Experimental specifications of the A-LBL experiment T2K-II.	97
3.4	Experimental specifications of the A-LBL experiment NO ν A-II.	98
3.5	Detection efficiencies(%) ^a of signal and background events in appearance samples. Normal mass hierarchy and $\delta_{CP} = 0$ are assumed.	99
3.6	Detection efficiencies(%) of signal and background events in disappearance samples. Normal mass hierarchy is assumed	100
3.7	JUNO simulated specifications	104

List of Tables

4.1	Varying $\theta_{13}, \theta_{23}, \delta_{CP}, \Delta m_{31}^2$ for the marginalisation procedure	115
4.2	Systematics of $\nu_{\mu}(\bar{\nu}_{\mu})$ disappearance and $\nu_e(\bar{\nu}_e)$ appearance channels at the FD in T2K-II and NO ν A.	115
4.3	Systematics of $\bar{\nu}_e$ disappearance channel in JUNO.	115
4.4	Fractional region of δ_{CP} , depending on $\sin^2 \theta_{23}$, can be explored with 3σ or higher significance	123

Chapter 1

Introduction

*“Dear Radioactive Ladies and Gentlemen[,]
As the bearer of these lines, to whom I graciously ask you to listen,
will explain to you in more detail, because of the ‘wrong statistics of N
and $Li-6$ nuclei and the continuous beta spectrum’, I have hit upon a
desperate remedy to save the ‘exchange theorem’ of statistics and the
law of conservation of energy. . . .”*

- W. Pauli, Dec 4, 1930

1.1 β Decay and the Neutrino

In the 1920s, three elementary particles were known: the electron, the proton and the photon. The models of the atomic nuclei were built out of these particles. A nucleus of atomic number \mathbf{A} and charge \mathbf{Z} was assumed to be made of \mathbf{A} positive protons and $\mathbf{A}-\mathbf{Z}$ negative electrons. As such, beta (β) decay was believed to be two-body decay process,

$$N(A, Z) \rightarrow N(A, Z + 1) + e^- \quad (1.1)$$

This model suffered from three very severe problems:

1. Order of magnitude of the energy of electrons measured in β -decay:

The electrons emitted in β -decay process were thought to be present in the nucleus even before the decay. In such cases, their wave function had to be confined in the nuclear size (of the order of 10^{-15} m). And, the uncertainty principle predicts a typical electron momentum and kinetic energy of about 100 MeV. But the observed maximum energies in beta decays were one order of magnitude smaller.

2. The continuous β -decay energy spectra:

If the β -decay takes place as in Equation 1.1, the electron energy spectra should be a line at the mass difference $m(A, Z) - m(A, Z + 1)$. But experiments showed a continuous spectrum ending at that mass difference [1].

3. The nuclear statistics:

Between 1928 and 1929, Rasetti measured the Raman rotation spectra of a number of diatomic gases[2], particularly of homonuclear molecules like H_2 , N_2 and O_2 . The rotational bands he observed showed a sequence of lines of alternate intensity. From the spectra of Rasetti and the explanation of Fermi in his book, it was learned that N_2 nuclei obey Bose statistics [3]. However, N_2 nucleus contained 14 protons and 7 electrons, a total of 21 spin-half particles and its spin should have been half-integral.

In 1930, Wolfgang Pauli postulated a hypothesis[4] stating that a new 'invisible' particle is emitted together with the electron in β -decay, such that the sum of energies of the particle and the electron is constant. This idea explains the continuous energy spectrum of β -electrons. Enrico Fermi, in 1933, formulated the theory of β -decay[5] based on Pauli's hypothesis and the new particle was named '*neutrino*' (ν).

Previously, in 1932, J. Chadwick discovered the neutron[6] and its presence in the nucleus together with the protons could solve the problem of the *wrong statistics*. Further, in December 1933, Fermi published his article titled "*Tentativo di una teoria dell'emissione di raggi beta*"[7] and in an extended version, in *Il Nuovo Cimento* where he explained the theory of β -decay of radioactive substances, built on the hypothesis that the electrons emitted by the nuclei do not exist before the decay. Thus, all β -decays were due to the same underlying three-body decay

1.2. Neutrinos in the Standard Model

process

$$n \rightarrow p + e^- + \bar{\nu} \quad (1.2)$$

The first-ever experimental evidence of neutrino took place by observing inverse β -decay reaction in 1956 from the Savannah River reactor plant in South Carolina by F. Reines and C. L. Cowan[8]. Thereafter, the physics community in various corners of the world started conducting underground experiments and a few experiments have been upgraded from time to time to understand this elusive particle. The other two active neutrinos, viz. muon neutrino (ν_μ) and tau neutrino (ν_τ) were directly observed in 1962[9] and 2000[10] respectively.

1.2 Neutrinos in the Standard Model

The discoveries of different fundamental particles (including neutrinos) in the middle of the 20th century necessitated the formulation of a basic theory to understand the properties of these particles and how they interact. The Standard Model (SM) [11, 12] of particle physics, which unifies the electromagnetic, weak, and strong forces, was developed over the course of the second half of the 20th century. Upon experimental verification of quark existence in the middle of the 1970s, the current formulation was finalised. Mathematically, SM is a non-abelian gauge theory based on the symmetry group $U(1)_Y \times SU(2)_L \times SU(3)_c$. Right-handed fermions are SU(2) singlets in this model, while left-handed fermion fields are SU(2) doublets. SM has three generations of leptons and quarks as tabulated in Table 1.1. Every quark has three SU(3) colour charges: red, green and blue. The weak force is carried by the W^\pm and Z^0 bosons, the electromagnetic force is carried by the photon, and the strong force is carried by the gluons. By exchanging

Table 1.1: The structure of quarks and leptons in the SM. ‘L’ and ‘R’ stand for left and right-handed particles.

Quarks			Leptons		
$\begin{pmatrix} u \\ d \end{pmatrix}_L$	$\begin{pmatrix} c \\ s \end{pmatrix}_L$	$\begin{pmatrix} t \\ b \end{pmatrix}_L$	$\begin{pmatrix} \nu_e \\ e \end{pmatrix}_L$	$\begin{pmatrix} \nu_\mu \\ \mu \end{pmatrix}_L$	$\begin{pmatrix} \nu_\tau \\ \tau \end{pmatrix}_L$
u_R	c_R	t_R	ν_{eR}	$\nu_{\mu R}$	$\nu_{\tau R}$
d_R	s_R	b_R	e_R	μ_R	τ_R

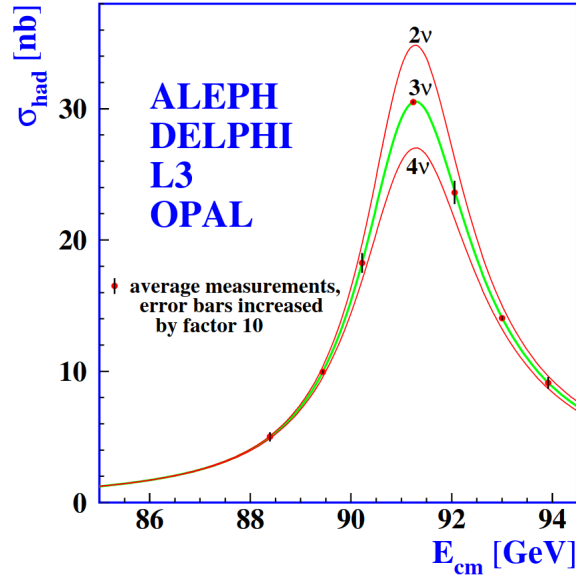


Figure 1-1: Measurements of the hadron production cross-section around the Z^0 resonance. The curves indicate the predicted cross-section for two, three and four neutrino species with SM couplings and negligible mass [13].

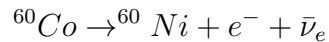
W^\pm and Z^0 bosons, neutrinos interact weakly with the other leptonic fields in this model. Charge current (CC) interactions are those mediated by the W^\pm boson, whereas neutral current (NC) interactions are those mediated by the Z^0 boson.

The number of light neutrino species in SM with the typical electroweak interactions can be counted as follows: The Z^0 boson can decay to the invisible $\nu\bar{\nu}$ pairs according to SM. The difference between Z^0 -boson's total decay width and it's visible decay width is known as the invisible decay width. The sum of the Z-boson's partial widths of decay into quarks and charged leptons is referred to as the visible decay width. The ratio of the invisible decay width of Z-boson and the it's decay width to charged leptons (Γ_{inv}/Γ_l) is measured using data from the LEP, and it is found to be 5.943 ± 0.016 . ($\Gamma_{\nu\nu}/\Gamma_l$) is the ratio of the partial widths to neutrinos and to charged leptons, and its SM value is 1.99125 ± 0.00083 . The number of the light active neutrino species N_ν can be calculated to be 2.9840 ± 0.0082 using this formula ($\Gamma_{inv}/\Gamma_l = N_\nu \Gamma_{\nu\nu}/\Gamma_l$) [13]. This is consistent with the fact that there are only three light active neutrinos known from experiments till date.

Even though SM has a strong track record of success in making predictions that can be verified experimentally and is a mathematically self-consistent model, there

1.3. Neutrino Oscillation

are some limitations. The neutrinos' mass is one of them. Prior to symmetry breaking of the group in SM, the masses of the fermions and gauge bosons are zero. After the spontaneous symmetry breaking, the Higgs mechanism provides masses to the gauge bosons. The masses of the fermions are also determined by the Higgs mechanism. The mass term of the fermions arise from the Yukawa term which is written as: $-y\bar{\psi}_L\psi_R\langle\phi\rangle$, where y is the Yukawa coupling, ψ_L , ψ_R are the left-handed and right-handed fermionic fields respectively and $\langle\phi\rangle$ is the vacuum expectation value (VEV) of the Higgs field. Because there is no suitable right-handed partner, neutrinos cannot have a gauge invariant mass term. Due to the observation of parity violation in weak interactions, right-handed neutrinos are absent in SM. In 1956, Lee and Yang hypothesised that parity is broken in weak interactions, as a solution to the $\tau - \theta$ puzzle[14]. Wu's experiment was the first to observe the parity violation in weak interactions. When the nuclear spins of ^{60}Co were aligned by an external magnetic field, an asymmetry in the direction of the emitted electrons were observed[15]. The decay process under consideration was



It was discovered that the electron's nuclear spin always acted in opposite direction to its momentum. In other words, the presence of e_L and $\bar{\nu}_R$ alone can account for the observed correlation between the nuclear spin and the electron momentum. The lack of "mirror image" states $\bar{\nu}_L$ and ν_R revealed a blatant parity violation. According to an experimental measurement made by Goldhaber, Grodzins, and Sunyar in 1958, neutrinos are left-handed and antineutrinos are right-handed [16]. Neutrinos are massless in the Standard Model (SM), but the experimentally observed phenomenon known as "neutrino oscillation" suggests that neutrinos have a mass.

1.3 Neutrino Oscillation

The three known neutrino flavour states (ν_e , ν_μ , ν_τ) are expressed as quantum superpositions of three massive states ν_k ($k = 1, 2, 3$) with different masses m_k

with a 3×3 unitary mixing matrix $U_{\alpha k}$ ($\alpha = e, \mu, \tau$), known as PMNS (Pontecorvo-Maki-Nakagawa-Sakata) matrix U_{PMNS} [17, 18], given by

$$U_{PMNS} = U_{\alpha k} = \begin{bmatrix} U_{e1} & U_{e2} & U_{e3} \\ U_{\mu 1} & U_{\mu 2} & U_{\mu 3} \\ U_{\tau 1} & U_{\tau 2} & U_{\tau 3} \end{bmatrix}$$

The U_{PMNS} matrix can be decomposed as:

$$\begin{bmatrix} \cos \theta_{12} & \sin \theta_{12} & 0 \\ -\sin \theta_{12} & \cos \theta_{12} & 0 \\ 0 & 0 & 1 \end{bmatrix} \begin{bmatrix} \cos \theta_{13} & 0 & \sin \theta_{13} e^{-i\delta_{CP}} \\ 0 & 1 & 0 \\ -\sin \theta_{13} e^{i\delta_{CP}} & 0 & \cos \theta_{13} \end{bmatrix} \begin{bmatrix} 1 & 0 & 0 \\ 0 & \cos \theta_{23} & \sin \theta_{23} \\ 0 & -\sin \theta_{23} & \cos \theta_{23} \end{bmatrix} \cdot M \quad (1.3)$$

and characterized by three non-zero angles $\theta_{kl} \in [0, \frac{\pi}{2}]$ ($k, l = 1, 2, 3$ and $k < l$) and a charge-parity violating phase $\delta_{CP} \in [0, 2\pi]$. The matrix M has a value of $\det M = 1$ for the Dirac neutrinos and $M = \text{diag}(1, e^{i\alpha_2}, e^{i\alpha_3})$ for Majorana neutrinos[19]. The mixing angles θ_{kl} are associated with solar, atmospheric and reactor neutrinos given by θ_{12} , θ_{23} and θ_{13} respectively, the mass-squared differences i.e. the mass splitting terms being Δm_{21}^2 , Δm_{32}^2 and Δm_{31}^2 with $\Delta m_{kl}^2 = m_k^2 - m_l^2$. Thus, the PMNS matrix for Dirac neutrinos can be written as:

$$U_{PMNS} = \begin{pmatrix} c_{12}c_{13} & s_{12}c_{13} & s_{13}e^{-i\delta_{CP}} \\ -s_{12}c_{23} - c_{12}s_{13}s_{23}e^{i\delta_{CP}} & c_{12}c_{23} - s_{12}s_{13}s_{23}e^{i\delta_{CP}} & c_{13}s_{23} \\ s_{12}s_{23} - c_{12}s_{13}c_{23}e^{i\delta_{CP}} & -c_{12}s_{23} - s_{12}s_{13}c_{23}e^{i\delta_{CP}} & c_{13}c_{23} \end{pmatrix} \quad (1.4)$$

The mass splitting terms can be expressed as:

$$\Delta m_{21}^2 = m_2^2 - m_1^2, \quad \Delta m_{3n}^2 = m_3^2 - \frac{(m_2^2 + m_1^2)}{2} \quad (1.5)$$

such that, $\Delta m_{21}^2 > 0$ and $\Delta m_{3n}^2 \equiv \Delta m_{31}^2 > 0$ is positive for Normal Mass Ordering (NO) and $\Delta m_{3n}^2 \equiv \Delta m_{32}^2 < 0$ is negative for Inverted Mass Ordering (IO) for the neutrino mass spectrum. In neutrino oscillations, the diagonal Majorana phase matrix \mathbf{M} does not have any effect.

Neutrino oscillation is typically measured by comparing the flux of produced α -flavor neutrinos and flux of β -flavor neutrinos observed in a detector placed at

1.4. Sources of Neutrinos

some distance from the production source. The probability for an α -flavor to oscillate into β -flavor, $P_{(\nu_\alpha \rightarrow \nu_\beta)}$, depends on three mixing angles ($\theta_{12}, \theta_{13}, \theta_{23}$), CP violation phase δ_{CP} , two mass-squared splittings ($\Delta m_{21}^2, \Delta m_{31}^2$), its energy E_ν , propagation distance L , and the density of matter passed through by the neutrino ρ , given by

$$P_{(\nu_\alpha \rightarrow \nu_\beta)} = f(\theta_{12}, \theta_{13}, \theta_{23}, \delta_{CP}; \Delta m_{21}^2, \Delta m_{31}^2; E_\nu, L, \rho).$$

It is well-established from the contribution of many neutrino experiments [12] using both the natural neutrino sources (solar and atmospheric neutrinos) and the man-made neutrino sources (reactor and accelerator neutrinos) that the two leptonic mixing angles θ_{12} and θ_{23} are large, θ_{13} is relatively small but non-zero, the mass-squared splitting $|\Delta m_{31}^2|$ is about 30 times larger than Δm_{21}^2 . A detailed formulation of neutrino oscillation probabilities has been addressed in Chapter 2.

1.4 Sources of Neutrinos

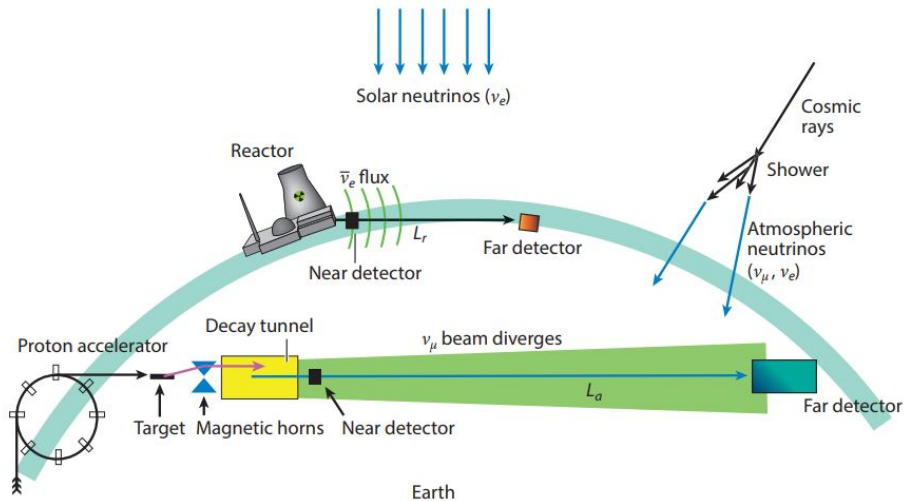


Figure 1-2: Natural and artificial sources of neutrino in a nutshell[20].

Neutrinos are the most abundant massive particles in the universe. They are produced in the stars, Earth's atmosphere, supernovae and active galactic nuclei. The man-made sources include neutrino production in nuclear fission in

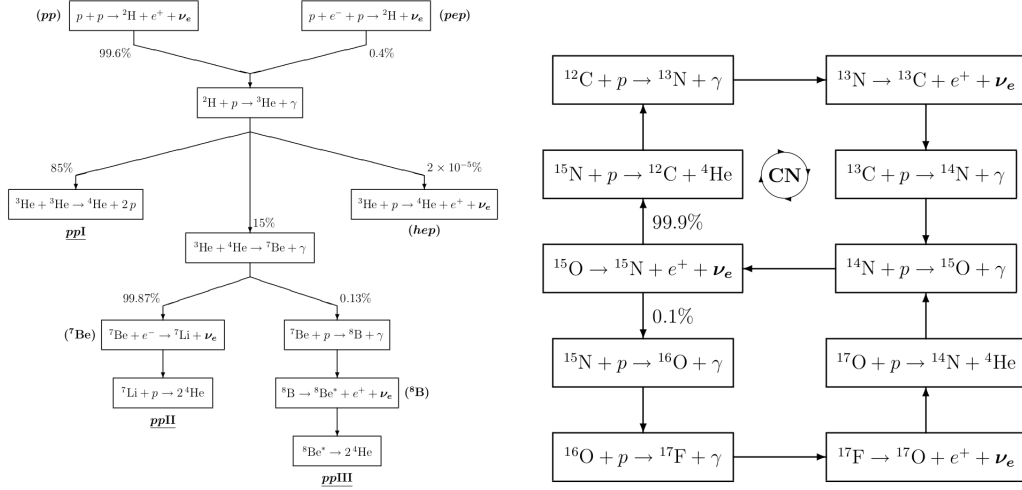


Figure 1-3: The pp (CNO) chain of the solar thermonuclear reaction in shown in the left (right) figure. The produced neutrinos are depicted in bold fonts [21] .

reactors and through pion decay in accelerators. Neutrinos are also produced in the core of the sun through nuclear fusion reactions.

1.4.1 Natural Sources

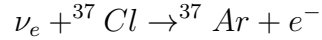
1.4.1.1 Solar Neutrinos

The major contribution comes from proton-proton (pp) and CNO reactions. More than 99% of the solar neutrinos are produced in the pp process. Neutrino are also produced during production of ${}^7\text{Li}$ and ${}^8\text{B}$ nuclei. The solar neutrinos are electron neutrinos in nature. The deuteron with another proton produces a Helium (${}^3\text{He}$) nuclues and gamma ray which further results in production of ${}^4\text{He}$ isotope. Both the Helium isotopes now fuse to form Beryllium (${}^7\text{Be}$) and a gamma ray. The ${}^7\text{Be}$, then, undergoes electron/proton capture to produce ${}^7\text{Li}/{}^8\text{B}$ and electron-neutrino. Detection of electron neutrinos are also reported from depth of the solar core through carbon-nitrogen-oxygen (CNO) cycle.

The processes involved in the pp and CNO reactions are given in Figure 1-3. Solar neutrinos were first detected in 1968 in the Homestake experiment[22], confirmed by Kamiokande. The low-energy neutrinos produced in the pp-reaction were measured by the gallium experiments.

1.4. Sources of Neutrinos

The Homestake experiment is a radiochemical experiment which detect solar neutrinos using Inverse beta decay (IBD) reaction[23, 24], given by



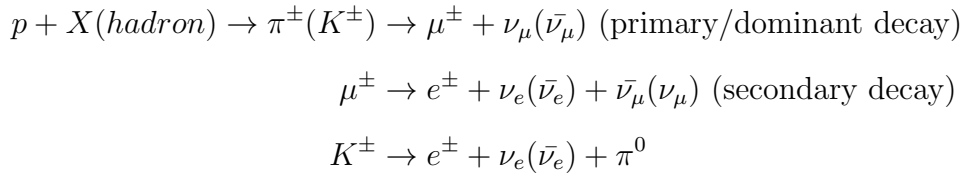
with a neutrino threshold energy of 0.814 MeV, and thus, can detect only intermediate and high-energy neutrinos. The experiment is mainly sensitive to the high-energy ${}^8\text{B}$ neutrinos. The solar neutrino flux recorded by the experiment was less than 3 Solar Neutrino Units (SNU)¹, which about 1/3 of that predicted by the Standard Solar Model (SSM)[25]. The gallium experiments like GALLEX [26–30], GNO [31, 32] and SAGE [33–37] detected solar neutrinos using gallium (${}^{71}\text{Ga}$) as the detection target, with low neutrino energy threshold of 233 keV[38]. Thus, these experiments are sensitive to all sources of solar neutrinos. The solar neutrino flux measured by these experiments are about 1/2 of that predicted by the SSM. The Kamiokande [39, 40] (Super-Kamiokande [41]) experiment, with a water Cherenkov detector, is sensitive to ${}^8\text{B}$ solar neutrinos with the neutrino energy threshold range of 6.7-9.0 (4.7-6.2) MeV. The experiment measured the solar neutrino flux via the elastic scattering (ES) reaction, and the average flux of ${}^8\text{B}$ ν_e obtained is about half the SSM flux.

In the late 20th century, another breakthrough experiment, SNO [42] provided measurements on the high energy part of the solar neutrino flux. SNO detects solar neutrino through three reactions on the deuterium target: the charged current (CC), the Neutral current (NC) and ES. Due to high backgrounds at low energies, the corresponding neutrino energy threshold are 6.9, 2.224 and 5.7 MeV respectively, all of the reactions being sensitive to ${}^8\text{B}$ solar neutrinos. The results confirmed the solar ν_e deficits [43], observed by the previous experiments. The NC measurement of the total flux observed that two ν_e out of three converts into ν_μ or ν_τ on their way from the center of the Sun to the Earth [44]. Thus, SNO experiment is significant for it proved that the solar neutrino problem (SNP) is due to neutrino flavour transitions.

¹1SNU \equiv 10^{-36} events/atom/s

1.4.1.2 Atmospheric Neutrinos

Atmospheric neutrinos are typically produced around 15 kilometers above Earth's surface. They form when a cosmic ray, high energetic particles (mostly protons) from space interact with the Earth's atmosphere. When they strike an atomic nucleus in our atmosphere, there is a cascade of particles. Short-lived particles called mesons form, most of them pions (and a few kaons). These are unstable particles made of two quarks, and they rapidly decay into muons and muon antineutrinos (or antimuons and muon neutrinos). A muon, being unstable, also undergoes decay into an electron, electron antineutrino, and muon neutrino. About two-thirds of atmospheric neutrinos are muon neutrinos and antineutrinos, and the remainder are electron neutrinos and antineutrinos. The reactions involved in the process are-



Atmospheric neutrinos were first detected in the mines of Kolar Gold Fields [45] of India and at the same time in a gold mine of South Africa [46]. From the above decay chain, the expected number of muon neutrinos (N_μ) are about twice that of electron neutrinos (N_e).

$$\text{i.e. } \frac{N_\mu + N_{\bar{\mu}}}{N_e + N_{\bar{e}}} \sim 2 \tag{1.6}$$

However, experiments like Kamiokande [47], IMB [48, 49] and Sudan2 [50] reported the ratio of observed N_μ/N_e to that of Monte-Carlo simulation, to be significantly less than one. This is known as the ‘‘Atmospheric Neutrino Anomaly’’. The Super-Kamiokande (SK) [51] detector started the operation in 1996 and concluded that the anomaly is due to $\nu_\mu \rightarrow \nu_e$ or $\nu_\mu \rightarrow \nu_\tau$ flavour oscillations. Apart from that, the oscillatory behaviour can be tested by observing neutrinos with different incoming directions that have travelled different distances to the detector. This

1.4. Sources of Neutrinos

is parameterised by the zenith angle². Atmospheric neutrino flux peaks at zenith angle $\sim 90^\circ$ (near the horizon), due to larger length of the atmosphere in that direction. For downward moving neutrinos, different zenith angles have path length of range $\sim 10 - 30km$, whereas, the upward moving neutrinos suffers significant oscillatory behaviors due to its larger path length of $\sim 10^4km$ for different zenith angles. Neutrinos are also produced in distant astrophysical sources [52] such as supernovae [53, 54], active galactic nuclei (AGN) [55] and gamma ray burst (GRB) [56].

Neutrino oscillation experiments are classified on the basis of the sources of the neutrinos and the measurements of appearance and disappearance channels. Their classification also depends on the average value of the ratio $\frac{L}{E}$ for an experiment, which determines the sensitivity to the mass-squared differences Δm_{ij}^2 ($i = 1, 2, 3$). It is to be noted that,

$$UU^\dagger = 1 \text{ gives } \sum_{k=1}^3 U_{\alpha k} U_{\beta k}^\dagger = \delta_{\alpha\beta} \quad (1.7)$$

which implies $P_{\nu_\alpha \rightarrow \nu_\beta}(L = 0, E) = \delta_{\alpha\beta}$. For $L > 0$, the amplitude of the oscillations is specified by the elements of the lepton mixing matrix U and the phases allow us to obtain information on the values of mass-squared differences Δm_{ij}^2 . The oscillation length L_{ij}^{osc} is the distance at which the phase generated by Δm_{ij}^2 becomes maximum, equal to 2π .

$$L_{ij}^{osc} = \frac{4\pi E}{\Delta m_{ij}^2} \quad (1.8)$$

Considering the above fact, different experiments are designed in order to be sensitive to Δm_{ij}^2 , for which

$$\frac{4\pi E}{\Delta m_{ij}^2 L} = 2\pi \Leftrightarrow \frac{\Delta m_{ij}^2 L}{2E} \sim 1 \Leftrightarrow \Delta m_{ij}^2 \propto \frac{E}{L} \quad (1.9)$$

The classification of neutrino oscillation experiments with their source-detector distance (L), energy (E) and sensitivity to Δm_{ij}^2 [which is given by E/L, E in MeV

²Zenith angle is the angle between the neutrino direction and the vertical.

Table 1.2: Classification of neutrino oscillation experiments with their source-detector distance (L), energy (E) and sensitivity to Δm_{ij}^2 .

Type of Experiments	L	E	Δm_{ij}^2 sensitivity
Reactor SBL	$\sim 10\text{m}$	$\sim 1\text{ MeV}$	$\sim 0.1\text{ eV}^2$
Accelerator SBL (Pion DIF)	$\sim 1\text{km}$	$\geq 1\text{ GeV}$	$\geq 1\text{ eV}^2$
Accelerator SBL (Muon DAR)	$\sim 10\text{m}$	$\sim 10\text{ MeV}$	$\sim 1\text{ eV}^2$
Accelerator SBL (Beam Dump)	$\sim 1\text{km}$	$\sim 100\text{ GeV}$	$\sim 10^2\text{ eV}^2$
Reactor LBL	$\sim 1\text{km}$	$\sim 1\text{ MeV}$	$\sim 10^{-3}\text{ eV}^2$
Accelerator LBL	$\sim 10^3\text{km}$	$\geq 1\text{ GeV}$	$\geq 10^{-3}\text{ eV}^2$
Reactor VLB	$\sim 10^2\text{km}$	$\sim 1\text{ MeV}$	$\sim 10^{-3}\text{ eV}^2$
Accelerator VLB	$\sim 10^4\text{km}$	$\geq 1\text{ GeV}$	$\geq 10^{-4}\text{ eV}^2$

(GeV) and L in m (km) for reactor (accelerator-based) neutrino experiments] is listed in Table 1.2.

1.4.2 Terrestrial Neutrino Sources

Terrestrial neutrino oscillation experiments (TNE) use neutrinos produced in reactors and accelerators. The sensitivity *i.e. the capability of an experiment to measure the oscillation parameters* depends importantly on source-detector distance, the neutrino energy, the power of the source, the detection cross-section and the backgrounds. In TNEs, one can control the values of these factors.

1.4.2.1 Reactor-based neutrino

When neutrinos have enough energy to produce charged particles like the electron (0.511 MeV), muon (105.7 MeV), or tau (1776.8 MeV), they can be detected through charged current interactions. Only reactions that produce positrons are feasible because the reactor neutrino energy is low. The inverse neutron decay process allows for the detection of reactor electron antineutrinos. This reaction liberates a total visible energy $E_e + m_e$, where E_e is the energy of the positron, which annihilates with the surrounding electron. This energy can be seen in scintillation detectors. The antineutrinos can be distinguished from the background by the coincidence of the prompt signal with the delayed signal produced by the nuclear capture of the neutron. Neglecting the small recoil energy

1.4. Sources of Neutrinos

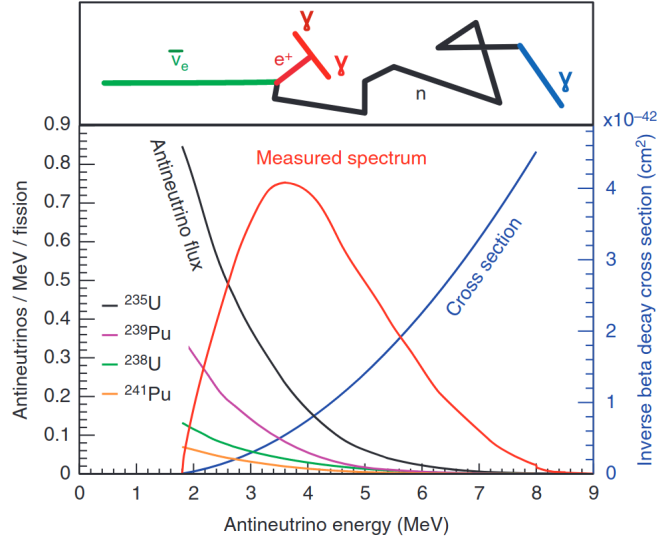


Figure 1-4: An observable electron anti-neutrino ($\bar{\nu}_e$) spectrum in reactor neutrino experiment [57].

of the neutron, the neutrino and positron energies are related by

$$E_\nu = E_e + T_n + m_n - m_p \simeq E_e + 1.293 \text{ MeV} \quad (1.10)$$

where T_n is the negligibly small recoil kinetic energy of the neutron. Thus, the neutrino energy threshold is given by

$$E_\nu^{th} = m_n + m_e - m_p \simeq 1.804 \text{ eV} \quad (1.11)$$

The response of a detector to a reactor electron anti-neutrino ($\bar{\nu}_e$) flux is illustrated in Fig. 1-4 which is proportional to the product of the

- antineutrino fluxes from each isotope, and
- the detection cross-section.

R-SBL experiments have source-detector distances between 10-100m. ILL [58], Gosgen [59], Rovno [60], Krasnoyarsk [61], Bugey [62] and Savannah River [63] were operative in the 1970s, but none of them observed a $\bar{\nu}_e$ disappearance. Their L values were sufficient to reach the sensitivity to the small values of Δm_{ij}^2 . Long baseline (LBL) reactor-based neutrino oscillation experiments with baselines of

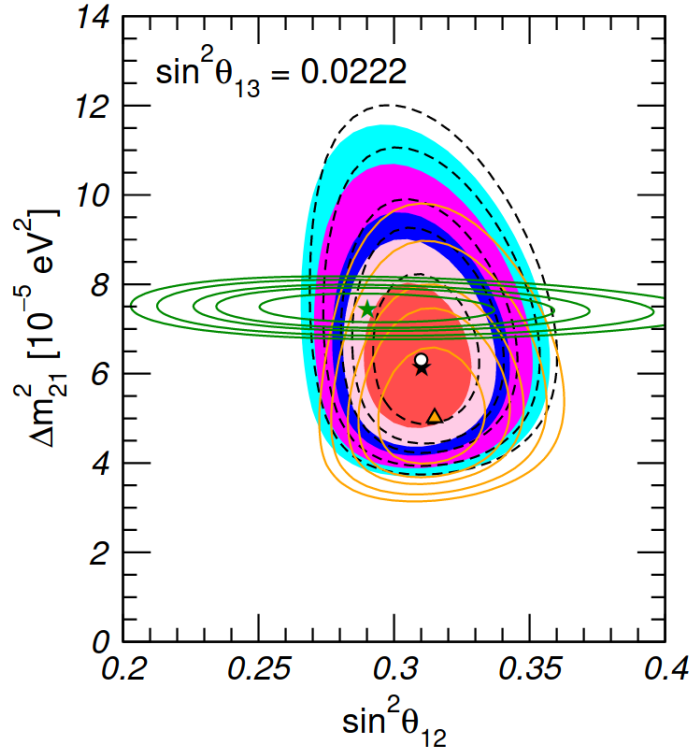


Figure 1-5: Allowed regions of $\sin^2 \theta_{12} - \Delta m_{21}^2$ for fixed $\theta_{13} = 8.6^\circ$ for solar and KamLAND data, with and without Super Kamiokande results. The updated allowed regions are showed at 1σ , 90%, 2σ , 99% and 3σ C.L for 2 d.o.f.. The analysis for KamLAND is given by solid green contours with best fit marked by a green star [75].

the order of 1 km have the sensitivity of Δm^2 of about $10^{-3} eV^2$, corresponding to atmospheric mass-squared difference. Chooz [64–66] and Palo Verde [67–69] are the notable experiments that were carried out in the 1990s. Although, these experiments were important to understand the reactor neutrino flux and spectrum, yet unable to observe the oscillation of $\bar{\nu}_e$ disappearance. However, they obtained an upper limit of $\sin^2 \theta_{13} < 0.10$ at 90% C.L. [65].

In the next-generation reactor experiments, Daya-Bay[70, 71], RENO [72] and Double Chooz [73, 74], our knowledge of the value of the element U_{e3} of the lepton mixing matrix in the case of three-neutrino mixing was further clarified. They solved the puzzle of the value of the mixing angle, θ_{13} , which finally turned out to be non-zero. The present best-fit value of the mixing angle from the reactor experiments is $\sim 8.6^\circ$, dominated by Daya Bay result [75, 76].

The KamLAND experiment [77] has been designed to detect electron

1.4. Sources of Neutrinos

antineutrinos produced by 53 nuclear power reactors in Japan, with a small contribution from reactors in South Korea ($\sim 2\%$), at distances varying from 80 km to 800 km. About 80% of the detected neutrinos come from reactors at distances between 140 km and 215 km, with an average distance of about 180 km. The large source–detector distance allowed the KamLAND experiment to measure the $\bar{\nu}_e$ disappearance due to the small solar Δm_{21}^2 . The ratio of measured to expected $\bar{\nu}_e$ events in KamLAND from March 2002 to January 2004 [78] is

$$R = 0.658 \pm 0.044 \pm 0.047$$

which deviates from unity by about 5σ . It showed that the earlier solar neutrino measurements were indeed caused by oscillations. It also measures the most accurate value of the mass-squared difference Δm_{21}^2 . The present allowed regions of $\sin^2 \theta_{12} - \Delta m_{21}^2$ plane obtained with a combined fit of KamLAND and solar data is presented in Figure 1-5. The present best-fit values [75] of the solar mixing parameters are:

$$\Delta m_{21}^2 = 7.42 \times 10^{-5} eV^2, \quad \sin^2 \theta_{12} = 0.304 \text{ (for both the mass hierarchies)}$$

Another type of experiments are reactor-based medium baselines (MBLs) like JUNO which due to its unique baseline of 52.5 km is sensitive to both the solar and atmospheric mass-squared differences.

1.4.2.2 Accelerator-based neutrino

In accelerator neutrino oscillation experiments, neutrinos and anti-neutrinos are produced when high energetic proton beam collide a fixed hadronic target. The proton beam is accelerated by a set of linear and cycling synchotrons to achieve a higher energy before hitting the target. The proton collision with the fixed target mainly produces pions (π^\pm) and kaons (K^\pm). This meson beam is aligned (*defocused, to be accurate*), into a decay pipe, where they decay primarily into charged muons and muon neutrinos or muon anti-neutrinos depending on the parent mesons. The charged muons can further undergo secondary decay into

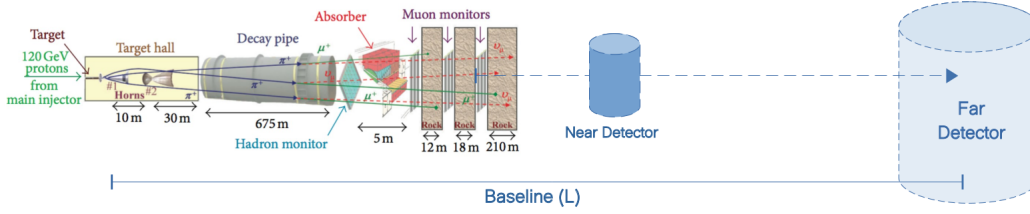


Figure 1-6: Process of neutrino production, propagation and detection in accelerator neutrino oscillation experiments. The left portion of the image is the NuMI beamline [79] which are employed in the MINOS [80], MINOS+ [81] and NO ν A [82] experiments.

electron neutrino and anti-neutrino, resulting in the contamination of the highly intense muon neutrino (anti-neutrino) beam. The following processes take place:

$$\pi^\pm(K^\pm) \longrightarrow \mu^\pm + \nu_\mu(\bar{\nu}_\mu) \quad (\text{most dominant})$$

Secondary decay may take place resulting in ν_e , given by

$$\mu^\pm \longrightarrow e^\pm + \nu_e(\bar{\nu}_e) + \bar{\nu}_\mu(\nu_\mu)$$

$$K^\pm \longrightarrow e^\pm + \nu_e(\bar{\nu}_e) + \pi^0$$

The charged leptons are stopped by the absorber and, the neutrinos and anti-neutrinos travel to the far detector (FD) traversing a distance L(in km) beneath the earth's surface where the oscillation analysis is performed. In present days, near detectors (ND) are placed close to the source of production to reduce the uncertainty in flux and cross-section information. ND monitors the un-oscillated ν_μ and $\bar{\nu}_\mu$ fluxes from the production site. Figure 1-6 illustrates the production, propagation and detection of the neutrino beam as described above.

Accelerator experiments can be classified according to their source-detector baselines (L) in Table 1.2 and the method of production of the neutrino beam are pion decay in flight (DIF), muon decay at rest (DAR) and beam dump.

1. **Pion Decay in Flight (DIF):** Neutrino beam is produced by the decay of mesons, most dominantly pions, created by a proton beam after hitting a target. The pions and kaons are aligned in a decay tunnel for decay

1.4. Sources of Neutrinos

of mesons to neutrinos and antineutrinos. The neutrino thus produced is primarily composed of ν_μ or $\bar{\nu}_\mu$. The typical energy of the neutrinos vary from sub-GeV to few GeV depending on the energy of the initial proton beam.

They can also be further sub-divided based on the neutrino beams generated by pion decay in flight, in three categories:

- a. *Wide band beam:* These are experiments having a high-intensity neutrino beam with a wide energy spectrum which can span one or two orders of magnitude. This type of beam is convenient for investigating new oscillation signals in a wide range of values of Δm_{ij}^2 .
- b. *Narrow band Beam:* The neutrino beams of these experiments have a narrow energy spectrum, which is obtained by selecting the momenta of the parent pion and kaons. The resulting intensity of the neutrino flux of a narrow-band beam is reduced comparing with a wide-band beam obtained from the same proton beam. Narrow-band beams are convenient for precise measurements of Δm_{ij}^2 .
- c. *Off-Axis Beam:* These are experiments which use a high-intensity wide-band beam with the detector shifted by a small angle from the axis of the beam, where the neutrino energy is almost monochromatic. The off-axis principle is a new concept, which is exploited by LBL experiments T2K and NO ν A. The neutrino energy as a function of the parent pion energy (E_π) and off-axis angle (θ), for pions, is given by:

$$E_\nu = \frac{\left[1 - \frac{m_\mu^2}{m_\pi^2}\right] E_\pi}{1 + \gamma^2 \theta^2}, \quad (1.12)$$

And the expression for the neutrino flux as a function of the angle is,

$$\phi_\nu(\theta) \propto \left(\frac{2\gamma}{1 + \gamma^2 \theta^2}\right)^2, \quad (1.13)$$

to the lowest order of θ , where $\gamma = \frac{E_\pi}{m_\pi}$, is the Lorentz factor. For $\theta = 0$, the neutrino energy linearly varies with pion energy, whereas it

tails off for $\theta > 0$. To obtain a narrow band beam, one can look for a non-zero off-axis angle and baselines at the ν_e -appearance oscillation maximum. For $\text{NO}\nu\text{A}$, $\theta = 14.6\text{mrad}$ at a baseline of 810 km results in the neutrino flux peak at $\sim 2\text{GeV}$ (Figure 1-7). Similar Off-axis technique is utilized by the T2K experiment with $L = 295\text{km}$ with $\theta = 2.5^\circ$ to obtain a peak in neutrino flux at 0.6GeV .

2. **Muon Decat At Rest (DAR):** A beam of low-energetic muon antineutrinos are produced from the decay of the μ^+ produced in the pion decay (the π^- are mostly absorbed by nuclei) and stopped in the target. The process is

$$\mu^+ \rightarrow e^+ + \nu_e + \bar{\nu}_\mu$$

$$\pi^+ \rightarrow \mu^+ + \nu_\mu$$

The antineutrinos have energies of the order of several tens of MeV.

3. **Beam Dump:** In this method, a proton beam of the order of some hundreds of GeV, hit a thick target, called the beam dump, where the proton-nucleon interactions generate heavy hadrons. The charmed heavy hadrons decay promptly with practically equal branching ratios into electrons and muons, emitting equal fluxes of electron and muon neutrinos with energies of the order of 10^2 GeV. A detector at a distance of the order of 1 km can measure the ratio of the electron and muon neutrino fluxes, whose deviations from unity would signal the presence of oscillations [21].

SBL accelerator experiments like CHARM [84], CDHSW [85], CCFR [86], BEBC [87], LSND [88], NOMAD [89], KARMEN[90], CHORUS [91] among others have been carried out to explore the different flavor transition channels. All other experiments except LSND failed to find any indication of neutrino oscillations [92, 93].

K2K is the first generation LBL accelerator-based neutrino oscillation experiment based in Japan, with a distance of 250 km from the source in the KEK laboratory to the Super-Kamiokande detector in the Kamioka mine [94–97]. The neutrino beam is a pulsed wide-band beam with a mean energy of 1.3 GeV. It is an almost

1.4. Sources of Neutrinos

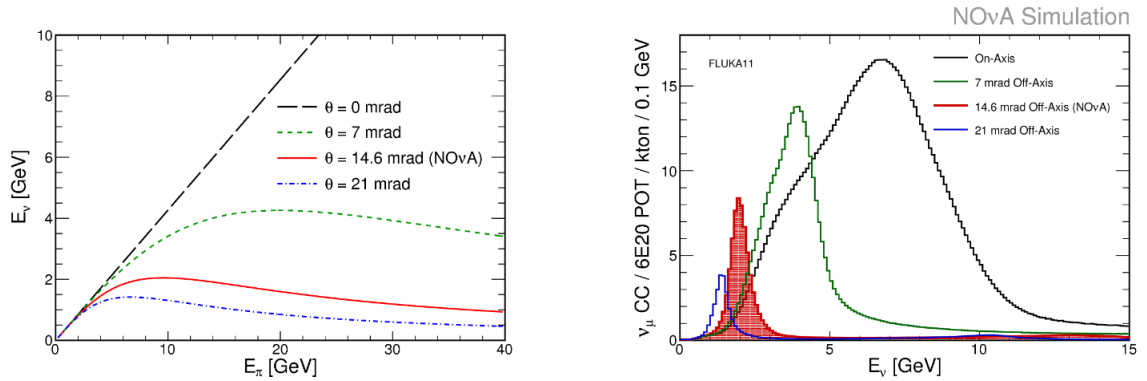


Figure 1-7: Neutrino energy as a function of the parent π -energy for different off-axis angles (*left*) and the overall predicted flux per given exposure (*right*). The figure is a description of the NO ν A experiment [83].

pure ν_μ beam ($\sim 98\%\nu_\mu + \sim 1\%\bar{\nu}_\mu + \sim 1\%\nu_e$). The protons are focused on an aluminum target and the produced positive pions are focused towards a decay tunnel 200 m long, where they decay into antimuons and muon neutrinos. At the end of the decay tunnel, there is an iron and concrete beam dump which stops all charged particles, except muons with energy greater than 5.5 GeV. After the beam dump, there is a muon monitor and after about 70 m of earth which eliminates all particles except neutrinos, there is a near neutrino detector system which is used to calibrate the neutrino beam (about 300 m from the production target). The near detector system consists of two detector sets: a 1 kton water Cherenkov detector and a fine-grained detector system. The water Cherenkov detector uses the same technology and analysis algorithms as the Super-Kamiokande far detector. Another notable accelerator-based LBL experiments include OPERA [98], ICARUS [99], MINOS and MINOS+ (based in the USA, which concluded their data taking in late 2019). Ongoing experiments include the second generation accelerator LBL experiments of Japan and the USA, T2K [100] and NO ν A [101] respectively which form the basis of the thesis, are discussed in greater details in the upcoming chapters.

The sources of neutrinos, their detection techniques, description of relevant neutrino experiments and their results are explored in our paper [102] and the literature cited within.

Neutrino Interactions

The neutrino energy accessible to A-LBL neutrinos makes them sensitive to different interaction types as represented by the Feynman diagram in Figure 1-8. The neutrino and anti-neutrino inclusive cross-sections at the intermediate energy range, appropriate for A-LBL, vary from 0.2 to 20 GeV. At these intermediate energies, several distinct neutrino scattering mechanisms start to play a role, as shown in Figure 1-9. They are:

- Quasi-Elastic (QE) scattering,
- Resonant Delta Production (RES),
- Deep Inelastic Scattering (DIS), and
- Meson Exchange Current (MEC).

Quasi-Elastic (QE) scattering: For neutrino energies less than $\sim 2\text{GeV}$, neutrino-hadron interactions are predominantly quasi-elastic (QE). They provide large source of signal events in many neutrino oscillation experiments operating in this energy range. In this process, the neutrino scatters off a single nucleon within the nucleus instead of its constituent parton. The target neutron in the detector is converted to a proton when a neutrino is involved, and vice-versa for a

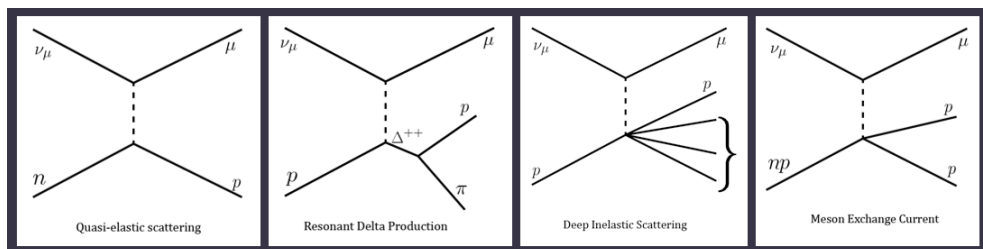


Figure 1-8: Feynman diagrams for different types of neutrinos interactions at the detector. The image is taken from <https://www.phys.ksu.edu/reu/2018/song.html>.

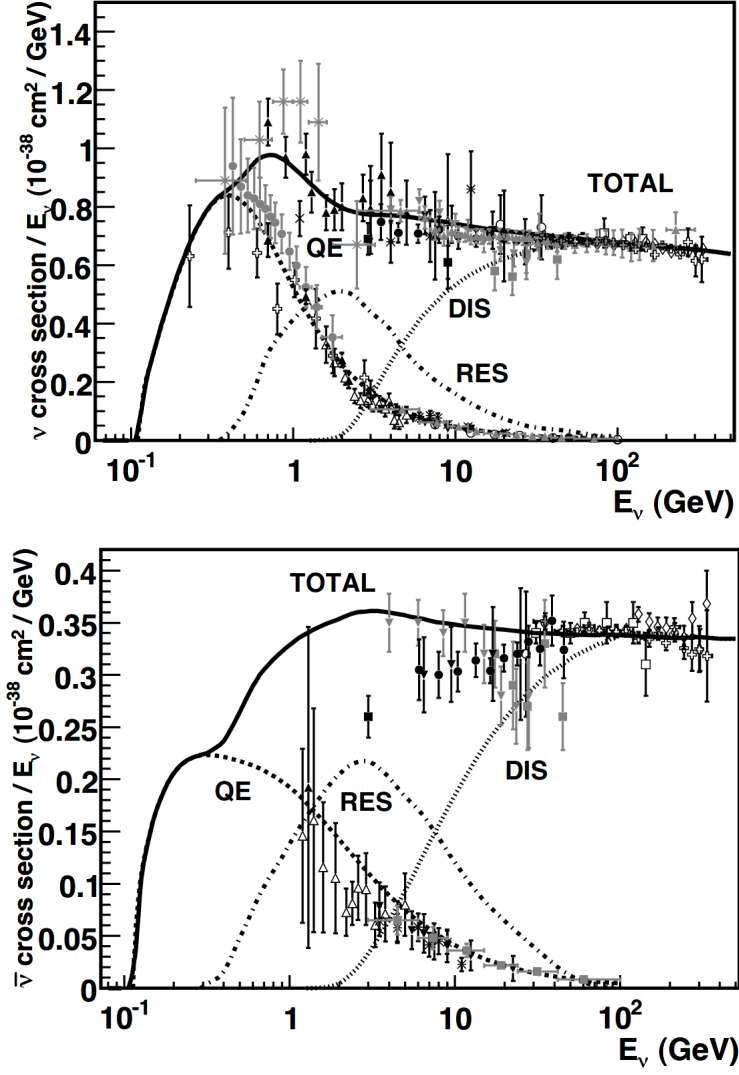


Figure 1-9: The neutrino and antineutrino per nucleon CC cross sections (for an isoscalar target) divided by neutrino energy as a function of energy [103].

antineutrino.

$$\nu_\mu + n \rightarrow \mu^- + p \quad (1.14)$$

$$\bar{\nu}_\mu + p \rightarrow \mu^+ + n \quad (1.15)$$

The overall $Q^2(= q^2)$ for this interaction is relatively low and QE events are generally characterized by clean lepton signatures travelling relatively in line with the beam direction and a small hadronic component which usually involves a single proton track for the neutrino case.

Resonant Delta Production (RES): These interactions produce baryon resonances in the final state (Δ) which decay into pions and protons. If a π^0 is produced that usually decays via $\pi^0 \rightarrow \gamma\gamma$. Sometimes a single γ can be produced by the Δ decay as well ($\Delta^+ \rightarrow p\gamma$). These can exhibit a variety of signatures but usually involve either charged pion tracks which can hard-scatter in the detector and produce kinks or a pair of electromagnetic shower cascades coming from π^0 decay. Sometimes multiple proton tracks can be seen as well.

Deep Inelastic Scattering (DIS): These are in general messy interactions at a very high Q^2 where the relevant initial state particles involved are the quark soup within each nucleon. The event signature is a large hadronic component due to the resulting hadronization of the final state quarks. Here the lepton signatures aren't very clean, being relatively small and travelling at a large angle with respect to the beam.

Meson Exchange Current (MEC): These are interactions at a slightly higher Q^2 where the neutrino scatters off a correlated nucleon pair instead of a single nucleus. The nucleon pair is predominantly a np pair which produces two protons (neutrons) in the final state for neutrinos (anti-neutrinos).

1.5 Knowns and Unknowns in Neutrino Physics

In the standard 3ν framework, there are six parameters that govern neutrino oscillations: θ_{12} , θ_{13} , θ_{23} , δ_{CP} , Δm_{21}^2 and $\Delta m_{31(2)}^2$. Global fit 1[75] and global fit 2[76] are the updated global analysis of the neutrino experiments' datasets and the previous results are available in Ref. [104, 105] respectively. Global fit 1 is also known as NuFit 5.0 and the previous corresponding is called NuFit 4.1. Global fit 1 & 2 include the updated results from Super-Kamiokande, IceCube DeepCore, SNO, short baseline reactor experiments Daya Bay and RENO, long baseline (LBL) accelerator-based neutrino experiments T2K and NO ν A upto July 2020 when the Neutrino 2020 conference took place. In Global Fit 1, the authors

1.5. Knowns and Unknowns in Neutrino Physics

Table 1.3: The neutrino oscillation parameters, according to two different global fits- Global Fit 1[75] & Global Fit 2[76].

Global Fit 1	Parameters ^a	Mass Ordering	Best Fit	3 σ
	$\Delta m_{21}^2 (\times 10^{-5} eV^2)$	NH,IH	7.42	6.82-8.04
	$\theta_{12} (^{\circ})$	NH	33.44	31.27-35.86
		IH	33.45	31.27-35.87
	$ \Delta m_{3n}^2 (\times 10^{-3} eV^2)$	NH	2.517	2.435-2.598
		IH	2.498	2.581-2.414
	$\theta_{23} (^{\circ})$	NH	49.2	40.1-51.7
		IH	49.3	40.3-51.8
	$\theta_{13} (^{\circ})$	NH	8.57	8.20-8.93
		IH	8.60	8.24-8.96
	$\sigma (^{\circ})$	NH	197	120-369
		IH	282	193-352
Global Fit 2	$\Delta m_{21}^2 (\times 10^{-5} eV^2)$	NH,IH	7.50	6.94-8.14
	$\theta_{12} (^{\circ})$	NH,IH	34.3	31.4-37.4
	$ \Delta m_{3n}^2 (\times 10^{-3} eV^2)$	NH	2.55	2.47-2.63
		IH	2.45	2.37-2.53
	$\theta_{23} (^{\circ})$	NH	49.26	41.20-51.33
		IH	49.46	41.16-51.25
	$\theta_{13} (^{\circ})$	NH	8.53	8.13-8.92
		IH	8.58	8.17-8.96
	$\sigma (^{\circ})$	NH	194	128-359
		IH	284	200-353

^a $\Delta m_{3n}^2 \equiv \Delta m_{31}^2 > 0$, for Normal Hierarchy, Δm_{31}^2 being the reactor mass squared difference. $\Delta m_{3n}^2 \equiv \Delta m_{32}^2 < 0$, for Inverted Hierarchy, Δm_{32}^2 being the atmospheric mass squared difference.

assume that the Wilk's theorem holds to convert $\Delta\chi^2$ values into confidence levels and equivalent numbers of Gaussian standard deviations (σ). In Global Fit 2, the authors have considered both Bayesian and frequentist method for oscillation data analysis to arrive at their results.

The global fits give more accurate measurements of oscillation parameters of θ_{12} , θ_{13} , Δm_{21}^2 and $|\Delta m_{31,32}^2|$. The sign of $\Delta m_{31,32}^2$ referred as mass hierarchy of the three mass-eigenstates, the resolving of the octant degeneracy of mixing angle θ_{23} and determination of δ_{CP} have been studied extensively in the two global fits. Presently, the 3σ relative precision³, marginalised over both hierarchies, for the oscillation parameters stands at 4% for θ_{12} , 9% for θ_{13} , 25% for θ_{23} , 16%

³Relative precision is defined as $\frac{2(x_1-x_2)}{(x_1+x_2)}$, where x_1 is the upper and x_2 is the lower bound in Table 1.3.

for Δm_{21}^2 and 6.5% for $|\Delta m_{31,32}^2|$. The solar mixing angle is well measured by solar experiment while the corresponding mass-squared difference Δm_{21}^2 is better constrained by KamLAND. The recent evidence of neutrino flux from CNO fusion chain by Borexino is not included in these analyses. In these updated global fits, the disagreement between solar and KamLAND data has decreased significantly after the inclusion of the updated Super Kamiokande solar neutrino results. The short baseline reactor-based experiments Daya Bay and RENO are sensitive to θ_{13} and $|\Delta m_{31,32}^2|$. The upcoming reactor-based medium baseline experiment JUNO promises to measure the solar parameters apart from θ_{13} and Δm_{31}^2 with a better precision. NO ν A recently showed evidence of appearance of anti-neutrino with greater than 4σ C.L. T2K alone excludes the CP conserving values of δ_{CP} at almost 3σ C.L. The best fit value of δ_{CP} for T2K lies near $3\pi/2$ for NH, whereas for NO ν A, it is 0.82π - close to CP conserving value π . This tension has to be resolved and a joint-collaboration of T2K and NO ν A colleagues has started. However, for inverted hierarchy, the best fit of δ_{CP} is close to $3\pi/2$. T2K has better precision for θ_{13} measurement than NO ν A but it is not competitive to that of reactor-based short baseline experiments.

There are many open questions in neutrino physics and we divide them into two categories:

- (1) Questions within standard 3ν oscillation framework, and
- (2) beyond standard 3ν neutrino oscillation framework.

A few of them are described below.

1.5.1 Questions within standard 3ν oscillation framework

1.5.1.1 Neutrino Mass Hierarchy

The solar experiments confirmed that $\Delta m_{21}^2 > 0$ i.e. $m_2 > m_1$, but the sign of Δm_{31}^2 is still unknown. Thus, we are left with two possibilities for the mass eigenvalues. We refer them as the mass hierarchies (MH) of the three active neutrinos: (A) Normal Ordering, $m_3 > m_2 > m_1$, and (B) Inverted Ordering,

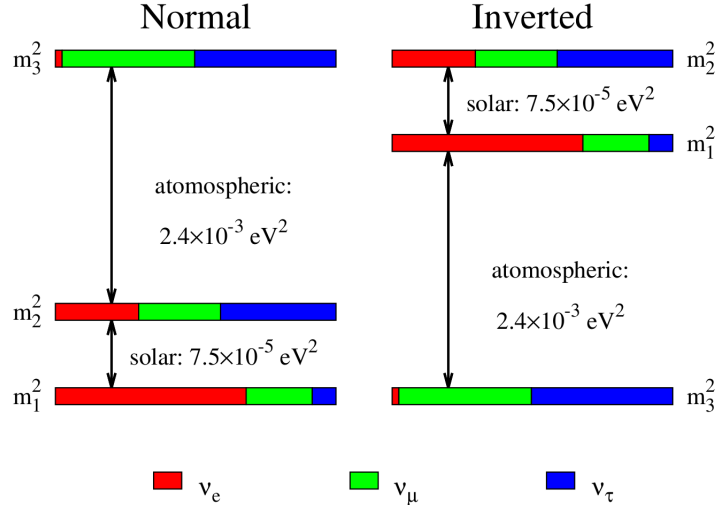


Figure 1-10: Illustration of normal and inverted neutrino mass hierarchies.

$m_2 > m_1 > m_3$. The sign of Δm_{31}^2 is of fundamental importance because it has many implications in particle physics and astrophysics. The behavior of neutrino oscillations in atmospheric and long baseline experiments are sensitive to Δm_{31}^2 [106]. The supernova neutrino oscillations are also affected for a similar reason [107]. The interference effects of two atmospheric mass-squared differences in reactor neutrino vacuum oscillations is also sensitive to it [108]. Moreover, preference to IO may help the seesaw and leptogenesis [109] mechanisms work well to interpret the tiny neutrino mass and explain the baryon asymmetry of the Universe (BAU) [110, 111]. If the hierarchy is inverted, it also provides a chance to observe neutrinoless double beta decay $0\nu\beta\beta$, and thus the Majorana nature of neutrino [112].

1.5.1.2 Leptonic CP Violation

The CP transformation combines charge conjugation C with parity P. Under C transformation, particles and antiparticles are interchanged, and the handedness of space is reversed under P transformation, $\vec{x} \rightarrow -\vec{x}$. For instance, CP can change a left-handed electron e_L^- into a right-handed positron, e_R^+ . The laws of nature would apply to both matter and antimatter if CP were an exact symmetry. Since most phenomena exhibit C and P symmetry, they are also CP symmetric. These symmetries are respected by the gravitational, electromagnetic, and strong

interactions. On the other hand, the weak interactions most severely violate C and P. The charged W bosons, for instance, couple to left-handed electrons, e_L^- , and to their CP conjugate right-handed positrons, e_R^+ , but not to their P conjugate right-handed electrons or their C conjugate left-handed positrons. Although weak interactions separately violate C and P, CP is still preserved in most weak interaction processes. However, the CP symmetry can be broken in some extremely rare processes, as seen in neutral K decays in 1964 [113] and later confirmed in B (2001) and D (2019) decays [12].

It is crucial to know whether or not the CP symmetry in the leptonic sector is violated because it will explain the observed baryon asymmetry of the universe (BAU) via leptogenesis. Under CPT invariance, CP violating asymmetries is measured by appearance channels, particularly in A-LBL, given by $A_{CP}^{\alpha\beta} = P(\nu_\alpha \rightarrow \nu_\beta) - P(\bar{\nu}_\alpha \rightarrow \bar{\nu}_\beta)$, where $\alpha, \beta = e, \mu, \tau$. $A_{CP}^{\alpha\beta}$ depends on all the six oscillation parameters. Given that θ_{12} and Δm_{21}^2 are well-constrained in solar experiments and KamLAND, θ_{13} ($\neq 0$) by R-SBL experiments, θ_{23} by atmospheric experiments and $|\Delta m_{31,32}^2|$ by atmospheric and A-LBL experiments, the uncertainties arise mostly due to the value of δ_{CP} . Presently, the best fit of δ_{CP} hints at $3\pi/2$ for IO, indicating maximal CP violation in the lepton sector. The upcoming A-LBL experiments such as DUNE and T2HK shall explore the CPV phase. In these experiments, the CP asymmetry can be intrinsic due to presence of $\sin \delta_{CP}$ term and can also be due to matter effect experienced by neutrinos and antineutrinos while propagating through Earth matter. This fake CPV due to matter effect must be disentangled from the genuine CPV parameter δ_{CP} . Other possible new physics effects like sterile neutrinos [114–116], non-standard interactions [117–120], that can induce fake CPV must also be taken into consideration in the measurement of δ_{CP} .

1.5.1.3 Octant Degeneracy

The PMNS matrix is yet to be fully fixed as the octant of θ_{23} and the value of δ_{CP} are unknown. If the value of θ_{23} is measured to be $\pi/4$, it means the mass eigenstate ν_3 is comprised of an approximately equal amount of ν_μ and

ν_τ , indicating some *unknown* symmetry between the second and the third lepton generations. Whether θ_{23} is exactly equal to 45° , in the lower octant (LO, $\theta_{23} < 45^\circ$), or in the higher octant (HO, $\theta_{23} > 45^\circ$) is of interest to pursue. Particularly, $\theta_{23} = \pi/4$ is allowed in many neutrino mass models as a consequence of the exact $\mu - \tau$ symmetry [121]. The deviation of θ_{23} from $\pi/4$ will serve as useful model discriminator [122, 123] and requires a precision measurement in the upcoming atmospheric and A-LBL experiments.

1.5.2 Beyond standard 3ν neutrino oscillation

1.5.2.1 Sterile neutrinos

Whether there exists additional species of neutrinos is one of the fundamental questions in neutrino physics and cosmology. Such neutrinos cannot take part directly in weak interactions, but with the active neutrinos. Experimentally, accelerator anomalies from LSND [88] and MiniBooNE [124], and reactor antineutrino anomalies [125] are explained using sterile-active oscillations with the assumption of one or two sterile neutrinos. The mass-squared difference that could explain the LSND $\bar{\nu}_e$ excess in $\bar{\nu}_\mu \rightarrow \bar{\nu}_e$ oscillation measurement is $\Delta m^2 = 1eV^2$, suggesting the presence of a sterile neutrino [126]. Event rate deficit of ν_e candidate in solar experiments GALLEX and SAGE also favour the sterile neutrino hypothesis in the measurement of $\nu_e \rightarrow \nu_e$ disappearance [127, 128]. Also, long-lived sterile neutrinos at the keV scale might serve as a warm dark matter candidate [129].

1.5.2.2 Nature of neutrino: Dirac or Majorana

A lepton and its antiparticle possess opposite lepton numbers and are distinguishable. But if neutrino is a Majorana particle, it is its own antiparticle [130], leading to lepton number violation as a direct consequence. The tiny masses of three known neutrinos make it extremely difficult to identify their nature, *i.e.*, whether they are the Dirac or Majorana particles. At present

the only experimentally feasible way to probe the Majorana nature of massive neutrinos is to observe $0\nu\beta\beta$ decays of some even-even nuclei, given by the process $N(A, Z) \rightarrow N(A, Z+2) + 2e^-$, which occur via an exchange of the virtual Majorana neutrinos between two beta decays [131].

1.5.2.3 Absolute scale of neutrino mass

It is important to note that the phenomenon of neutrino oscillation can only probe the mass squared differences of the neutrinos but not their absolute masses. A determination of absolute mass scale is performed by a number of non-oscillation experiments. There are tritium beta decay experiments which measure the absolute mass of neutrinos. The effective electron antineutrino mass is measured in the beta decay ${}^3_1\text{H} \rightarrow {}^3_2\text{H} + e^- + \bar{\nu}_e$, given by

$$\langle m_e \rangle \equiv \sqrt{\sum_{i=1}^3 m_i^2 |U_{ei}|^2} \quad (1.16)$$

The combined data of Troitsk [132] and Mainz [133] experiments give the upper bound of electron neutrino mass as < 1.8 eV. The combined result of first and second campaign of neutrino-mass measurement of KATRIN gives an improved upper limit of < 0.8 eV [134] for the mass of electron antineutrino. There are also weak bounds on muon neutrino [135] and tau neutrino [136] masses coming from pion and tau decay as < 0.17 MeV and < 18.2 MeV respectively. The neutrinoless double beta decay ($0\nu\beta\beta$) experiments which can probe Majorana nature of the neutrinos can also put constraint on the effective Majorana neutrino mass. The decay width of a particular Neutrinoless Double Beta Decay (NDBD) process mediated by light neutrino can be written as,

$$\Gamma^{0\nu} = 1/T_{1/2}^{0\nu} = G^\nu(Q, Z) |M^{0\nu\beta\beta}|^2 \frac{|m_{\beta\beta}|^2}{m_e^2}$$

, where $G^\nu(Q, Z)$ is the phase factor, $M^{0\nu\beta\beta}$ is the nuclear matrix element (NME) and $m_{\beta\beta}$ is the effective Majorana mass. $T_{1/2}^{0\nu}$ represents the half-life of the decay of the isotope under consideration. The effective Majorana mass is $|\sum_{i=1}^3 U_{ei}^2 m_i|$,

1.5. Knowns and Unknowns in Neutrino Physics

where m_i are the Majorana masses of the three light neutrinos.

Experiments like CUORE, Gerda and KamLAND-Zen have set lower limits on the half-life of isotopes ^{130}Te ($T_{1/2}^{0\nu} > 3.2 \times 10^{25}$), ^{76}Ge ($T_{1/2}^{0\nu} > 9 \times 10^{25}$) and ^{136}Xe ($T_{1/2}^{0\nu} > 1.07 \times 10^{26}$), respectively. These bounds on the half-life from the above experiments give the upper limits on the effective mass of $m_{\beta\beta} < 75 - 350$ meV by CUORE [137], $m_{\beta\beta} < 104 - 228$ meV by Gerda [138] and $m_{\beta\beta} < 104 - 228$ meV by KamLAND-Zen [139], respectively where the bounds on the corresponding NMEs can be found in Ref [140]. An upper bound on the sum of active neutrino masses as 0.118 eV comes from cosmology [141]. From the neutrino oscillation experiments we know that the two mass squared differences which govern the oscillation of the three generations of neutrinos are of the order of 10^{-5} eV² and 10^{-3} eV². Thus, the oscillation data together with the cosmological bound signify that the neutrino masses are much smaller than the masses of the charged leptons.

1.5.2.4 CPT/Lorentz Violation

CPT violation are related to Lorentz symmetry breaking in local field theories [142]. CPT interchanges the $\nu_\alpha \rightarrow \nu_\beta$ and $\bar{\nu}_\beta \rightarrow \bar{\nu}_\alpha$ ($\alpha, \beta = e, \mu, \tau$) oscillation channels. Hence, CPT violation can be explored by measuring the difference of these two channels, given by CPT asymmetry, $\mathcal{A}^{CPT} = P_{\nu_\alpha \rightarrow \nu_\beta} - P_{\bar{\nu}_\beta \rightarrow \bar{\nu}_\alpha}$. Ongoing accelerator neutrino experiments measure $\nu_\mu \rightarrow \nu_e$ and $\nu_\mu \rightarrow \nu_\mu$ oscillation channels and anti-neutrino counterparts. As there is no experiments presently that can measure the CPT asymmetry in appearance channels as the $\bar{\nu}_e \rightarrow \bar{\nu}_\mu$ is missing, CPT violation can be explored via the disappearance channels. For CPT violation to be observed, there has to be a finite difference between the set of oscillation parameters defining the neutrino and anti-neutrino oscillation probabilities, defined as $\delta_{\nu\bar{\nu}}(X) = X - \bar{X}$, where X are the six parameters in neutrino oscillation and \bar{X} are the corresponding parameters describing anti-neutrino oscillation. An interesting work on CPT violation is recently published and can be found in Ref [143].

1.6 Scope of the Thesis

The work of this thesis involves the sensitivity of three terrestrial experiments: two A-LBL experiments (T2K-II and NO ν A) and one R-MBL experiments JUNO to address the three outstanding problems in neutrino oscillation physics *viz.* determination of neutrino mass hierarchy, exploring leptonic CP violation and resolving the octant degeneracy of θ_{23} .

Chapter 2 forms the motivation of the thesis. We describe the three neutrino oscillation phenomenology in great details. We present a derivation of neutrino oscillation probabilities relevant to A-LBL experiments and discuss the significance of the relevant oscillation channels. We also revisit the parameter degeneracy in neutrino oscillation in context of the present global data fits. We describe the limitations of A-LBL experiments due to the degeneracies and emphasize on our framework.

In chapter 3, we give the description of the oscillation experiments which we have studied in the thesis. We describe the configurations of the above experiments and present the simulated event spectra of the selected appearance and disappearance channels.

Chapter 4 covers the results of our neutrino oscillation analysis. We discuss the sensitivities of T2K-II, NO ν A and JUNO to mass hierarchy and CPV by taking their projected exposures. We also comment on the effect of varying T2K-II exposure on the above issues.

In chapter 5, we present our results on the precision measurements of the oscillation parameters θ_{13} , θ_{23} , Δm_{31}^2 and δ_{CP} , and the combined sensitivity to resolving the octant degeneracy by the considered experiments.

Finally, we summarize the thesis and give the impact of our work.

Bibliography

- [1] Ellis, C. D. & Wooster, W. A. The average energy of disintegration of radium E. *Proceedings of the Royal Society of London. Series A, Containing Papers of a Mathematical and Physical Character* **117** (776), 109–123, 1927.
- [2] Dickinson, R. *et al.* Raman spectra of polyatomic gases. *Physical Review* **34** (4), 582, 1929.
- [3] Heitler, W. & Herzberg, G. Gehorchen die stickstoffkerne der boseschen statistik? *Naturwissenschaften* **17** (34), 673–674, 1929.
- [4] Pauli, W. Pauli letter collection: letter to lise meitner. Tech. Rep., 1930.
- [5] Fermi, E. An attempt at a theory of ‘beta’ray emission. *Ricerca Scientifica* **4** (2), 491–495, 1933.
- [6] Chadwick, J. Possible existence of a neutron. *Nature* **129** (3252), 312–312, 1932.
- [7] Fermi, E. Tentativo di una teoria dei raggi β . *Ricerca Scient* **2**, 12, 1933.
- [8] Cowan, C. *et al.* A test of neutrino-antineutrino identity. *Il Nuovo Cimento (1955-1965)* **3** (3), 649–651, 1956.
- [9] Danby, G. *et al.* Observation of high-energy neutrino reactions and the existence of two kinds of neutrinos. *Physical Review Letters* **9** (1), 36, 1962.
- [10] Kodama, K. *et al.* Observation of tau neutrino interactions. *Physics Letters B* **504** (3), 218–224, 2001.
- [11] Weinberg, S. A Model of Leptons. *Phys. Rev. Lett.* **19**, 1264–1266, 1967.
- [12] Zyla, P. *et al.* Particle Data Group. *Prog. Theor. Exp. Phys.* **083C01**, 2020.
- [13] Schael, S. *et al.* Precision electroweak measurements on the Z resonance. *Phys. Rept.* **427**, 257–454, 2006. [hep-ex/0509008](https://arxiv.org/abs/hep-ex/0509008).
- [14] Lee, T. D. & Yang, C.-N. Question of Parity Conservation in Weak Interactions. *Phys. Rev.* **104**, 254–258, 1956.

- [15] Wu, C. S. *et al.* Experimental Test of Parity Conservation in β Decay. *Phys. Rev.* **105**, 1413–1414, 1957.
- [16] Goldhaber, M. *et al.* Helicity of Neutrinos. *Phys. Rev.* **109**, 1015–1017, 1958.
- [17] Maki, Z. *et al.* Remarks on the unified model of elementary particles. *Progress of Theoretical Physics* **28** (5), 870–880, 1962.
- [18] Pontecorvo, B. Neutrino experiments and the problem of conservation of leptonic charge. *Sov. Phys. JETP* **26** (984-988), 165, 1968.
- [19] Nakamura, K. & Petcov, S. Neutrino mass, mixing, and oscillations. *K. Nakamura et al. (Particle Data Group), J. Phys. G* **37**, 075021, 2010.
- [20] Diwan, M. V. *et al.* Long-Baseline Neutrino Experiments. *Ann. Rev. Nucl. Part. Sci.* **66**, 47–71, 2016. [1608.06237](#).
- [21] Giunti, C. & Kim, C. W. *Fundamentals of Neutrino Physics and Astrophysics*, 2007.
- [22] Davis, R., Jr. *et al.* Search for neutrinos from the sun. *Phys. Rev. Lett.* **20**, 1205–1209, 1968.
- [23] Pontecorvo, B. Inverse beta process. *Camb. Monogr. Part. Phys. Nucl. Phys. Cosmol.* **1**, 25–31, 1991.
- [24] Alvarez, L. W. A Proposed Experimental Test of the Neutrino Theory , 1949.
- [25] Bahcall, J. N. *et al.* Solar models: Current epoch and time dependences, neutrinos, and helioseismological properties. *Astrophys. J.* **555**, 990–1012, 2001. [astro-ph/0010346](#).
- [26] Anselmann, P. *et al.* Implications of the GALLEX determination of the solar neutrino flux. *Physics Letters B* **285** (4), 390–397, 1992.
- [27] Anselmann, P. *et al.* Solar neutrinos observed by GALLEX at Gran Sasso. *Physics Letters B* **285** (4), 376–389, 1992.

- [28] Anselmann, P. *et al.* GALLEX solar neutrino observations. The results from GALLEX I and early results from GALLEX II. *Physics Letters B* **314** (3-4), 445–458, 1993.
- [29] Anselmann, P. *et al.* GALLEX results from the first 30 solar neutrino runs. *Phys. Lett. B* **327**, 377–385, 1994.
- [30] Anselmann, P. *et al.* GALLEX solar neutrino observations: Complete results for GALLEX II. *Phys. Lett. B* **357**, 237–247, 1995. [Erratum: *Phys.Lett.B* 361, 235–236 (1995)].
- [31] Altmann, M. *et al.* GNO solar neutrino observations: Results for GNO I. *Phys. Lett. B* **490**, 16–26, 2000. [hep-ex/0006034](https://arxiv.org/abs/hep-ex/0006034).
- [32] Altmann, M. *et al.* Complete results for five years of GNO solar neutrino observations. *Physics Letters B* **616** (3-4), 174–190, 2005.
- [33] Abazov, A. I. *et al.* Search for neutrinos from sun using the reaction ${}^{71}\text{Ga}(\nu_e, e^-){}^{71}\text{Ge}$. *Phys. Rev. Lett.* **67**, 3332–3335, 1991.
- [34] Abdurashitov, J. N. *et al.* Results from SAGE. *Phys. Lett. B* **328**, 234–248, 1994.
- [35] Abdurashitov, J. N. *et al.* Measurement of the solar neutrino capture rate by SAGE and implications for neutrino oscillations in vacuum. *Phys. Rev. Lett.* **83**, 4686–4689, 1999. [astro-ph/9907131](https://arxiv.org/abs/astro-ph/9907131).
- [36] Abdurashitov, J. N. *et al.* Measurement of the solar neutrino capture rate with gallium metal. *Phys. Rev. C* **60**, 055801, 1999. [astro-ph/9907113](https://arxiv.org/abs/astro-ph/9907113).
- [37] Abdurashitov, J. N. *et al.* Solar neutrino flux measurements by the Soviet-American Gallium Experiment (SAGE) for half the 22 year solar cycle. *J. Exp. Theor. Phys.* **95**, 181–193, 2002. [astro-ph/0204245](https://arxiv.org/abs/astro-ph/0204245).
- [38] Kuzmin, V. Zhetf, 49 (1965), 1532; kuz'min va. *Sov. Phys. JETP* **22**, 1051, 1966.
- [39] Koshiya, M. Observational neutrino astrophysics. *Phys. Rept.* **220**, 229–381, 1992.

- [40] Fukuda, Y. *et al.* Solar neutrino data covering solar cycle 22. *Phys. Rev. Lett.* **77**, 1683–1686, 1996.
- [41] Hosaka, J. *et al.* Solar neutrino measurements in Super-Kamiokande-I. *Phys. Rev. D* **73**, 112001, 2006. [hep-ex/0508053](#).
- [42] Boger, J. *et al.* The Sudbury neutrino observatory. *Nucl. Instrum. Meth. A* **449**, 172–207, 2000. [nucl-ex/9910016](#).
- [43] Ahmad, Q. R. *et al.* Measurement of the rate of $\nu_e + d \rightarrow p + p + e^-$ interactions produced by ^8B solar neutrinos at the Sudbury Neutrino Observatory. *Phys. Rev. Lett.* **87**, 071301, 2001. [nucl-ex/0106015](#).
- [44] Ahmad, Q. R. *et al.* Direct evidence for neutrino flavor transformation from neutral current interactions in the Sudbury Neutrino Observatory. *Phys. Rev. Lett.* **89**, 011301, 2002. [nucl-ex/0204008](#).
- [45] Achar, C. V. *et al.* Detection of muons produced by cosmic ray neutrinos deep underground. *Phys. Lett.* **18**, 196–199, 1965.
- [46] Reines, F. *et al.* Evidence for high-energy cosmic ray neutrino interactions. *Phys. Rev. Lett.* **15**, 429–433, 1965.
- [47] Hirata, K. S. *et al.* Experimental Study of the Atmospheric Neutrino Flux. *Phys. Lett. B* **205**, 416, 1988.
- [48] Casper, D. *et al.* Measurement of atmospheric neutrino composition with IMB-3 detector. *Phys. Rev. Lett.* **66**, 2561–2564, 1991.
- [49] Becker-Szendy, R. *et al.* Electron- and muon-neutrino content of the atmospheric flux. *Phys. Rev. D* **46**, 3720–3724, 1992.
- [50] Goodman, M. C. The Atmospheric neutrino anomaly in Soudan-2. *Nucl. Phys. B Proc. Suppl.* **38**, 337–342, 1995.
- [51] Fukuda, Y. *et al.* Evidence for oscillation of atmospheric neutrinos. *Phys. Rev. Lett.* **81**, 1562–1567, 1998. [hep-ex/9807003](#).

- [52] Hulth, P. O. Ultra high energy neutrino telescopes. *Int. J. Mod. Phys. A* **21**, 1914–1924, 2006.
- [53] Hirata, K. *et al.* Observation in the Kamiokande-II detector of the neutrino burst from supernova SN1987A. *Physical Review D* **38** (2), 448, 1988.
- [54] Alexeyev, E. *et al.* Detection of the neutrino signal from SN 1987A in the LMC using the INR Baksan underground scintillation telescope. *Physics Letters B* **205** (2-3), 209–214, 1988.
- [55] Nellen, L. *et al.* Neutrino production through hadronic cascades in AGN accretion disks. *Physical Review D* **47** (12), 5270, 1993.
- [56] Waxman, E. & Bahcall, J. N. High-energy neutrinos from cosmological gamma-ray burst fireballs. *Phys. Rev. Lett.* **78**, 2292–2295, 1997. [astro-ph/9701231](#).
- [57] Vogel, P. *et al.* Neutrino oscillation studies with reactors. *Nature Communications* **6** (1), 1–12, 2015.
- [58] Kwon, H. *et al.* Search for Neutrino Oscillations at a Fission Reactor. *Phys. Rev. D* **24**, 1097–1111, 1981.
- [59] Zacek, G. *et al.* Neutrino Oscillation Experiments at the Gosgen Nuclear Power Reactor. *Phys. Rev. D* **34**, 2621–2636, 1986.
- [60] Afonin, A. I. *et al.* $\bar{\nu}_e$ Spectra at Two Distances From the Reactor of the Rovno Nuclear Power Plant: Search for Oscillations. *JETP Lett.* **45**, 247–251, 1987.
- [61] Vidyakin, G. S. *et al.* Limitations on the characteristics of neutrino oscillations. *JETP Lett.* **59**, 390–393, 1994.
- [62] Declais, Y. *et al.* Search for neutrino oscillations at 15-meters, 40-meters, and 95-meters from a nuclear power reactor at Bugey. *Nucl. Phys. B* **434**, 503–534, 1995.
- [63] Greenwood, Z. D. *et al.* Results of a two position reactor neutrino oscillation experiment. *Phys. Rev. D* **53**, 6054–6064, 1996.

- [64] Apollonio, M. *et al.* Initial results from the CHOOZ long baseline reactor neutrino oscillation experiment. *Phys. Lett. B* **420**, 397–404, 1998. [hep-ex/9711002](#).
- [65] Apollonio, M. *et al.* Limits on neutrino oscillations from the CHOOZ experiment. *Phys. Lett. B* **466**, 415–430, 1999. [hep-ex/9907037](#).
- [66] Apollonio, M. *et al.* Search for neutrino oscillations on a long base-line at the CHOOZ nuclear power station. *The European Physical Journal C-Particles and Fields* **27** (3), 331–374, 2003.
- [67] Boehm, F. *et al.* Results from the Palo Verde neutrino oscillation experiment. *Phys. Rev. D* **62**, 072002, 2000. [hep-ex/0003022](#).
- [68] Boehm, F. *et al.* Search for neutrino oscillations at the Palo Verde nuclear reactors. *Phys. Rev. Lett.* **84**, 3764–3767, 2000. [hep-ex/9912050](#).
- [69] Boehm, F. *et al.* Final results from the Palo Verde neutrino oscillation experiment. *Physical Review D* **64** (11), 112001, 2001.
- [70] An, F. *et al.* Observation of electron-antineutrino disappearance at Daya Bay. *Physical Review Letters* **108** (17), 171803, 2012.
- [71] An, F. P. *et al.* Spectral measurement of electron antineutrino oscillation amplitude and frequency at Daya Bay. *Phys. Rev. Lett.* **112**, 061801, 2014. [1310.6732](#).
- [72] Ahn, J. K. *et al.* Observation of Reactor Electron Antineutrino Disappearance in the RENO Experiment. *Phys. Rev. Lett.* **108**, 191802, 2012. [1204.0626](#).
- [73] Abe, Y. *et al.* Indication of Reactor $\bar{\nu}_e$ Disappearance in the Double Chooz Experiment. *Phys. Rev. Lett.* **108**, 131801, 2012. [1112.6353](#).
- [74] Abe, Y. *et al.* Background-independent measurement of θ_{13} in Double Chooz. *Phys. Lett. B* **735**, 51–56, 2014. [1401.5981](#).
- [75] Esteban, I. *et al.* The fate of hints: updated global analysis of three-flavor neutrino oscillations. *JHEP* **09**, 178, 2020. [2007.14792](#).

- [76] de Salas, P. F. *et al.* 2020 global reassessment of the neutrino oscillation picture. *JHEP* **02**, 071, 2021. [2006.11237](#).
- [77] Eguchi, K. *et al.* First results from KamLAND: Evidence for reactor anti-neutrino disappearance. *Phys. Rev. Lett.* **90**, 021802, 2003. [hep-ex/0212021](#).
- [78] Araki, T. *et al.* Measurement of neutrino oscillation with KamLAND: Evidence of spectral distortion. *Phys. Rev. Lett.* **94**, 081801, 2005. [hep-ex/0406035](#).
- [79] Adamson, P. *et al.* The NuMI Neutrino Beam. *Nucl. Instrum. Meth. A* **806**, 279–306, 2016. [1507.06690](#).
- [80] Diwan, M. V. Status of the MINOS experiment. *eConf* **C0209101**, TH08, 2002. [hep-ex/0211026](#).
- [81] Tzanankos, G. *et al.* MINOS+: a Proposal to FNAL to run MINOS with the medium energy NuMI beam , 2011.
- [82] Ayres, D. S. *et al.* NOvA: Proposal to Build a 30 Kiloton Off-Axis Detector to Study $\nu_\mu \rightarrow \nu_e$ Oscillations in the NuMI Beamline , 2004. [hep-ex/0503053](#).
- [83] Nayak, N. *A Joint Measurement of ν_μ -Disappearance and ν_e -Appearance in the NuMI Beam Using the NOvA Experiment*. Ph.D. thesis, University of California, Irvine, 2021.
- [84] Bergsma, F. *et al.* A Search for Neutrino Oscillations. *Z. Phys. C* **40**, 171, 1988.
- [85] Dydak, F. *et al.* A search for ν_μ oscillations in the Δm^2 range 0.3-90 eV^2 . *Phys. Lett. B* **134** (281), 90688–9, 1984.
- [86] Stockdale, I. E. *et al.* Search for ν_μ and $\bar{\nu}$ Oscillations in the Mass Range $15 - eV^2/c^4 < \delta M^2 < 1000 - eV^2/c^4$. *Conf. Proc. C* **841031**, 258, 1984.
- [87] Angelini, C. *et al.* New Experimental Limits on $\nu_\mu \rightarrow \nu_e$ Oscillations. *Phys. Lett., B* **179** (3), 307–312, 1986.

- [88] Aguilar-Arevalo, A. *et al.* Evidence for neutrino oscillations from the observation of $\bar{\nu}_e$ appearance in a $\bar{\nu}_\mu$ beam. *Phys. Rev. D* **64**, 112007, 2001. [hep-ex/0104049](#).
- [89] Astier, P. *et al.* Search for $\nu_\mu \rightarrow \nu_e$ oscillations in the NOMAD experiment. *Phys. Lett. B* **570**, 19–31, 2003. [hep-ex/0306037](#).
- [90] Armbruster, B. *et al.* Upper limits for neutrino oscillations $\nu_\mu \rightarrow \nu_e$ from muon decay at rest. *Physical Review D* **65** (11), 112001, 2002.
- [91] Eskut, E. *et al.* New results from a search for $\nu_\mu \rightarrow \nu_\tau$ and $\nu_e \rightarrow \nu_\tau$ oscillation. *Phys. Lett. B* **497**, 8–22, 2001.
- [92] Aguilar-Arevalo, A. *et al.* Evidence for neutrino oscillations from the observation of $\bar{\nu}_e$ appearance in a $\bar{\nu}_\mu$ beam. *Phys. Rev. D* **64**, 112007, 2001. [hep-ex/0104049](#).
- [93] Athanassopoulos, C. *et al.* Evidence for $\nu_\mu \rightarrow \nu_e$ neutrino oscillations from LSND. *Phys. Rev. Lett.* **81**, 1774–1777, 1998. [nucl-ex/9709006](#).
- [94] Ahn, M. H. *et al.* Indications of neutrino oscillation in a 250 km long baseline experiment. *Phys. Rev. Lett.* **90**, 041801, 2003. [hep-ex/0212007](#).
- [95] Ahn, M. H. *et al.* Search for electron neutrino appearance in a 250 km long baseline experiment. *Phys. Rev. Lett.* **93**, 051801, 2004. [hep-ex/0402017](#).
- [96] Ahn, S. H. *et al.* Detection of accelerator produced neutrinos at a distance of 250 km. *Phys. Lett. B* **511**, 178–184, 2001. [hep-ex/0103001](#).
- [97] Yamamoto, S. *et al.* Improved Search for $\nu_\mu \rightarrow \nu_e$ Oscillation in a Long-Baseline Accelerator Experiment. *Physical Review Letters* **96** (18), 181801, 2006.
- [98] Komatsu, M. *et al.* Sensitivity to θ_{13} of the CERN to Gran Sasso neutrino beam. *Journal of Physics G: Nuclear and Particle Physics* **29** (2), 443, 2003.
- [99] Arneodo, F. *et al.* The ICARUS experiment: A Second generation proton decay experiment and neutrino observatory at the Gran Sasso Laboratory, 2001. [hep-ex/0103008](#).

- [100] Itow, Y. *et al.* The JHF-Kamioka neutrino project. In *3rd Workshop on Neutrino Oscillations and Their Origin (NOON 2001)*. 239–248, 2001. [hep-ex/0106019](#).
- [101] Ayres, D. *et al.* Letter of Intent to build an Off-axis Detector to study neutrino oscillations with the NuMI Neutrino Beam, 2002. [hep-ex/0210005](#).
- [102] Nath, A. & Francis, N. K. Detection techniques and investigation of different neutrino experiments. *Int. J. Mod. Phys. A* **36** (13), 2130008, 2021. [1804.08467](#).
- [103] Formaggio, J. A. & Zeller, G. P. From eV to EeV: Neutrino Cross Sections Across Energy Scales. *Rev. Mod. Phys.* **84**, 1307–1341, 2012. [1305.7513](#).
- [104] Esteban, I. *et al.* Global analysis of three-flavour neutrino oscillations: synergies and tensions in the determination of θ_{23} , δ_{CP} , and the mass ordering. *JHEP* **01**, 106, 2019. [1811.05487](#).
- [105] de Salas, P. *et al.* Status of neutrino oscillations 2017. *arXiv:1708.01186*, 2017.
- [106] Bernabeu, J. *et al.* Atmospheric neutrino oscillations, θ_{13} and neutrino mass hierarchy. *Nucl. Phys. B* **669**, 255–276, 2003. [hep-ph/0305152](#).
- [107] Dighe, A. S. & Smirnov, A. Y. Identifying the neutrino mass spectrum from the neutrino burst from a supernova. *Phys. Rev. D* **62**, 033007, 2000. [hep-ph/9907423](#).
- [108] Petcov, S. T. & Piai, M. The LMA MSW solution of the solar neutrino problem, inverted neutrino mass hierarchy and reactor neutrino experiments. *Phys. Lett. B* **533**, 94–106, 2002. [hep-ph/0112074](#).
- [109] Fukugita, M. & Yanagida, T. Baryogenesis Without Grand Unification. *Phys. Lett. B* **174**, 45–47, 1986.
- [110] Buchmuller, W. *et al.* Leptogenesis for pedestrians. *Annals Phys.* **315**, 305–351, 2005. [hep-ph/0401240](#).

- [111] Davidson, S. *et al.* Leptogenesis. *Phys. Rept.* **466**, 105–177, 2008. [0802.2962](#).
- [112] Bilenky, S. M. & Giunti, C. Neutrinoless double-beta decay: A brief review. *Mod. Phys. Lett. A* **27**, 1230015, 2012. [1203.5250](#).
- [113] Christenson, J. H. *et al.* Evidence for the 2π Decay of the K_2^0 Meson. *Phys. Rev. Lett.* **13**, 138–140, 1964.
- [114] Gandhi, R. *et al.* The impact of sterile neutrinos on CP measurements at long baselines. *JHEP* **11**, 039, 2015. [1508.06275](#).
- [115] Dutta, D. *et al.* Capabilities of long-baseline experiments in the presence of a sterile neutrino. *JHEP* **11**, 122, 2016. [1607.02152](#).
- [116] Berryman, J. M. *et al.* Sterile neutrino at the deep underground neutrino experiment. *Physical Review D* **92** (7), 073012, 2015.
- [117] Esteban, I. *et al.* Updated constraints on non-standard interactions from global analysis of oscillation data. *Journal of High Energy Physics* **2018** (8), 1–33, 2018.
- [118] Grossman, Y. Non-standard neutrino interactions and neutrino oscillation experiments. *Physics Letters B* **359** (1-2), 141–147, 1995.
- [119] Masud, M. *et al.* Probing the CP violation signal at DUNE in the presence of non-standard neutrino interactions. *Journal of Physics G: Nuclear and Particle Physics* **43** (9), 095005, 2016.
- [120] Coloma, P. Non-standard interactions in propagation at the Deep Underground Neutrino Experiment. *Journal of High Energy Physics* **2016** (3), 1–27, 2016.
- [121] Xing, Z.-z. & Zhou, S. A partial $\mu - \tau$ symmetry and its prediction for leptonic CP violation. *Phys. Lett. B* **737**, 196–200, 2014. [1404.7021](#).
- [122] Luo, S. & Xing, Z.-z. Resolving the octant of θ_{23} via radiative $\mu - \tau$ symmetry breaking. *Phys. Rev. D* **90** (7), 073005, 2014. [1408.5005](#).

- [123] Zhou, Y.-L. μ - τ reflection symmetry and radiative corrections , 2014. [1409.8600](#).
- [124] Aguilar-Arevalo, A. A. *et al.* Event Excess in the MiniBooNE Search for $\bar{\nu}_\mu \rightarrow \bar{\nu}_e$ Oscillations. *Phys. Rev. Lett.* **105**, 181801, 2010. [1007.1150](#).
- [125] Mention, G. *et al.* The Reactor Antineutrino Anomaly. *Phys. Rev. D* **83**, 073006, 2011. [1101.2755](#).
- [126] Gariazzo, S. *et al.* Updated global 3+ 1 analysis of short-baseline neutrino oscillations. *Journal of High Energy Physics* **2017** (6), 1–38, 2017.
- [127] Acero, M. A. *et al.* Limits on ν_e and $\bar{\nu}_e$ disappearance from Gallium and reactor experiments. *Physical Review D* **78** (7), 073009, 2008.
- [128] Giunti, C. & Laveder, M. Statistical Significance of the Gallium Anomaly. *Physical Review C* **83** (6), 065504, 2011.
- [129] Bode, P. *et al.* Halo formation in warm dark matter models. *Astrophys. J.* **556**, 93–107, 2001. [astro-ph/0010389](#).
- [130] Majorana, E. Teoria simmetrica dell’elettrone e del positrone. *Nuovo Cim.* **14**, 171–184, 1937.
- [131] Furry, W. H. On transition probabilities in double beta-disintegration. *Phys. Rev.* **56**, 1184–1193, 1939.
- [132] Aseev, V. N. *et al.* An upper limit on electron antineutrino mass from Troitsk experiment. *Phys. Rev. D* **84**, 112003, 2011. [1108.5034](#).
- [133] Kraus, C. *et al.* Final results from phase II of the Mainz neutrino mass search in tritium β decay. *The European Physical Journal C-Particles and Fields* **40** (4), 447–468, 2005.
- [134] Aker, M. *et al.* Direct neutrino-mass measurement with sub-electronvolt sensitivity. *Nature Phys.* **18** (2), 160–166, 2022. [2105.08533](#).
- [135] Assamagan, K. *et al.* Upper limit of the muon-neutrino mass and charged pion mass from momentum analysis of a surface muon beam. *Phys. Rev. D* **53**, 6065–6077, 1996.

- [136] Barate, R. *et al.* An Upper limit on the tau-neutrino mass from three-prong and five-prong tau decays. *Eur. Phys. J. C* **2**, 395–406, 1998.
- [137] Adams, D. Q. *et al.* Improved Limit on Neutrinoless Double-Beta Decay in ^{130}Te with CUORE. *Phys. Rev. Lett.* **124** (12), 122501, 2020. [1912.10966](#).
- [138] Agostini, M. *et al.* Probing Majorana neutrinos with double- β decay. *Science* **365**, 1445, 2019. [1909.02726](#).
- [139] Gando, A. *et al.* Search for Majorana Neutrinos near the Inverted Mass Hierarchy Region with KamLAND-Zen. *Phys. Rev. Lett.* **117** (8), 082503, 2016. [Addendum: *Phys.Rev.Lett.* 117, 109903 (2016)], [1605.02889](#).
- [140] Vergados, J. D. *et al.* Neutrinoless double beta decay and neutrino mass. *Int. J. Mod. Phys. E* **25** (11), 1630007, 2016. [1612.02924](#).
- [141] Roy Choudhury, S. & Choubey, S. Updated Bounds on Sum of Neutrino Masses in Various Cosmological Scenarios. *JCAP* **09**, 017, 2018. [1806.10832](#).
- [142] Greenberg, O. W. CPT Violation Implies Violation of Lorentz Invariance. *Physical Review Letters* **89** (23), 231602, 2002.
- [143] Ngoc, T. V. *et al.* Stringent constraint on CPT violation with the synergy of T2K-II, NO ν A extension, and JUNO. *Phys. Rev. D* **107** (1), 016013, 2023. [2210.13044](#).

Chapter 2

Neutrino Oscillation

Phenomenology at Terrestrial

Neutrino Experiments

2.1 PMNS matrix parametrization

A general $n \times n$ matrix has $2n^2$ real parameters. However, the unitary condition implies

$$\sum_{i=1}^n U_{\alpha,i} U_{\beta,i}^* = \delta_{\alpha\beta} \quad (2.1)$$

This condition yields n constraints for $\alpha = \beta$, and $n^2 - n$ constraints for $\alpha \neq \beta$. An unitary $n \times n$ matrix therefore has n^2 independent real parameters, with $\frac{1}{2}n(n-1)$ angles (magnitudes) and $\frac{1}{2}n(n+1)$ phases. However, in the case of fermions not all these phases are physical. In fact, in a theory with n generations of leptons, we have $2n$ fields that can be rephased. This means that $2n-1$ of these phases can be reabsorbed in a redefinition of the lepton fields. The actual number of physical phases is $\frac{1}{2}n(n+1) - (2n-1) = \frac{1}{2}(n-1)(n-2)$ in case of Dirac neutrino and $\frac{1}{2}n(n-1)$ in case of Majorana neutrino.

For example, in two-flavor oscillation, if we consider ν_e and ν_μ , there should be $\frac{1}{2}2(2-1) = 1$ angle and $\frac{1}{2}2(2+1) = 3$ phases, in which there is 0 physical phase.

In order to prove above conclusion, let us assume

$$\begin{pmatrix} \nu_e \\ \nu_\mu \end{pmatrix} = \begin{pmatrix} U_{e1} & U_{e2} \\ U_{\mu1} & U_{\mu2} \end{pmatrix} \begin{pmatrix} \nu_1 \\ \nu_2 \end{pmatrix}, \quad (2.2)$$

where in general

$$U = \begin{pmatrix} U_{e1} & U_{e2} \\ U_{\mu1} & U_{\mu2} \end{pmatrix} = \begin{pmatrix} e^{i\delta_1} \cos \theta & e^{i\delta_2} \sin \theta \\ -e^{i\delta_3} \sin \theta & e^{i\delta_4} \cos \theta \end{pmatrix} \quad (2.3)$$

We now can compute

$$\begin{aligned} UU^\dagger &= \begin{pmatrix} ce^{i\delta_1} & se^{i\delta_2} \\ -se^{i\delta_3} & ce^{i\delta_4} \end{pmatrix} \begin{pmatrix} ce^{-i\delta_1} & -se^{-i\delta_3} \\ se^{-i\delta_2} & ce^{-i\delta_4} \end{pmatrix} \\ &= \begin{pmatrix} 1 & cs(e^{i(\delta_2-\delta_4)} - e^{i(\delta_1-\delta_3)}) \\ cs(e^{i(\delta_4-\delta_2)} - e^{i(\delta_3-\delta_1)}) & 1 \end{pmatrix} \end{aligned}$$

In order to satisfy the unitary condition ($UU^\dagger = 1$), we require

$$e^{i(\delta_2-\delta_4)} - e^{i(\delta_1-\delta_3)} = 0$$

and

$$e^{i(\delta_4-\delta_2)} - e^{i(\delta_3-\delta_1)} = 0$$

From these we derive $\delta_4 = \delta_3 + \delta_2 - \delta_1$. It is obviously seen that among 4 imaginary phases, there are only 3 independent phases. We now prove that these 3 phases can be absorbed into the definition of the lepton fields. The general 2×2 unitary matrix can be of the form

$$U = \begin{pmatrix} ce^{i\delta_1} & se^{i\delta_2} \\ -se^{i\delta_3} & ce^{i(\delta_3+\delta_2-\delta_1)} \end{pmatrix} \quad (2.4)$$

Let us now consider the transformation

$$l_\alpha \rightarrow l_\alpha e^{i(\theta_e + \theta'_\alpha)}, \quad \nu_k \rightarrow \nu_k e^{i(\theta_e + \theta'_k)}, \quad U_{\alpha k} = U_{\alpha k} e^{i(\theta'_\alpha - \theta'_k)}$$

2.1. PMNS matrix parametrization

Under this transformation, the matrix U in equation (2.4) is transformed as

$$U \rightarrow \begin{pmatrix} ce^{i(\delta_1 + \theta'_e - \theta'_1)} & se^{i(\delta_2 + \theta'_e - \theta'_2)} \\ -se^{i(\delta_3 + \theta'_\mu - \theta'_1)} & ce^{i(\delta_3 + \delta_2 - \delta_1 + \theta'_\mu - \theta'_2)} \end{pmatrix} \quad (2.5)$$

and the two-flavor weak charged current is invariant

$$-i \frac{g_W}{\sqrt{2}} (\bar{e} \quad \bar{\mu}) \gamma^\mu \frac{1}{2} (1 - \gamma^5) \begin{pmatrix} U_{e1} & U_{e2} \\ U_{\mu 1} & U_{\mu 2} \end{pmatrix} \begin{pmatrix} \nu_1 \\ \nu_2 \end{pmatrix} \quad (2.6)$$

To eliminate all complex phases, we require

$$\theta'_1 - \theta'_e = \delta_1, \quad \theta'_2 - \theta'_e = \delta_2$$

$$\theta'_1 - \theta'_\mu = \delta_3, \quad \theta'_2 - \theta'_\mu = \delta_3 + \delta_2 - \delta_1$$

By writing all the phases relative to the phase of the electron, means setting $\theta'_e = 0$, we have

$$\theta'_1 = \delta_1, \quad \theta'_2 = \delta_2, \quad \theta'_\mu = \delta_1 - \delta_3$$

In general, by redefining the phases of the lepton fields using

$$\begin{aligned} \theta'_e &= \phi \\ \theta'_\mu &= \phi + \delta_1 - \delta_3 \\ \theta'_1 &= \phi + \delta_1 \\ \theta'_2 &= \phi + \delta_2 \end{aligned}$$

all complex phases can be removed from the 2×2 analogue of the PMNS matrix, where the ϕ fixes the overall phase of (for example) the electron field.

In three-flavor neutrino oscillation framework, the flavor definitive eigenstates are related to the mass definitive eigenstates by a 3×3 unitary PMNS matrix, shown in Eq. 2.7,

$$\begin{pmatrix} \nu_e \\ \nu_\mu \\ \nu_\tau \end{pmatrix} = U_{\text{PMNS}} \begin{pmatrix} \nu_1 \\ \nu_2 \\ \nu_3 \end{pmatrix} = \begin{pmatrix} U_{e1} & U_{e2} & U_{e3} \\ U_{\mu1} & U_{\mu2} & U_{\mu3} \\ U_{\tau1} & U_{\tau2} & U_{\tau3} \end{pmatrix} \begin{pmatrix} \nu_1 \\ \nu_2 \\ \nu_3 \end{pmatrix}. \quad (2.7)$$

If the PMNS matrix were real, it could be described by three rotation angles θ_{12} , θ_{13} and θ_{23} via orthogonal rotation matrix R

$$R = \begin{pmatrix} 1 & 0 & 0 \\ 0 & c_{23} & s_{23} \\ 0 & -s_{23} & c_{23} \end{pmatrix} \begin{pmatrix} c_{13} & 0 & s_{13} \\ 0 & 1 & 0 \\ -s_{13} & 0 & c_{13} \end{pmatrix} \begin{pmatrix} c_{12} & s_{12} & 0 \\ -s_{12} & c_{12} & 0 \\ 0 & 0 & 1 \end{pmatrix} \quad (2.8)$$

where $s_{ij} = \sin \theta_{ij}$ and $c_{ij} = \cos \theta_{ij}$. Since PMNS matrix is unitary and not real, it must contain six more additional degrees of freedom in term of complex phase $e^{i\delta}$. Five among these six phases can be absorbed into the definition of the particles and leaves only one single phase δ . This can be seen as follow.

The charged currents for leptonic weak interaction

$$-i \frac{g_W}{\sqrt{2}} (\bar{e}, \bar{\mu}, \bar{\tau}) \gamma^\mu \frac{1}{2} (1 - \gamma^5) \begin{pmatrix} U_{e1} & U_{e2} & U_{e3} \\ U_{\mu1} & U_{\mu2} & U_{\mu3} \\ U_{\tau1} & U_{\tau2} & U_{\tau3} \end{pmatrix} \begin{pmatrix} \nu_1 \\ \nu_2 \\ \nu_3 \end{pmatrix}$$

The four-vector currents are unchanged by transformation

$$l_\alpha \rightarrow l_\alpha e^{i\theta_\alpha}, \quad \nu_k \rightarrow \nu_k e^{i\theta_k} \quad \text{and} \quad U_{\alpha k} \rightarrow U_{\alpha k} e^{i(\theta_\alpha - \theta_k)} \quad (2.9)$$

where l_α is the charged lepton of the type $\alpha = e, \mu, \tau$. Since the phases are arbitrary, all other phases can be defined in term of θ_e :

$$\theta_\alpha = \theta_e + \theta'_\alpha, \quad \theta_k = \theta_e + \theta'_k$$

2.1. PMNS matrix parametrization

The transformation (2.9) therefore becomes

$$l_\alpha \rightarrow l_\alpha e^{i(\theta_e + \theta'_\alpha)}, \quad \nu_k \rightarrow \nu_k e^{i(\theta_e + \theta'_k)} \quad \text{and} \quad U_{\alpha k} \rightarrow U_{\alpha k} e^{i(\theta'_\alpha - \theta'_k)}$$

For electron $\theta_e = \theta_e + \theta'_e \Rightarrow \theta'_e = 0$. It can be seen now that only five phases are independent and can be absorbed into the particle definitions.

2.1.1 Majorana phase in neutrino oscillation

We will start by Majorana mass term as follow

$$\mathcal{L}_M = -\frac{1}{2}M(\bar{\nu}_R^c \nu_R + \bar{\nu}_R \nu_R^c), \quad (2.10)$$

where $\bar{\nu}_R = (\bar{\nu}_{1R}, \bar{\nu}_{2R}, \dots, \bar{\nu}_{nR})$ and $\nu_R^c \equiv C\bar{\nu}_R^T = \nu_L$. The Majorana mass eigenstate is

$$N = N_L + N_R = N_L + N_L^c = N^c \quad (2.11)$$

Then the relations between mass eigenstates and flavor eigenstates are

$$|\nu_i\rangle = \sum_j U_{ij}^* |N_j\rangle \quad (2.12)$$

All phases of U_{ij} are fixed completely by requiring that the mass m_j of N_j is real positive definite.

Since Majorana field must satisfy the condition (2.11) $N = N^c$, there is no freedom to do transformation

$$N_j \rightarrow e^{i\theta_j} N_j$$

Now we can see for the charged lepton current

$$-i\frac{g_W}{\sqrt{2}}(\bar{e}, \bar{\mu}, \bar{\tau})\gamma^\mu \frac{1}{2}(1 - \gamma^5) \begin{pmatrix} U_{e1} & U_{e2} & U_{e3} \\ U_{\mu1} & U_{\mu2} & U_{\mu3} \\ U_{\tau1} & U_{\tau2} & U_{\tau3} \end{pmatrix} \begin{pmatrix} N_1 \\ N_2 \\ N_3 \end{pmatrix}$$

Chapter 2. Neutrino Oscillation Phenomenology at Terrestrial Neutrino Experiments

some phases of mixing matrix U can only be absorbed by the charged leptons l_α , but not Majorana fields N_j . The number of CP violating phases, therefore in n-Majorana generations are

$$n^2 - \frac{1}{2}n(n-1) - n = \frac{1}{2}n(n-1) \quad (2.13)$$

Hence, if the neutrinos are Majorana particles, we should have $\frac{1}{2}3(3-1) = 3$ phases for 3 generations ($n=3$), in which we have 1 Dirac phase and 2 Majorana phases. If $n = 2$, there is one Majorana CPV phase and no Dirac CPV phase in the mixing matrix. Correspondingly, in contrast to the Dirac case, there can exist CP violating effects even in the system of two mixed massive Majorana neutrinos (particles).

The mixing matrix now is rewritten as

$$V = UP \quad (2.14)$$

where $U \equiv U_{PMNS}$ is the PMNS matrix containing 1 Dirac CP violating phase δ and $P = \text{diag}(1, e^{i\delta_1}, e^{i\delta_2})$.

We now show that the Majorana phases do not enter into the expressions of the probabilities of oscillations involving the flavour neutrinos and antineutrinos. The oscillation probabilities of neutrino mode and antineutrino mode are defined as in (2.28)

$$P(\nu_\alpha \rightarrow \nu_\beta) = \left| \sum_{i=1}^3 V_{\beta i} V_{i\alpha}^\dagger e^{-i\phi_i} \right|^2. \quad (2.15)$$

$$P(\bar{\nu}_\alpha \rightarrow \bar{\nu}_\beta) = \left| \sum_{i=1}^3 V_{\alpha i} V_{i\beta}^\dagger e^{-i\phi_i} \right|^2. \quad (2.16)$$

Inserting equation (2.14) into, for example equation (2.15) we have

2.2. Three Neutrino Flavour Oscillation in Vacuum

$$\begin{aligned}
 P(\nu_\alpha \rightarrow \nu_\beta) &= \left| \sum_{i=1}^3 V_{\beta i} V_{i\alpha}^\dagger e^{-i\phi_i} \right|^2 \\
 &= \left| \sum_{i=1}^3 (UP)_{\beta i} (UP)_{i\alpha}^\dagger e^{-i\phi_i} \right|^2 \\
 &= \left| \sum_{i=1}^3 U_{\beta i} (P_{\beta i} P_{i\alpha}^\dagger) U_{i\alpha}^\dagger e^{-i\phi_i} \right|^2 \\
 &= \left| \sum_{i=1}^3 U_{\beta i} U_{i\alpha}^\dagger e^{-i\phi_i} \right|^2
 \end{aligned}$$

We see that oscillation probability does not depend on P or equivalently does not contain Majorana phases. Therefore the neutrino oscillation experiment can not tell us whether the nature of neutrinos are Dirac or Majorana particles.

2.2 Three Neutrino Flavour Oscillation in Vacuum

The flavor eigenstates are related to the mass eigenstates by the 3×3 unitary PMNS matrix.

$$\begin{pmatrix} \nu_e \\ \nu_\mu \\ \nu_\tau \end{pmatrix} = \begin{pmatrix} U_{e1} & U_{e2} & U_{e3} \\ U_{\mu1} & U_{\mu2} & U_{\mu3} \\ U_{\tau1} & U_{\tau2} & U_{\tau3} \end{pmatrix} \begin{pmatrix} \nu_1 \\ \nu_2 \\ \nu_3 \end{pmatrix} \quad (2.17)$$

Chapter 2. Neutrino Oscillation Phenomenology at Terrestrial Neutrino Experiments

The PMNS matrix can be parameterized by three mixing angles ($\theta_{12}, \theta_{13}, \theta_{23}$) and a single Dirac phase δ_{CP} as expressed in equation (2.18).

$$\begin{aligned}
 U_{PMNS} &= \begin{pmatrix} U_{e1} & U_{e2} & U_{e3} \\ U_{\mu1} & U_{\mu2} & U_{\mu3} \\ U_{\tau1} & U_{\tau2} & U_{\tau3} \end{pmatrix} \\
 &= \begin{pmatrix} 1 & 0 & 0 \\ 0 & c_{23} & s_{23} \\ 0 & -s_{23} & c_{23} \end{pmatrix} \begin{pmatrix} c_{13} & 0 & s_{13}e^{-i\delta} \\ 0 & 1 & 0 \\ -s_{13}e^{i\delta} & 0 & c_{13} \end{pmatrix} \begin{pmatrix} c_{12} & s_{12} & 0 \\ -s_{12} & c_{12} & 0 \\ 0 & 0 & 1 \end{pmatrix} \\
 &= \begin{pmatrix} c_{12}c_{13} & s_{12}c_{13} & s_{13}e^{-i\delta} \\ -s_{12}c_{23} - c_{12}s_{23}s_{13}e^{i\delta} & c_{12}c_{23} - s_{12}s_{23}s_{13}e^{i\delta} & s_{23}c_{13} \\ s_{12}s_{23} - c_{12}c_{23}s_{13}e^{i\delta} & -c_{12}s_{23} - s_{12}c_{23}s_{13}e^{i\delta} & c_{23}c_{13} \end{pmatrix} \quad (2.18)
 \end{aligned}$$

where $s_{ij} = \sin \theta_{ij}$, $c_{ij} = \cos \theta_{ij}$ and δ_{CP} Dirac phase represents the CP violation in lepton sector ¹.

The PMNS matrix is unitary so $U^{-1} = U^\dagger \equiv (U^*)^T$. And hence, the mass eigenstates also can be performed via flavor eigenstates as

$$\begin{pmatrix} \nu_1 \\ \nu_2 \\ \nu_3 \end{pmatrix} = \begin{pmatrix} U_{e1}^* & U_{\mu1}^* & U_{\tau1}^* \\ U_{e2}^* & U_{\mu2}^* & U_{\tau2}^* \\ U_{e3}^* & U_{\mu3}^* & U_{\tau3}^* \end{pmatrix} \begin{pmatrix} \nu_e \\ \nu_\mu \\ \nu_\tau \end{pmatrix} \quad (2.19)$$

The unitary condition $UU^\dagger = I$ implies:

$$\begin{pmatrix} U_{e1} & U_{e2} & U_{e3} \\ U_{\mu1} & U_{\mu2} & U_{\mu3} \\ U_{\tau1} & U_{\tau2} & U_{\tau3} \end{pmatrix} \begin{pmatrix} U_{e1}^* & U_{\mu1}^* & U_{\tau1}^* \\ U_{e2}^* & U_{\mu2}^* & U_{\tau2}^* \\ U_{e3}^* & U_{\mu3}^* & U_{\tau3}^* \end{pmatrix} = \begin{pmatrix} 1 & 0 & 0 \\ 0 & 1 & 0 \\ 0 & 0 & 1 \end{pmatrix} \quad (2.20)$$

In compact form

$$\sum_{i=1}^3 U_{\alpha,i} U_{\beta,i}^* = \delta_{\alpha\beta} \quad (2.21)$$

¹If neutrino is Majorana particle, the mixing matrix includes two additional phases which do not appear in the expression of oscillation probabilities.

2.2. Three Neutrino Flavour Oscillation in Vacuum

From (2.17), we derive wave function at time $t = 0$

$$|\nu_\mu\rangle_0 \equiv |\psi(0)\rangle = U_{\mu 1}^* |\nu_1\rangle + U_{\mu 2}^* |\nu_2\rangle + U_{\mu 3}^* |\nu_3\rangle \quad (2.22)$$

Time-dependent wave function

$$|\nu_\mu\rangle \equiv |\psi(\vec{x}, t)\rangle = U_{\mu 1}^* |\nu_1\rangle e^{-i\phi_1} + U_{\mu 2}^* |\nu_2\rangle e^{-i\phi_2} + U_{\mu 3}^* |\nu_3\rangle e^{-i\phi_3} \quad (2.23)$$

In compact form

$$|\nu_\alpha\rangle = \sum_{i=1}^3 U_{\alpha,i}^* |\nu_i\rangle e^{-i\phi_i}, \quad (2.24)$$

where $\phi_i = p_i \cdot x_i = E_i t - \vec{p}_i \cdot \vec{x}_i$. From (2.19) we have

$$|\nu_1\rangle = U_{e1} |\nu_e\rangle + U_{\mu 1} |\nu_\mu\rangle + U_{\tau 1} |\nu_\tau\rangle$$

$$|\nu_2\rangle = U_{e2} |\nu_e\rangle + U_{\mu 2} |\nu_\mu\rangle + U_{\tau 2} |\nu_\tau\rangle$$

$$|\nu_3\rangle = U_{e3} |\nu_e\rangle + U_{\mu 3} |\nu_\mu\rangle + U_{\tau 3} |\nu_\tau\rangle$$

The equation (2.23) can be rewritten as

$$\begin{aligned} |\nu_\mu\rangle &= U_{\mu 1}^* (U_{e1} |\nu_e\rangle + U_{\mu 1} |\nu_\mu\rangle + U_{\tau 1} |\nu_\tau\rangle) e^{-i\phi_1} \\ &+ U_{\mu 2}^* (U_{e2} |\nu_e\rangle + U_{\mu 2} |\nu_\mu\rangle + U_{\tau 2} |\nu_\tau\rangle) e^{-i\phi_2} \\ &+ U_{\mu 3}^* (U_{e3} |\nu_e\rangle + U_{\mu 3} |\nu_\mu\rangle + U_{\tau 3} |\nu_\tau\rangle) e^{-i\phi_3} \\ &= (U_{\mu 1}^* U_{e1} e^{-i\phi_1} + U_{\mu 2}^* U_{e2} e^{-i\phi_2} + U_{\mu 3}^* U_{e3} e^{-i\phi_3}) |\nu_e\rangle \\ &+ (U_{\mu 1}^* U_{\mu 1} e^{-i\phi_1} + U_{\mu 2}^* U_{\mu 2} e^{-i\phi_2} + U_{\mu 3}^* U_{\mu 3} e^{-i\phi_3}) |\nu_\mu\rangle \\ &+ (U_{\mu 1}^* U_{\tau 1} e^{-i\phi_1} + U_{\mu 2}^* U_{\tau 2} e^{-i\phi_2} + U_{\mu 3}^* U_{\tau 3} e^{-i\phi_3}) |\nu_\tau\rangle \\ &= c_e |\nu_e\rangle + c_\mu |\nu_\mu\rangle + c_\tau |\nu_\tau\rangle. \end{aligned} \quad (2.25)$$

In compact form

$$|\nu_\mu\rangle = \sum_{\beta} \sum_{i=1}^3 U_{\mu i}^* U_{\beta i} e^{-i\phi_i} |\nu_\beta\rangle. \quad (2.26)$$

The oscillation probability from muon neutrino to electron neutrino is

defined as

$$\begin{aligned}
 P(\nu_\mu \rightarrow \nu_e) &= |\langle \nu_e | \nu_\mu \rangle|^2 = c_e c_e^* \\
 &= |U_{\mu 1}^* U_{e 1} e^{-i\phi_1} + U_{\mu 2}^* U_{e 2} e^{-i\phi_2} + U_{\mu 3}^* U_{e 3} e^{-i\phi_3}|^2. \quad (2.27)
 \end{aligned}$$

In compact form

$$P(\nu_\alpha \rightarrow \nu_\beta) = \left| \sum_{i=1}^3 U_{\alpha i}^* U_{\beta i} e^{-i\phi_i} \right|^2. \quad (2.28)$$

Since $v_\nu = c$ and in natural unit $c = 1$, we have $t = L$. Also from relativity relation $E^2 = p^2 + m^2 \Rightarrow E - P = \frac{m^2}{E+p} \approx \frac{m^2}{2E}$. Therefore at distance $x = L$ from the neutrino source, we have

$$\phi_i = p_i \cdot x_i = E_i t - \vec{p}_i \cdot \vec{x}_i = (E_i - p_i)L \approx \frac{m_i^2 L}{2E}$$

If $\phi_1 = \phi_2 = \phi_3 (\approx \frac{m^2 L}{2E})$, from unitary condition (2.21) we have

$$P(\nu_\alpha \rightarrow \nu_\beta) = \left| \sum_{i=1}^3 U_{\alpha i}^* U_{\beta i} \right|^2 e^{i\frac{m^2 L}{2E}} e^{-i\frac{m^2 L}{2E}} = \delta_{\alpha\beta}$$

This means that the oscillations occur if the neutrinos have mass ($m_i \neq 0$) and the masses are not the same ($m_1 \neq m_2 \neq m_3$).

Using the identity properties of complex number:

$$|z_1 + z_2 + z_3|^2 = |z_1|^2 + |z_2|^2 + |z_3|^2 + 2\text{Re}[z_1 z_2^* + z_1 z_3^* + z_2 z_3^*] \quad (2.29)$$

Then equation (2.27) becomes

$$\begin{aligned}
 P(\nu_\mu \rightarrow \nu_e) &= |U_{\mu 1}^* U_{e 1} e^{-i\phi_1} + U_{\mu 2}^* U_{e 2} e^{-i\phi_2} + U_{\mu 3}^* U_{e 3} e^{-i\phi_3}|^2 \\
 &= |U_{\mu 1}^* U_{e 1}|^2 + |U_{\mu 2}^* U_{e 2}|^2 + |U_{\mu 3}^* U_{e 3}|^2 \\
 &\quad + 2\text{Re}[U_{\mu 1}^* U_{e 1} U_{\mu 2} U_{e 2}^* e^{i(\phi_2 - \phi_1)}] \\
 &\quad + 2\text{Re}[U_{\mu 1}^* U_{e 1} U_{\mu 3} U_{e 3}^* e^{i(\phi_3 - \phi_1)}] \\
 &\quad + 2\text{Re}[U_{\mu 2}^* U_{e 2} U_{\mu 3} U_{e 3}^* e^{i(\phi_3 - \phi_2)}] \quad (2.30)
 \end{aligned}$$

2.2. Three Neutrino Flavour Oscillation in Vacuum

In compact form

$$P(\nu_\alpha \rightarrow \nu_\beta) = \sum_{i=1}^3 |U_{\alpha i}^* U_{\beta i}|^2 + 2 \sum_{j>i} \text{Re}[U_{\alpha i}^* U_{\beta i} U_{\alpha j} U_{\beta j}^* e^{i(\phi_j - \phi_i)}] \quad (2.31)$$

From the unitary condition we derive

$$\begin{aligned} & |U_{\mu 1}^* U_{e 1} + U_{\mu 2}^* U_{e 2} + U_{\mu 3}^* U_{e 3}|^2 = 0 \\ \Rightarrow & |U_{\mu 1}^* U_{e 1}|^2 + |U_{\mu 2}^* U_{e 2}|^2 + |U_{\mu 3}^* U_{e 3}|^2 \\ & + 2\text{Re}[U_{\mu 1}^* U_{e 1} U_{\mu 2} U_{e 2}^* + U_{\mu 1}^* U_{e 1} U_{\mu 3} U_{e 3}^* + U_{\mu 2}^* U_{e 2} U_{\mu 3} U_{e 3}^*] \\ = & 0 \end{aligned} \quad (2.32)$$

In compact form

$$\sum_i |U_{\alpha i}^* U_{\beta i}|^2 + 2 \sum_{j>i} \text{Re}[U_{\alpha i}^* U_{\beta i} U_{\alpha j} U_{\beta j}^*] = \delta_{\alpha\beta} \quad (2.33)$$

It is followed from (2.30) and (2.32):

$$\begin{aligned} P(\nu_\mu \rightarrow \nu_e) &= 2\text{Re}[U_{\mu 1}^* U_{e 1} U_{\mu 2} U_{e 2}^* (e^{i(\phi_2 - \phi_1)} - 1)] \\ &+ 2\text{Re}[U_{\mu 1}^* U_{e 1} U_{\mu 3} U_{e 3}^* (e^{i(\phi_3 - \phi_1)} - 1)] \\ &+ 2\text{Re}[U_{\mu 2}^* U_{e 2} U_{\mu 3} U_{e 3}^* (e^{i(\phi_3 - \phi_2)} - 1)] \end{aligned} \quad (2.34)$$

In compact form

$$P(\nu_\alpha \rightarrow \nu_\beta) = \delta_{\alpha\beta} + 2 \sum_{j>i} \text{Re}[U_{\alpha i}^* U_{\beta i} U_{\alpha j} U_{\beta j}^* (e^{i(\phi_j - \phi_i)} - 1)] \quad (2.35)$$

We have

$$\begin{aligned} & \text{Re}[U_{\alpha i}^* U_{\beta i} U_{\alpha j} U_{\beta j}^* (e^{i(\phi_j - \phi_i)} - 1)] \\ = & \text{Re}[U_{\alpha i}^* U_{\beta i} U_{\alpha j} U_{\beta j}^* (\cos(\phi_j - \phi_i) - 1 + i \sin(\phi_j - \phi_i))] \\ = & \text{Re} \left\{ (\text{Re}[U_{\alpha i}^* U_{\beta i} U_{\alpha j} U_{\beta j}^*] + i \text{Im}[U_{\alpha i}^* U_{\beta i} U_{\alpha j} U_{\beta j}^*]) \left(-2 \sin^2 \left(\frac{\phi_j - \phi_i}{2} \right) + i \sin(\phi_j - \phi_i) \right) \right\} \\ = & -2\text{Re}[U_{\alpha i}^* U_{\beta i} U_{\alpha j} U_{\beta j}^*] \sin^2 \left(\frac{\phi_j - \phi_i}{2} \right) - \text{Im}[U_{\alpha i}^* U_{\beta i} U_{\alpha j} U_{\beta j}^*] \sin(\phi_j - \phi_i) \end{aligned} \quad (2.36)$$

From (2.36), we can write the oscillation probability in a normal form

$$\begin{aligned}
 P(\nu_\mu \rightarrow \nu_e) = & \\
 & - 4\text{Re} [U_{\mu 1}^* U_{e 1} U_{\mu 2} U_{e 2}^*] \sin^2\left(\frac{\phi_2 - \phi_1}{2}\right) - 2\text{Im} [U_{\mu 1}^* U_{e 1} U_{\mu 2} U_{e 2}^*] \sin(\phi_2 - \phi_1) \\
 & - 4\text{Re} [U_{\mu 1}^* U_{e 1} U_{\mu 3} U_{e 3}^*] \sin^2\left(\frac{\phi_3 - \phi_1}{2}\right) - 2\text{Im} [U_{\mu 1}^* U_{e 1} U_{\mu 3} U_{e 3}^*] \sin(\phi_3 - \phi_1) \\
 & - 4\text{Re} [U_{\mu 2}^* U_{e 2} U_{\mu 3} U_{e 3}^*] \sin^2\left(\frac{\phi_3 - \phi_2}{2}\right) - 2\text{Im} [U_{\mu 2}^* U_{e 2} U_{\mu 3} U_{e 3}^*] \sin(\phi_3 - \phi_2). \quad (2.37)
 \end{aligned}$$

In compact form

$$\begin{aligned}
 P(\nu_\alpha \rightarrow \nu_\beta) = \delta_{\alpha\beta} & - 4 \sum_{j>i} \text{Re} [U_{\alpha i}^* U_{\beta i} U_{\alpha j} U_{\beta j}^*] \sin^2\left(\frac{\phi_j - \phi_i}{2}\right) \\
 & - 2 \sum_{j>i} \text{Im} [U_{\alpha i}^* U_{\beta i} U_{\alpha j} U_{\beta j}^*] \sin(\phi_j - \phi_i) \quad (2.38)
 \end{aligned}$$

If the neutrinos interact at a time T and at a distance L along its direction of flight, the difference in phase of the three mass eigenstates are written as

$$\phi_j - \phi_i = p_j \cdot x_j - p_i \cdot x_i = (E_j - E_i)T - (p_j - p_i)L$$

With assuming that $p_j = p_i = p$ for neutrinos of the same source, then

$$\begin{aligned}
 \phi_j - \phi_i & = (E_j - E_i)T \approx \left[p_j \left(1 + \frac{m_j^2}{2p_j^2} \right) - p_i \left(1 + \frac{m_i^2}{2p_i^2} \right) \right] T \\
 & = \frac{m_j^2 - m_i^2}{2p} T = \frac{\Delta m_{ji}^2 L}{2E} \quad (2.39)
 \end{aligned}$$

In the above calculation, we used the approximation $T \approx L$ and $p \approx E$ for $v_\nu \approx c = 1$ and $m_\nu \ll E_\nu$. We finally get the most common form of the oscillation probability:

$$\begin{aligned}
 P(\nu_\alpha \rightarrow \nu_\beta) = \delta_{\alpha\beta} & - 4 \sum_{j>i} \text{Re} [U_{\alpha i}^* U_{\beta i} U_{\alpha j} U_{\beta j}^*] \sin^2 \left(\frac{\Delta m_{ji}^2 L}{4E} \right) \\
 & - 2 \sum_{j>i} \text{Im} [U_{\alpha i}^* U_{\beta i} U_{\alpha j} U_{\beta j}^*] \sin \left(\frac{\Delta m_{ji}^2 L}{2E} \right). \quad (2.40)
 \end{aligned}$$

For antineutrinos, we just take the complex conjugate of the product

2.2. Three Neutrino Flavour Oscillation in Vacuum

matrix and get

$$\begin{aligned}
P(\bar{\nu}_\alpha \rightarrow \bar{\nu}_\beta) = \delta_{\alpha\beta} & - 4 \sum_{j>i} \text{Re} [U_{\alpha i}^* U_{\beta i} U_{\alpha j} U_{\beta j}^*] \sin^2 \left(\frac{\Delta m_{ji}^2}{4E} L \right) \\
& + 2 \sum_{j>i} \text{Im} [U_{\alpha i}^* U_{\beta i} U_{\alpha j} U_{\beta j}^*] \sin \left(\frac{\Delta m_{ji}^2}{2E} L \right). \quad (2.41)
\end{aligned}$$

The probabilities (2.40) and (2.41) are called *transition probabilities*, and the *survival probability* for a flavor is

$$P(\nu_\alpha \rightarrow \nu_\alpha) = P(\bar{\nu}_\alpha \rightarrow \bar{\nu}_\alpha) = 1 - 4 \sum_{j>i} |U_{\alpha i}|^2 |U_{\alpha j}|^2 \sin^2 \left(\frac{\Delta m_{ji}^2}{4E} L \right). \quad (2.42)$$

From (2.40) and (2.41), the difference between the neutrino and antineutrino oscillation probability indicates CP violation in neutrino sector

$$\begin{aligned}
\mathcal{A}_{\text{CP}} & = P(\nu_\alpha \rightarrow \nu_\beta) - P(\bar{\nu}_\alpha \rightarrow \bar{\nu}_\beta) \\
& = 4 \sum_{j>i} \text{Im} [U_{\alpha i}^* U_{\beta i} U_{\alpha j} U_{\beta j}^*] \sin \left(\frac{\Delta m_{ji}^2}{2E} L \right). \quad (2.43)
\end{aligned}$$

If CP is violated, $U_{\alpha i}^* U_{\beta i} U_{\alpha j} U_{\beta j}^*$ has to contain an imaginary component. For $\alpha = \mu$ and $\beta = e$, then

$$\begin{aligned}
\mathcal{A}_{\text{CP}} & = P(\nu_\mu \rightarrow \nu_e) - P(\bar{\nu}_\mu \rightarrow \bar{\nu}_e) \\
& = 4 \sum_{j>i} \text{Im} [U_{\mu i}^* U_{e i} U_{\mu j} U_{e j}^*] \sin \left(\frac{\Delta m_{ji}^2}{2E} L \right) \\
& = 4 \text{Im} [U_{\mu 1}^* U_{e 1} U_{\mu 2} U_{e 2}^*] \sin \left(\frac{\Delta m_{21}^2}{2E} L \right) \\
& + 4 \text{Im} [U_{\mu 1}^* U_{e 1} U_{\mu 3} U_{e 3}^*] \sin \left(\frac{\Delta m_{31}^2}{2E} L \right) \\
& + 4 \text{Im} [U_{\mu 2}^* U_{e 2} U_{\mu 3} U_{e 3}^*] \sin \left(\frac{\Delta m_{32}^2}{2E} L \right). \quad (2.44)
\end{aligned}$$

From the unitary condition we have

$$U_{\mu 1} U_{e 1}^* + U_{\mu 2} U_{e 2}^* + U_{\mu 3} U_{e 3}^* = 0. \quad (2.45)$$

Multiply two sides of the equation (2.45) with $U_{\mu 1}^* U_{e 1}$ and $U_{\mu 2}^* U_{e 2}$ respectively and

then add them up, we have

$$\begin{aligned}
& U_{\mu 1}^* U_{e 1} U_{\mu 1} U_{e 1}^* + U_{\mu 1}^* U_{e 1} U_{\mu 2} U_{e 2}^* + U_{\mu 1}^* U_{e 1} U_{\mu 3} U_{e 3}^* \\
& + U_{\mu 2}^* U_{e 2} U_{\mu 1} U_{e 1}^* + U_{\mu 2}^* U_{e 2} U_{\mu 2} U_{e 2}^* + U_{\mu 2}^* U_{e 2} U_{\mu 3} U_{e 3}^* = 0 \\
\Leftrightarrow & 0 = |U_{\mu 1}|^2 |U_{e 1}|^2 + |U_{\mu 2}|^2 |U_{e 2}|^2 \\
& + \operatorname{Re}[U_{\mu 1}^* U_{e 1} U_{\mu 2} U_{e 2}^*] + \operatorname{Re}[U_{\mu 2}^* U_{e 2} U_{\mu 1} U_{e 1}^*] + \operatorname{Re}[U_{\mu 1}^* U_{e 1} U_{\mu 3} U_{e 3}^*] + \operatorname{Re}[U_{\mu 2}^* U_{e 2} U_{\mu 3} U_{e 3}^*] \\
& + i \{ \operatorname{Im}[U_{\mu 1}^* U_{e 1} U_{\mu 2} U_{e 2}^*] + \operatorname{Im}[U_{\mu 2}^* U_{e 2} U_{\mu 1} U_{e 1}^*] + \operatorname{Im}[U_{\mu 1}^* U_{e 1} U_{\mu 3} U_{e 3}^*] + \operatorname{Im}[U_{\mu 2}^* U_{e 2} U_{\mu 3} U_{e 3}^*] \} \\
\Rightarrow & \operatorname{Im}[U_{\mu 1}^* U_{e 1} U_{\mu 2} U_{e 2}^*] + \operatorname{Im}[U_{\mu 2}^* U_{e 2} U_{\mu 1} U_{e 1}^*] + \operatorname{Im}[U_{\mu 1}^* U_{e 1} U_{\mu 3} U_{e 3}^*] + \operatorname{Im}[U_{\mu 2}^* U_{e 2} U_{\mu 3} U_{e 3}^*] = 0.
\end{aligned} \tag{2.46}$$

Note that

$$[U_{\mu 1}^* U_{e 1} U_{\mu 2} U_{e 2}^*]^* = U_{\mu 2}^* U_{e 2} U_{\mu 1} U_{e 1}^* \Rightarrow \operatorname{Im}[U_{\mu 1}^* U_{e 1} U_{\mu 2} U_{e 2}^*] = -\operatorname{Im}[U_{\mu 2}^* U_{e 2} U_{\mu 1} U_{e 1}^*]$$

Therefore, from (2.46) we get

$$\operatorname{Im}[U_{\mu 1}^* U_{e 1} U_{\mu 3} U_{e 3}^*] = -\operatorname{Im}[U_{\mu 2}^* U_{e 2} U_{\mu 3} U_{e 3}^*]. \tag{2.47}$$

Multiply two sides of the equation (2.45) with $U_{\mu 1}^* U_{e 1}$ and $U_{\mu 3}^* U_{e 3}$ respectively and then add them up, we have

$$\begin{aligned}
& U_{\mu 1}^* U_{e 1} U_{\mu 1} U_{e 1}^* + U_{\mu 1}^* U_{e 1} U_{\mu 2} U_{e 2}^* + U_{\mu 1}^* U_{e 1} U_{\mu 3} U_{e 3}^* \\
& + U_{\mu 3}^* U_{e 3} U_{\mu 1} U_{e 1}^* + U_{\mu 3}^* U_{e 3} U_{\mu 2} U_{e 2}^* + U_{\mu 3}^* U_{e 3} U_{\mu 3} U_{e 3}^* = 0 \\
\Leftrightarrow & 0 = |U_{\mu 1}|^2 |U_{e 1}|^2 + |U_{\mu 3}|^2 |U_{e 3}|^2 \\
& + \operatorname{Re}[U_{\mu 1}^* U_{e 1} U_{\mu 3} U_{e 3}^*] + \operatorname{Re}[U_{\mu 3}^* U_{e 3} U_{\mu 1} U_{e 1}^*] + \operatorname{Re}[U_{\mu 1}^* U_{e 1} U_{\mu 2} U_{e 2}^*] + \operatorname{Re}[U_{\mu 3}^* U_{e 3} U_{\mu 2} U_{e 2}^*] \\
& + i \{ \operatorname{Im}[U_{\mu 1}^* U_{e 1} U_{\mu 3} U_{e 3}^*] + \operatorname{Im}[U_{\mu 3}^* U_{e 3} U_{\mu 1} U_{e 1}^*] + \operatorname{Im}[U_{\mu 1}^* U_{e 1} U_{\mu 2} U_{e 2}^*] + \operatorname{Im}[U_{\mu 3}^* U_{e 3} U_{\mu 2} U_{e 2}^*] \} \\
\Rightarrow & \operatorname{Im}[U_{\mu 1}^* U_{e 1} U_{\mu 3} U_{e 3}^*] + \operatorname{Im}[U_{\mu 3}^* U_{e 3} U_{\mu 1} U_{e 1}^*] + \operatorname{Im}[U_{\mu 1}^* U_{e 1} U_{\mu 2} U_{e 2}^*] + \operatorname{Im}[U_{\mu 3}^* U_{e 3} U_{\mu 2} U_{e 2}^*] = 0.
\end{aligned} \tag{2.48}$$

Note that

$$[U_{\mu 1}^* U_{e 1} U_{\mu 3} U_{e 3}^*]^* = U_{\mu 3}^* U_{e 3} U_{\mu 1} U_{e 1}^* \Rightarrow \operatorname{Im}[U_{\mu 1}^* U_{e 1} U_{\mu 3} U_{e 3}^*] = -\operatorname{Im}[U_{\mu 3}^* U_{e 3} U_{\mu 1} U_{e 1}^*]$$

2.2. Three Neutrino Flavour Oscillation in Vacuum

and

$$[U_{\mu 3}^* U_{e 3} U_{\mu 2} U_{e 2}^*]^* = U_{\mu 2}^* U_{e 2} U_{\mu 3} U_{e 3}^* \Rightarrow \text{Im}[U_{\mu 3}^* U_{e 3} U_{\mu 2} U_{e 2}^*] = -[U_{\mu 2}^* U_{e 2} U_{\mu 3} U_{e 3}^*]$$

Therefore, from (2.48) we get

$$\text{Im}[U_{\mu 1}^* U_{e 1} U_{\mu 2} U_{e 2}^*] = \text{Im}[U_{\mu 2}^* U_{e 2} U_{\mu 3} U_{e 3}^*]. \quad (2.49)$$

By using (2.47) and (2.49), we can rewrite (2.44) as

$$\begin{aligned} \mathcal{A}_{\text{CP}} &= P(\nu_{\mu} \rightarrow \nu_e) - P(\bar{\nu}_{\mu} \rightarrow \bar{\nu}_e) \\ &= 4\text{Im}[U_{\mu 1}^* U_{e 1} U_{\mu 2} U_{e 2}^*] (\sin \Delta_{21} - \sin \Delta_{31} + \sin \Delta_{32}), \end{aligned} \quad (2.50)$$

where $\Delta_{31} = \frac{\Delta m_{31}^2}{2E} L$, $\Delta_{21} = \frac{\Delta m_{21}^2}{2E} L$ and $\Delta_{32} = \frac{\Delta m_{32}^2}{2E} L = \Delta_{31} - \Delta_{21}$. By a simple trigonometry calculation, we have

$$\begin{aligned} &\sin \Delta_{21} - \sin \Delta_{31} + \sin(\Delta_{31} - \Delta_{21}) \\ &= \sin \Delta_{21} - \sin \Delta_{31} + (\sin \Delta_{31} \cos \Delta_{21} - \cos \Delta_{31} \sin \Delta_{21}) \\ &= \sin \Delta_{21} (1 - \cos \Delta_{31}) - \sin \Delta_{31} (1 - \cos \Delta_{21}) \\ &= 2 \frac{\sin \Delta_{21}}{2} \frac{\cos \Delta_{21}}{2} \frac{2(1 - \cos 2\frac{\Delta_{31}}{2})}{2} - 2 \sin \frac{\Delta_{31}}{2} \cos \frac{\Delta_{31}}{2} \frac{2(1 - \cos 2\frac{\Delta_{21}}{2})}{2} \\ &= 4 \frac{\sin \Delta_{21}}{2} \frac{\cos \Delta_{21}}{2} \sin^2 \frac{\Delta_{31}}{2} - 4 \sin \frac{\Delta_{31}}{2} \cos \frac{\Delta_{31}}{2} \sin^2 \frac{\Delta_{21}}{2} \\ &= 4 \sin \frac{\Delta_{21}}{2} \sin \frac{\Delta_{31}}{2} \left(\cos \frac{\Delta_{21}}{2} \sin \frac{\Delta_{31}}{2} - \sin \frac{\Delta_{21}}{2} \cos \frac{\Delta_{31}}{2} \right) \\ &= 4 \sin \frac{\Delta_{21}}{2} \sin \frac{\Delta_{31}}{2} \sin \frac{\Delta_{32}}{2} \end{aligned}$$

Then we can rewrite (2.50) as

$$\begin{aligned} \mathcal{A}_{\text{CP}} &= P(\nu_{\mu} \rightarrow \nu_e) - P(\bar{\nu}_{\mu} \rightarrow \bar{\nu}_e) \\ &= 16\text{Im}[U_{\mu 1}^* U_{e 1} U_{\mu 2} U_{e 2}^*] \left(\sin \frac{\Delta_{21}}{2} \sin \frac{\Delta_{31}}{2} \sin \frac{\Delta_{32}}{2} \right) \\ &= 16\text{Im}[U_{\mu 1}^* U_{e 1} U_{\mu 2} U_{e 2}^*] \sin \frac{\Delta m_{21}^2 L}{4E} \sin \frac{\Delta m_{31}^2 L}{4E} \sin \frac{\Delta m_{32}^2 L}{4E} \quad (2.51) \\ &= 2 \cos \theta_{13} \sin 2\theta_{12} \sin 2\theta_{13} \sin 2\theta_{23} \sin \delta_{\text{CP}} \sin \frac{\Delta m_{21}^2 L}{4E} \sin \frac{\Delta m_{31}^2 L}{4E} \sin \frac{\Delta m_{32}^2 L}{4E}. \end{aligned}$$

In the last line, we already used

$$U_{e1} = c_{12}c_{13}, \quad U_{e2}^* = s_{12}c_{13}$$

$$U_{\mu 1}^* = -s_{12}c_{23} - c_{12}s_{23}s_{13}e^{-i\delta}, \quad U_{\mu 2} = c_{12}c_{23} - s_{12}s_{23}s_{13}e^{i\delta}$$

In practical, CP violation can be measured by comparing the rate of electron neutrinos appearance from muon neutrinos, $P(\nu_\mu \rightarrow \nu_e)$, with its of electron antineutrinos appearance from muon anti-neutrinos, $P(\bar{\nu}_\mu \rightarrow \bar{\nu}_e)$ in accelerator-based experiments or comparing the first with electron antineutrino disappearance in the reactor-based experiments.²

2.3 Three Neutrino Flavour Oscillation in Matter

In matter, unlike oscillation probabilities in vacuum, oscillation patterns are altered due to the MSW effect [1–3]. This occurs as a result of neutrinos experiencing potentials due to charged current(CC) and neutral current (NC) scattering on electrons, neutrons, and protons as they propagate through matter on Earth. The explicit expressions for these matter potentials can be found in much literature, and a brief sketch for how these quantities are derived is given in [4–6]. Neglecting Majorana phases that are irrelevant for oscillation experiments, the evolution of the mass eigenstates in vacuum is described by

$$i \frac{d}{dt} \Psi(x) = H_0^M \Psi(x) \tag{2.52}$$

where $H_0^M = \text{diag}(E_1, E_2, E_3)$ with $E_k = \sqrt{\vec{p}_k^2 + m_k^2} \simeq p_k + \frac{m_k^2}{2p_k}$, $k = 1, 2, 3$ being the energy eigenvalues of the mass eigen states. The Hamiltonian in the flavour space is obtained as $H_0 = UH_M^0U^\dagger$, where U is the lepton mixing matrix from Equation 2.18.

²Accelerator-based measurements lead to an intrinsic $\delta_{CP} - \theta_{13}$ degeneracy while reactor-based measurement can precisely measure θ_{13} . Their combined information thus can provide constraint on δ_{CP} .

2.3. Three Neutrino Flavour Oscillation in Matter

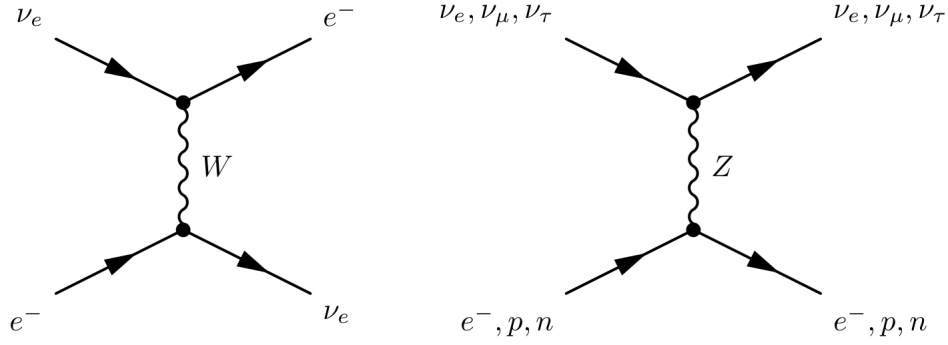


Figure 2-1: Feynman diagrams of the coherent forward elastic scattering processes experienced by neutrinos on the particles in matter.

When the neutrinos propagate through matter, the hamiltonian is modified as

$$H = H_0 + H_1 \quad (2.53)$$

where, in the interaction Hamiltonian H_1 , we add up the interaction terms from scattering on the particles present. Thus, we can write

$$H_1 = H_Z^n + H_Z^p + H_Z^e + H_W^e \quad (2.54)$$

In Equation 2.54, $H_Z^i = \text{diag}(V_Z^i, V_Z^i, V_Z^i)$, $i = n, p, e$ and $H_W^i = \text{diag}(V_W^i, 0, 0)$ such that V_W^e represents the effective matter potential due to CC scattering on electrons, V_Z^e represents the effective matter potential due to NC scattering on electrons, and so on. The reason we consider matter potentials from scattering with electrons, protons and neutrons, is because the compositions of μ and τ leptons is zero on Earth. The Feynman diagrams for coherent forward scattering process that the CC potential via W -boson exchange (*left*) and the NC potential through the Z -boson exchange (*right*) is given in Figure 2-1. The effective weak CC and NC interaction Hamiltonians are:

$$\mathcal{H}_W^{eff} = \frac{G_F}{\sqrt{2}} J_{W\mu} J_W^{\mu\dagger}, \quad (2.55)$$

$$\mathcal{H}_Z^{eff} = \frac{4G_F}{\sqrt{2}} J_Z^\mu J_{Z\mu}. \quad (2.56)$$

G_F is the weak Fermi constant and the currents are:

$$J_W^\mu = \sum_l \left[\bar{l} \gamma^\mu (1 - \gamma_5) \nu_l + \bar{d} \gamma^\mu (1 - \gamma_5) u \right], \quad (2.57)$$

$$J_Z^\mu = \frac{1}{2} \sum_i \bar{\psi}_i \gamma^\mu \left[I_i^3 (1 - \gamma_5) - 2Q_i \sin^2 \theta_W \right] \psi_i, \quad (2.58)$$

where $i = (l, \nu_l, u, d)$, I_i^3 is the associated particle isospin, and Q_i is the particle charge. The derivation of neutrino matter potentials has been studied also in Refs. [7, 8].

Now, the effective CC potential due to scattering on electrons is given by

$$V_W^e = \langle \nu_e(p_1, s_1) e(p_2, s_2) | H_W | \nu_e(p_1, s_1) e(p_2, s_2) \rangle, \quad (2.59)$$

The electron states correspond to the electrons in the left diagram in Figure 2-1. For the interaction to leave the medium unchanged in order to contribute coherently to the neutrino potential, it is fair to assume that the neutrinos and electrons conserve their momentum. The low-energy effective Hamiltonian density relevant for CC $\nu_e e$ scattering from Equation 2.55 is,

$$\mathcal{H}_W(x) = \frac{G_F}{\sqrt{2}} \left[\bar{e}(x) \gamma^\beta (1 - \gamma_5) \nu_e(x) \right] \left[\bar{\nu}_e(x) \gamma_\beta (1 - \gamma_5) e(x) \right] \quad (2.60)$$

The presence of electrons in a medium results in two observations. One is the statistical energy distribution of the electrons in the medium is accounted for by integration over the Fermi function $f(E_e, T)$ which is normalized to $\int f(E_e, T) dp_e = 1$, T being the temperature T of the electron background. The other is an averaging over spins $\frac{1}{2} \sum_s$, since we do not know the polarization of the electrons. Thus, Equation 2.60 is transformed as,

$$\mathcal{H}_W(x) = \int f(E_e, T) \frac{G_F}{2\sqrt{2}} \sum_s \left[\bar{e}(x) \gamma^\beta (1 - \gamma_5) \nu_e(x) \right] \left[\bar{\nu}_e(x) \gamma_\beta (1 - \gamma_5) e(x) \right] dp_2 \quad (2.61)$$

2.3. Three Neutrino Flavour Oscillation in Matter

Since, only electrons contribute to CC potential in Equation 2.59, we can write

$$\begin{aligned} & \left[\bar{e}(x)\gamma^\beta(1-\gamma_5)\nu_e(x) \right] \left[\bar{\nu}_e(x)\gamma_\beta(1-\gamma_5)e(x) \right] |\nu_e(p_1, s_1)e(p_2, s_2) \rangle \\ &= \frac{1}{2VE_2(p_2)} \left[a_{s_2}^\dagger(p_2)a_{s_2}(p_2)\bar{u}_{s_2}(p_2)\gamma^\beta(1-\gamma_5)\nu_e(x) \right] \left[\bar{\nu}_e(x)\gamma_\beta(1-\gamma_5)u_{s_2}(p_2) \right] |\nu_e e \rangle \end{aligned} \quad (2.62)$$

Now, considering $H_W = \int_V \mathcal{H}_W(x)dx$, substituting Equations 2.62 and 2.61 in 2.59, we have

$$\begin{aligned} V_W^e &= \langle \nu_e(p_1, s_1)e(p_2, s_2) | \frac{G_F}{4\sqrt{2}V} \int \int f(E_e, T) \sum_{s_2} \frac{a_{s_2}^\dagger(p_2)a_{s_2}(p_2)}{E_e(p_2)} \\ & \left[\bar{u}_{s_2}(p_2)\gamma^\beta(1-\gamma_5)\nu_e(x) \right] \left[\bar{\nu}_e(x)\gamma_\beta(1-\gamma_5)u_{s_2}(p_2) \right] dx dp_2 | \nu_e(p_1, s_1)e(p_2, s_2) \rangle \end{aligned} \quad (2.63)$$

We assume the medium to be isotropic and non-magnetic and, then, apply the Fierz transformation (page 64, [4]) to re-arrange the ν_e and e spinors. Using $\int p_2 f(E_e, T) dp_2 = 0$ for isotropy, and the total electron number density of the medium $\int f(E_e, T) N_e(p_2) dp_2 = N_e$, only integration over x remains. Hence, we have,

$$V_W^e = \langle \nu_e(p_1, s_1)e(p_2, s_2) | \frac{G_F N_e}{\sqrt{2}} \times \frac{1}{2VE_{\nu_e}} \int 4E_{\nu_e} dx | \nu_e(p_1, s_1)e(p_2, s_2) \rangle . \quad (2.64)$$

Assuming normalized state vectors, $|\nu_e(p_1, s_1)e(p_2, s_2) \rangle$, Equation 2.64 reduces to

$$\begin{aligned} V_W^e &= \frac{G_F N_e}{\sqrt{2}} \times \frac{2}{V} \int dx \langle \nu_e(p_1, s_1)e(p_2, s_2) | \nu_e(p_1, s_1)e(p_2, s_2) \rangle \\ V_W^e &= V_{CC} = \sqrt{2}G_F N_e \end{aligned} \quad (2.65)$$

For anti-neutrinos, $V_{CC} \rightarrow -V_{CC}$, because of the anti-commutation relation between the creation and annihilation operators.

The NC scattering is mediated by Z^0 boson and we use the NC hamiltonian from Equation 2.56 to obtain V_Z^n due to ν_α , $\alpha = e, \mu, \tau$ scattering. The effective

hamiltonian is given by,

$$\mathcal{H}_Z(x) = -\frac{G_F}{4\sqrt{2}} \int f(E_n, T) \sum_s \left[\bar{\psi}_n(x) \gamma^\mu (1 - \gamma_5) \psi_n(x) \right] \left[\bar{\nu}_\alpha(x) \gamma_\mu (1 - \gamma_5) \nu_\alpha(x) \right] dp_n \quad (2.66)$$

Here, we have introduced the statistical Fermi distribution for neutrons $f(E_n, T)$ and summation over the neutron spins due to the assumption of unpolarized medium, just as for the electrons. Equation 2.66 is of the form as in Equation 2.61. Applying the Fierz transformation and performing similar derivation of V_W^e , we find

$$V_Z^n = -\frac{G_F N_n}{\sqrt{2}} \quad (2.67)$$

The potentials V_Z^e and V_Z^p are equal in magnitude and opposite in sign, and therefore cancels out each other. Thus, the potential induced by NC scattering is,

$$V_{NC} = V_Z^n = -\frac{G_F N_n}{\sqrt{2}} \quad (2.68)$$

where, N_n is the neutron no. density of the medium.

2.3.1 Neutrino Oscillation Probability in Matter

The relation between mass eigenstates and flavor eigenstates

$$|\nu_\alpha\rangle = \sum_k U_{\alpha k}^* |\nu_k\rangle$$

The total Hamiltonian in matter is

$$H = H_0 + H_1,$$

where H_0 is the hamiltonian in vaccum and H_1 is the perturbed hamiltonian.

$$\begin{aligned} H_0 |\nu_k\rangle &= E_k |\nu_k\rangle; \quad \text{with} \quad E_k = \sqrt{\vec{p}_k^2 + m_k^2} \approx p_k + \frac{m_k^2}{2p_k} \\ H_1 |\nu_\alpha\rangle &= V_\alpha |\nu_\alpha\rangle = (V_{CC} + V_{NC}) |\nu_\alpha\rangle. \end{aligned}$$

2.3. Three Neutrino Flavour Oscillation in Matter

In the literature, many authors have considered perturbation/expansion H_1 around naturally appearing small parameters such as the matter potential $\frac{a}{\Delta m_{31}^2}$ [9], $\sin \theta_{13}$, $\sin^2 \theta_{13}$ [10, 11], the ratio of mass of mass-squared differences $\frac{\Delta m_{21}^2}{\Delta m_{31}^2}$ and $\frac{\Delta m_{21}^2}{\Delta m_{ee}^2}$ [9, 12–17], where $\Delta m_{ee}^2 \equiv \cos^2 \theta_{12} \Delta m_{31}^2 + \sin^2 \theta_{12} \Delta m_{32}^2$. In context of ongoing accelerator-based long baseline and reactor-based neutrino based medium baseline experiments, the oscillation channels $P_{\nu_\mu \rightarrow \nu_e}$ ($P_{\bar{\nu}_\mu \rightarrow \bar{\nu}_e}$), $P_{\nu_\mu \rightarrow \nu_\mu}$ ($P_{\bar{\nu}_\mu \rightarrow \bar{\nu}_\mu}$) and $P_{\bar{\nu}_e \rightarrow \bar{\nu}_e}$ are of great interest. We will use the S-matrix method to show a derivation, presented as in Ref.[9] for propagation of neutrinos in matter of constant density. The Schrodinger equation for neutrino in matter is

$$\begin{aligned} i \frac{d}{dt} |\nu_\alpha(t)\rangle &= H |\nu_\alpha(t)\rangle \\ &= (H_0 + H_1) |\nu_\alpha(t)\rangle \\ &= (E_k + V_\alpha) |\nu_\alpha(t)\rangle \\ &= \left[\left(p_k + \frac{m_k^2}{2p_k} \right) + V_\alpha \right] |\nu_\alpha(t)\rangle \end{aligned}$$

For $v \approx c = 1$ (means $t \approx x$) we have $p_k \approx E$. We can see that $E + V_{NC}$ is the same for all neutrinos. They generate a phase common to all flavors and will cancel out in transition. Hence we can ignore them here for simplicity. So we rewrite the above equation as

$$\begin{aligned} i \frac{d}{dt} |\nu_\alpha(t)\rangle &= \left[\left(p_k + \frac{m_k^2}{2p_k} \right) + V_\alpha \right] |\nu_\alpha(t)\rangle \\ &= \left[\left(\frac{m_k^2}{2E} + V_{CC} \delta_{\alpha e} \right) + (E + V_{NC}) \right] |\nu_\alpha(t)\rangle \\ &\implies \left(\frac{m_k^2}{2E} + V_{CC} \delta_{\alpha e} \right) |\nu_\alpha(t)\rangle \end{aligned}$$

Or in explicit form

$$i \frac{d}{dt} \begin{pmatrix} \nu_e \\ \nu_\mu \\ \nu_\tau \end{pmatrix} = \left[\frac{1}{2E} U \begin{pmatrix} m_1^2 & 0 & 0 \\ 0 & m_2^2 & 0 \\ 0 & 0 & m_3^2 \end{pmatrix} U^\dagger + \begin{pmatrix} V_{CC} & 0 & 0 \\ 0 & 0 & 0 \\ 0 & 0 & 0 \end{pmatrix} \right] \begin{pmatrix} \nu_e \\ \nu_\mu \\ \nu_\tau \end{pmatrix} \quad (2.69)$$

Chapter 2. Neutrino Oscillation Phenomenology at Terrestrial Neutrino Experiments

where U is an unitary matrix. We can rewrite the Schrodinger equation in matter as

$$i\frac{d\nu}{dx} = H\nu,$$

where

$$\begin{aligned} H &= H_0 + H_1 \\ &= \frac{1}{2E}U \begin{pmatrix} 0 & 0 & 0 \\ 0 & 0 & 0 \\ 0 & 0 & \Delta m_{31}^2 \end{pmatrix} U^\dagger + \frac{1}{2E} \left[U \begin{pmatrix} 0 & 0 & 0 \\ 0 & \Delta m_{21}^2 & 0 \\ 0 & 0 & 0 \end{pmatrix} U^\dagger + \begin{pmatrix} a & 0 & 0 \\ 0 & 0 & 0 \\ 0 & 0 & 0 \end{pmatrix} \right] \end{aligned}$$

and $a = 2EV_{CC} = 2\sqrt{2}G_F E N_e$. Since Δm_{21}^2 and $a \ll \Delta m_{31}^2$, we can treat H_1 as a perturbation. The Schrodinger equation has a solution of Dyson series form

$$\nu(x) = S(x)\nu(0), \quad (2.70)$$

with

$$S(x) \equiv T e^{\int_0^x H(s) ds},$$

T is the symbol of time ordering. The oscillation probability at distance L then can be calculate through $S(x)$

$$P(\nu_\alpha \rightarrow \nu_\beta) = |S_{\beta\alpha}(L)|^2. \quad (2.71)$$

We can calculate the perturbation to the first order in a and Δm_{21}^2 . We have

$$S_0(x) = e^{-iH_0 x} \quad (2.72)$$

and

$$S_1(x) = e^{-iH_0 x} (-i) \int_0^x ds H_1(s) = e^{-iH_0 x} (-i) \int_0^x ds e^{iH_0 s} H_1 e^{-iH_0 s} \quad (2.73)$$

2.3. Three Neutrino Flavour Oscillation in Matter

Substituting H_o and H_1 and calculating $(S(x))_{\beta\alpha} = (S_0(x))_{\beta\alpha} + (S_1(x))_{\beta\alpha}$, the general form of oscillation probability is given by,

$$\begin{aligned}
P(\nu_\alpha \rightarrow \nu_\beta) &= |(S(x))_{\beta\alpha}|^2 = \delta_{\alpha\beta} \left[1 - 4|U_{\alpha 3}|^2 \sin^2 \Delta_{31} \left(1 - \frac{2a}{\Delta m_{31}^2} (|U_{13}|^2 - \delta_{\alpha 1}) \right) \right] \\
&\quad - \delta_{\alpha\beta} \left[\frac{ax}{E} |U_{\alpha 3}|^2 |U_{13}|^2 \sin 2\Delta_{31} \right] \\
&\quad + 4 \sin^2 \Delta_{31} |U_{\beta 3}|^2 |U_{\alpha 3}|^2 \left[1 - 2 \frac{a}{\Delta m_{31}^2} (2|U_{13}|^2 - \delta_{\alpha 1} - \delta_{\beta 1}) \right] \\
&\quad - 8 \Delta_{21} \sin^2 \Delta_{31} \text{Im}(U_{\beta 3}^* U_{\alpha 3} U_{\beta 2} U_{\alpha 2}^*) \\
&\quad + 4 \sin 2\Delta_{31} \left[\Delta_{21} \text{Re}(U_{\beta 3}^* U_{\alpha 3} U_{\beta 2} U_{\alpha 2}^*) \right. \\
&\quad \left. + \frac{ax}{4E} (|U_{13}|^2 \delta_{\alpha 1} \delta_{\beta 1} + |U_{\beta 3}|^2 |U_{\alpha 3}|^2 (2|U_{13}|^2 - \delta_{\alpha 1} - \delta_{\beta 1})) \right] \\
&\quad + 4 \Delta_{21}^2 |U_{\beta 2}|^2 |U_{\alpha 2}|^2 \tag{2.74}
\end{aligned}$$

For $\alpha = \mu$ and $\beta = e$ we get the electron neutrino appearance probability from muon neutrino, given by

$$\begin{aligned}
P(\nu_\mu \rightarrow \nu_e) &= 4 \sin^2 \Delta_{31} |U_{e3}|^2 |U_{\mu 3}|^2 \\
&\quad - 8 \sin^2 \Delta_{31} |U_{e3}|^2 |U_{\mu 3}|^2 \frac{a}{\Delta m_{31}^2} (2|U_{e3}|^2 - 1) \\
&\quad + 4 \sin 2\Delta_{31} \frac{ax}{4E} |U_{e3}|^2 |U_{\mu 3}|^2 (2|U_{e3}|^2 - 1) \\
&\quad - 8 \Delta_{21} \sin^2 \Delta_{31} \text{Im}(U_{e3}^* U_{\mu 3} U_{e2} U_{\mu 2}^*) \\
&\quad + 4 \Delta_{21} \sin 2\Delta_{31} \text{Re}(U_{e3}^* U_{\mu 3} U_{e2} U_{\mu 2}^*) \\
&\quad + 4 \Delta_{21}^2 |U_{e2}|^2 |U_{\mu 2}|^2 \tag{2.75}
\end{aligned}$$

Substituting the elements from the PMNS matrix, we find

$$\begin{aligned}
P(\nu_\mu \rightarrow \nu_e) &= 4s_{13}^2 s_{23}^2 c_{13}^2 \sin^2 \Delta_{31} \\
&\quad - 8s_{13}^2 s_{23}^2 c_{13}^2 \frac{a}{\Delta m_{31}^2} (2s_{13}^2 - 1) \sin^2 \Delta_{31} \\
&\quad + 4s_{13}^2 s_{23}^2 c_{13}^2 \frac{ax}{4E} (2s_{13}^2 - 1) \sin 2\Delta_{31} \\
&\quad - 8s_{12} s_{13} s_{23} c_{12} c_{13}^2 c_{23} \sin \delta \Delta_{21} \sin^2 \Delta_{31} \\
&\quad + 4s_{12} s_{13} s_{23} c_{13}^2 (c_{12} c_{23} \cos \delta - s_{12} s_{13} s_{23}) \Delta_{21} \sin 2\Delta_{31} \\
&\quad + 4s_{12}^2 c_{13}^2 (c_{12}^2 c_{23}^2 + s_{12}^2 s_{13}^2 s_{23}^2 - 2s_{12} s_{13} s_{23} c_{12} c_{23} \cos \delta) \Delta_{21}^2 \tag{2.76}
\end{aligned}$$

Chapter 2. Neutrino Oscillation Phenomenology at Terrestrial Neutrino Experiments

For $\frac{\Delta m_{21}^2 x}{4E} \ll 1$ and $\Delta m_{31}^2 \approx \Delta m_{32}^2$, we can make a replacement with: $\Delta_{21} = \sin \Delta_{21}$; $\cos \Delta_{31} = \cos \Delta_{32}$; $\sin \Delta_{31} = \sin \Delta_{32}$ and the probability of $\nu_\mu \rightarrow \nu_e$ oscillation can be written as follows

$$\begin{aligned}
P(\nu_\mu \rightarrow \nu_e) \approx & 4s_{13}^2 s_{23}^2 c_{13}^2 \sin^2 \Delta_{31} \\
& - 8s_{13}^2 s_{23}^2 c_{13}^2 \frac{a}{\Delta m_{31}^2} (2s_{13}^2 - 1) \sin^2 \Delta_{31} \\
& + 8s_{13}^2 s_{23}^2 c_{13}^2 \frac{aL}{4E} (2s_{13}^2 - 1) \sin \Delta_{31} \cos \Delta_{32} \\
& - 8s_{12}s_{13}s_{23}c_{12}c_{13}^2 c_{23} \sin \delta_{CP} \sin \Delta_{21} \sin \Delta_{31} \sin \Delta_{32} \\
& + 8s_{12}s_{13}s_{23}c_{13}^2 (c_{12}c_{23} \cos \delta_{CP} - s_{12}s_{13}s_{23}) \sin \Delta_{21} \sin \Delta_{31} \cos \Delta_{32} \\
& + 4s_{12}^2 c_{13}^2 (c_{12}^2 c_{23}^2 + s_{12}^2 s_{13}^2 s_{23}^2 - 2s_{12}s_{13}s_{23}c_{12}c_{23} \cos \delta_{CP}) \sin^2 \Delta_{21},
\end{aligned} \tag{2.77}$$

where $\Delta_{ji} = \frac{\Delta m_{ji}^2}{4E} L$, and $a = 2\sqrt{2}G_F n_e E = 7.56 \times 10^{-5} [eV^2] (\frac{\rho}{g/cm^3}) (\frac{E}{GeV})$, n_e is the electron density of the matter and ρ is the density of the Earth.

- The appearances of a in the equation (2.77) is due to the matter effect which is rooted from the fact that electron neutrino when passing through ordinary matter will interact weakly with electrons.
- For anti-neutrino counterpart, $P(\bar{\nu}_\mu \rightarrow \bar{\nu}_e)$ can be obtained from Eq.(2.77) by replacing $\delta \rightarrow -\delta$ and $a \rightarrow -a$.
- The matter effect, represented by a constant, involves to the second and third terms.
- While the term proportional to $\sin \delta_{CP}$ is called *CP-violating* since their contribution for total probability are opposite for neutrino and antineutrino, the fifth, which contains $\cos \delta_{CP}$, is called *CP-conserving term* since their contributions are the same for neutrino and antineutrino.
- The last one depends on Δm_{21}^2 and can be ignored in the case of long baseline experiments. At present landscape of neutrino oscillations, this channels is the only hope to provide information about δ_{CP} .

Fig. 2-2 and Fig. 2-3 show the oscillation probabilities of $\nu_\mu \rightarrow \nu_e$ and $\bar{\nu}_\mu \rightarrow \bar{\nu}_e$ as a function of neutrino energy at different true value of δ_{CP} for T2K baseline

2.3. Three Neutrino Flavour Oscillation in Matter

Table 2.1: Global constraint of oscillation parameters with *normal* mass hierarchy assumed [18].

Parameter	Best fit $\pm 1\sigma$
$\sin^2 \theta_{12}$	$0.310^{+0.013}_{-0.012}$
$\sin^2 \theta_{13} (\times 10^{-2})$	$2.241^{+0.067}_{-0.066}$
$\sin^2 \theta_{23}$	$0.558^{+0.020}_{-0.033}$
$\delta_{CP} (^\circ)$	222^{+38}_{-28}
$\Delta m_{21}^2 (10^{-5} \text{eV}^2/c^4)$	$7.39^{+0.21}_{-0.20}$
$\Delta m_{31}^2 (10^{-3} \text{eV}^2/c^4)$	$2.523^{+0.032}_{-0.030}$

$L = 295$ km (with peak of neutrino flux at 0.6 GeV) and NO ν A baseline $L = 810$ km (with peak of neutrino flux at 2 GeV), respectively. In the figure 2-4, the difference between solid and dashed blue lines indicates the matter effect, and the difference between solid and dashed red lines shows the combined effect of both matter and CP-violation. In the case of T2K experiment, the matter effect is much smaller than the CP-violation effect. For NO ν A, due to its longer baseline the matter effect is larger. The plots are made with assumed values of oscillation parameters as listed Table 2.1.

However, challenges for this channel measurement are the smallness of oscillation amplitude and its degeneracy with other oscillation parameters. Along with the appearance channels, the accelerator-based long-baseline neutrino experiments typically can measure precisely the probability of $\nu_\mu \rightarrow \nu_\mu$ and $\bar{\nu}_\mu \rightarrow \bar{\nu}_\mu$.

Substituting $\alpha = \beta = \mu$ in Equation 2.74, we obtain the survival/disappearance probability for muon-neutrinos, given by

$$\begin{aligned}
 P(\nu_\mu \rightarrow \nu_\mu) = & 1 + 4 \sin^2 \Delta_{31} |U_{\mu 3}|^2 \left[(|U_{\mu 3}|^2 - 1) - \frac{2a}{\Delta m_{31}^2} |U_{e 3}|^2 (2|U_{\mu 3}|^2 - 1) \right] \\
 & + 4 \Delta_{31} \sin 2\Delta_{31} |U_{\mu 3}|^2 \left[\frac{\Delta m_{21}^2}{\Delta m_{31}^2} |U_{\mu 2}|^2 + \frac{a}{\Delta m_{31}^2} |U_{e 3}|^2 (2|U_{\mu 3}|^2 - 1) \right] \\
 & + 4 \Delta_{21}^2 |U_{\mu 2}|^4 \tag{2.78}
 \end{aligned}$$

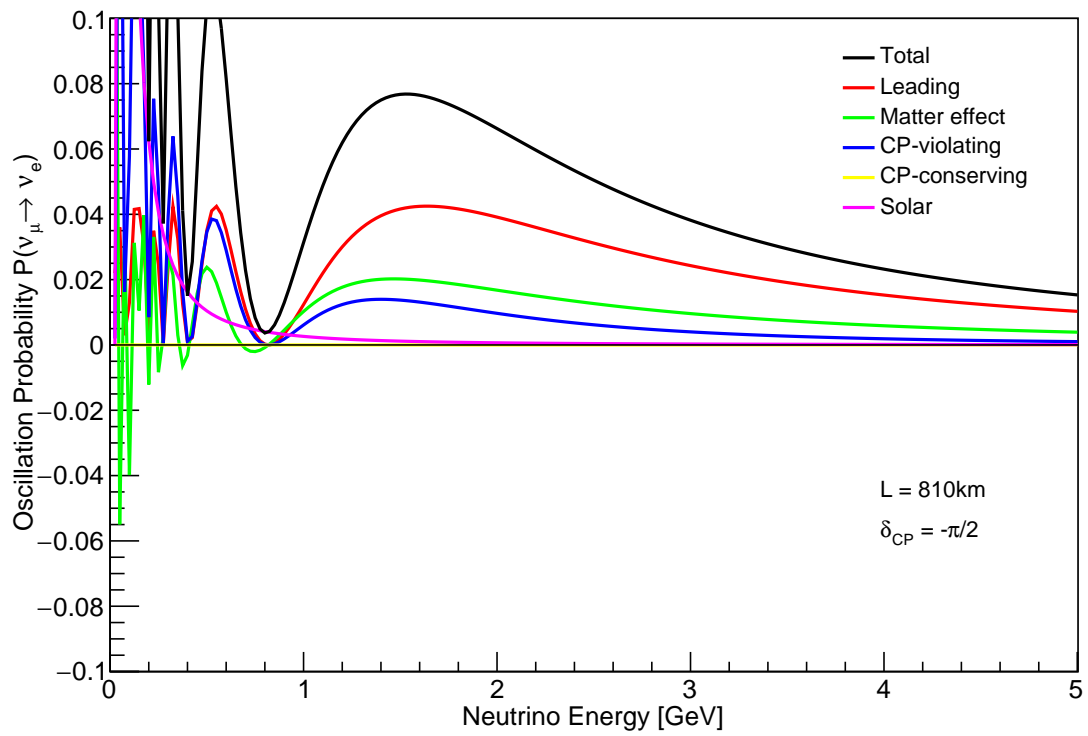
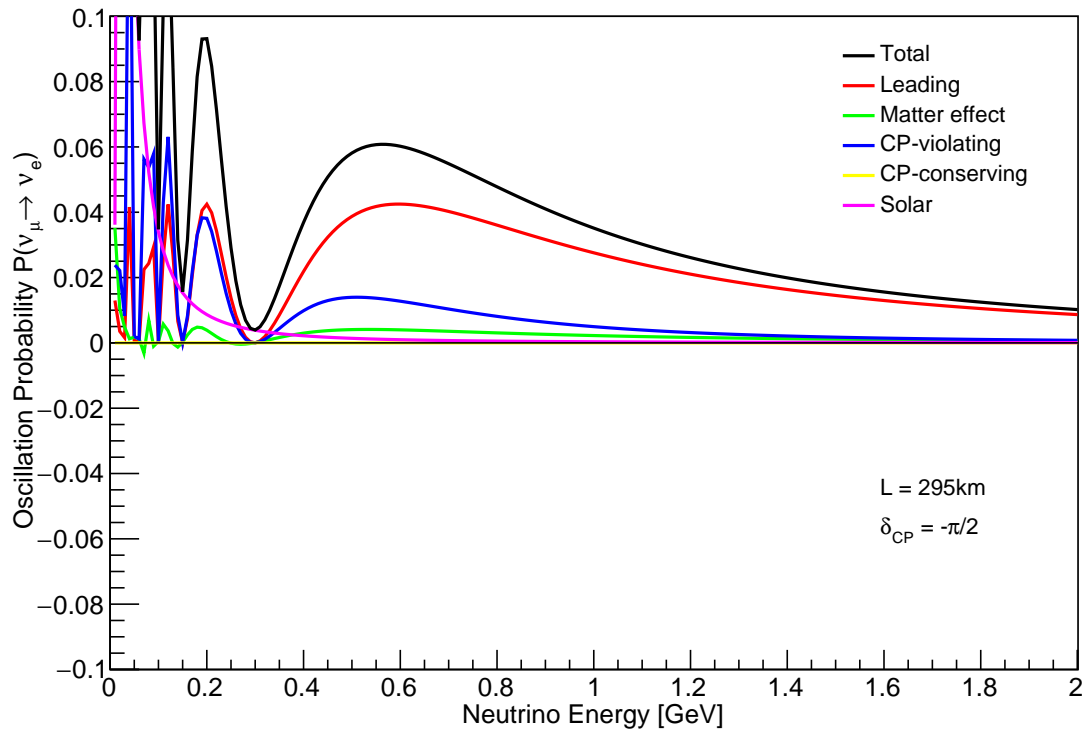


Figure 2-2: $P(\nu_\mu \rightarrow \nu_e)$ for $L = 295$ (top) and $L = 810$ km (bottom) for $\delta_{CP} = -\pi/2$.

2.3. Three Neutrino Flavour Oscillation in Matter

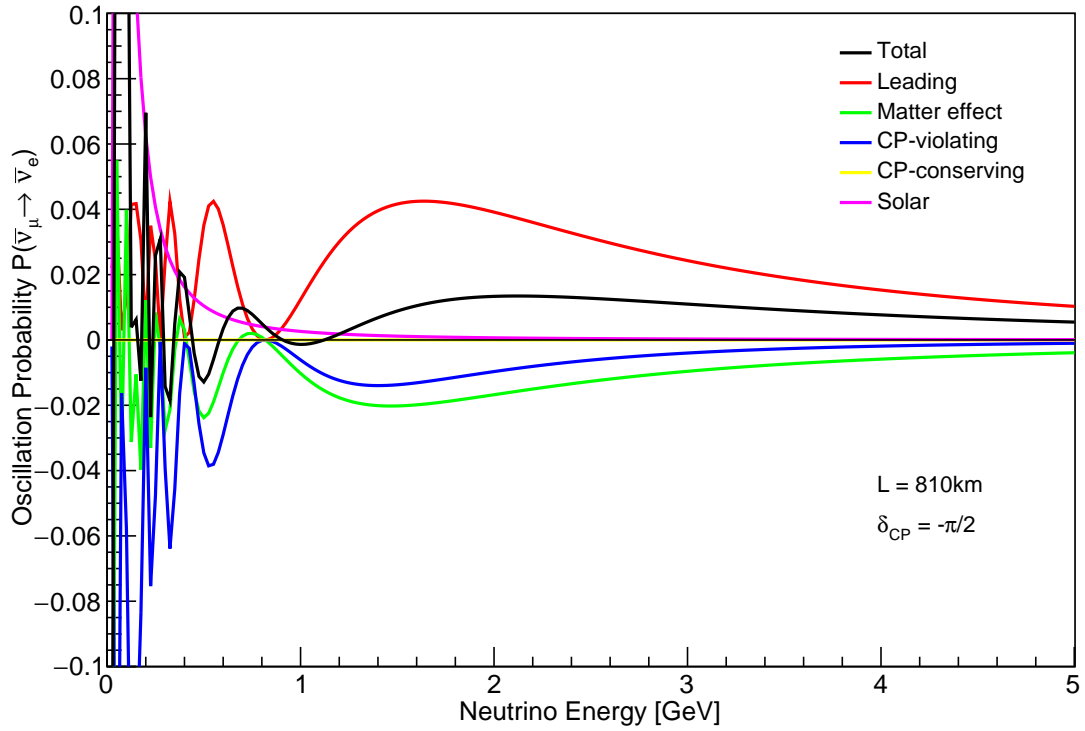
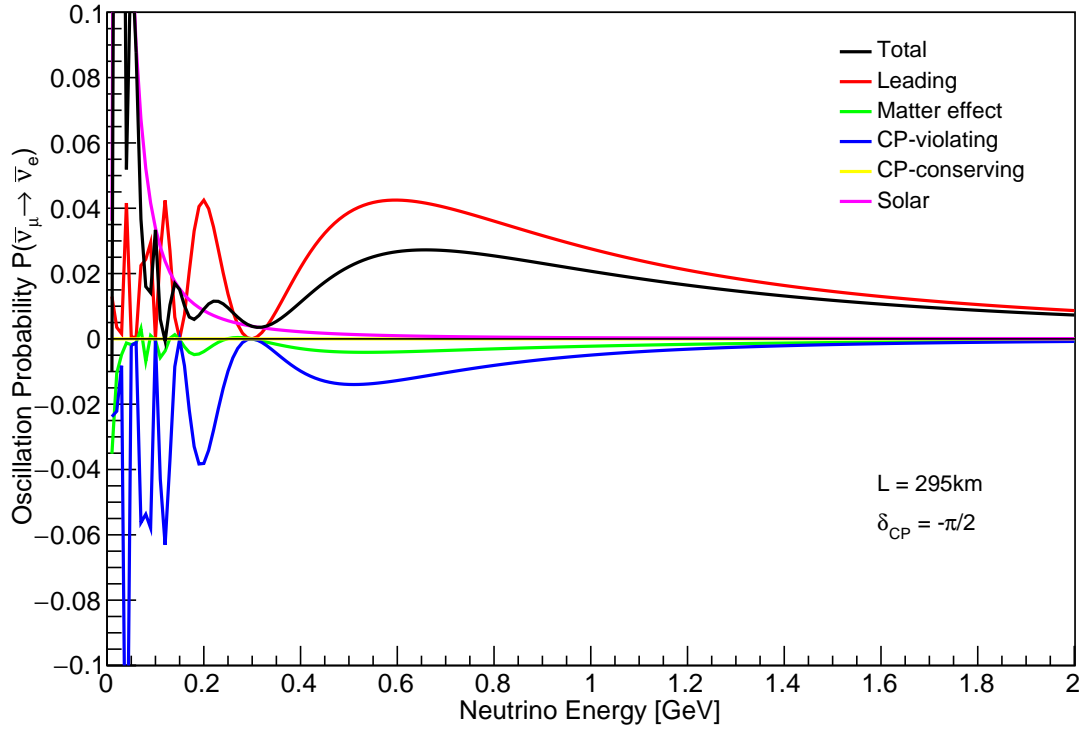
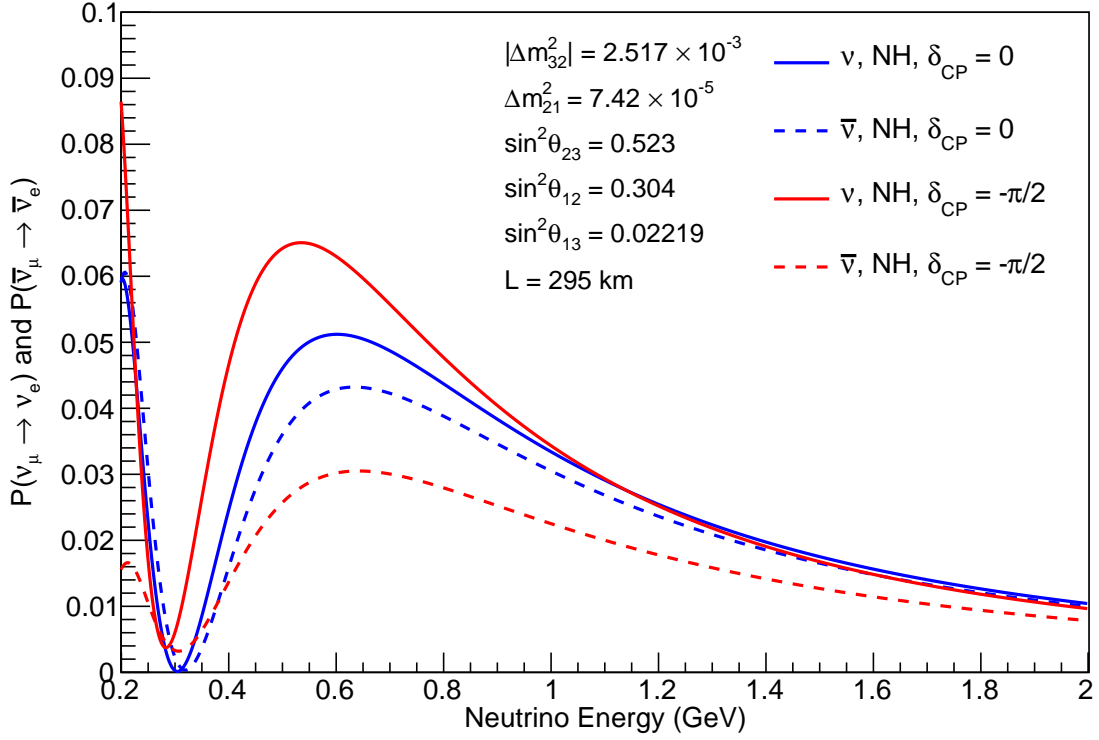


Figure 2-3: $P(\bar{\nu}_\mu \rightarrow \bar{\nu}_e)$ for $L = 295$ (top) and $L = 810$ km (bottom) for $\delta_{CP} = -\pi/2$.

Neutrino Oscillation in T2K



Neutrino Oscillation in NOvA

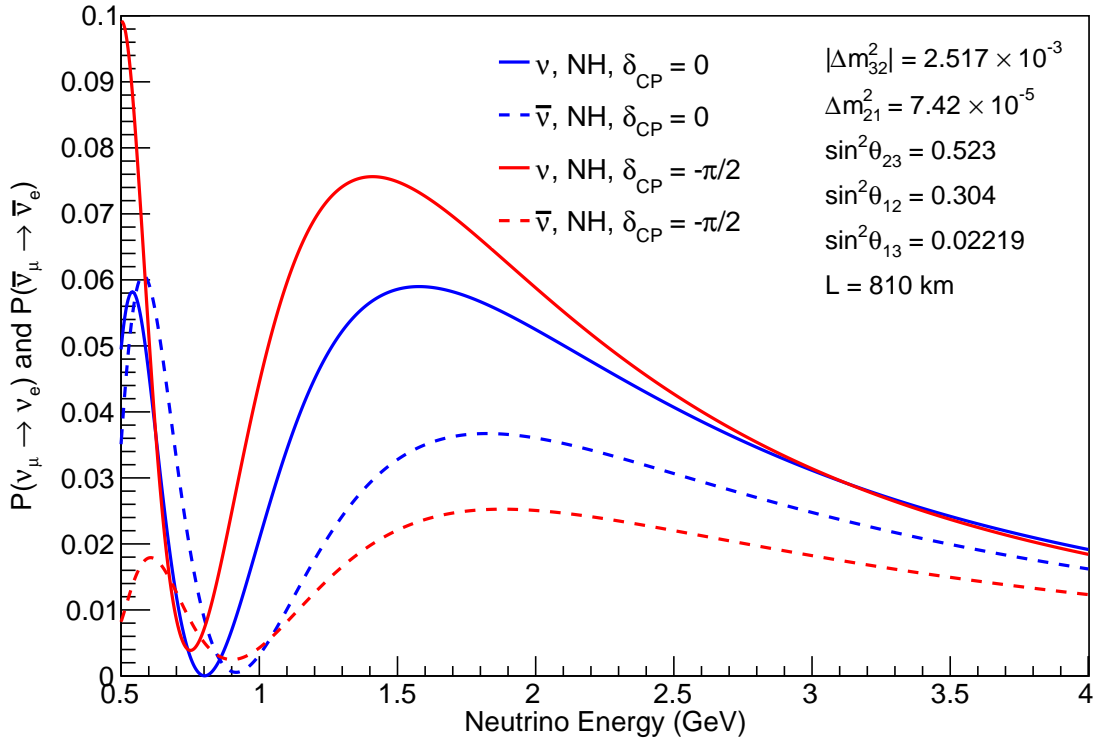


Figure 2-4: $P(\nu_\mu \rightarrow \nu_e)$ and $P(\bar{\nu}_\mu \rightarrow \bar{\nu}_e)$ for $L = 295$ (top) and $L = 810$ km (bottom) for $\delta_{CP} = 0, -\pi/2$.

2.4. Oscillation Parameter Degeneracy

Using the elements from the PMNS matrix, we obtain

$$\begin{aligned}
P(\nu_\mu \rightarrow \nu_\mu) = & 1 + 4s_{23}^2 c_{13}^2 (s_{23}^2 c_{13}^2 - 1) \sin^2 \Delta_{31} \\
& \pm 4s_{23}^2 c_{13}^2 s_{13}^2 (2s_{23}^2 c_{13}^2 - 1) \frac{2a}{\Delta m_{31}^2} \sin^2 \Delta_{31} \\
& \pm 4s_{23}^2 c_{13}^2 s_{13}^2 (2s_{23}^2 c_{13}^2 - 1) \frac{a}{\Delta m_{31}^2} \Delta_{31} \sin 2\Delta_{31} \\
& + 4s_{23}^2 c_{13}^2 (c_{12}^2 c_{23}^2 + s_{12}^2 s_{13}^2 s_{23}^2 - 2s_{12} s_{13} s_{23} c_{12} c_{23} \cos \delta) \Delta_{21} \sin 2\Delta_{31} \\
& + 4(c_{12}^2 c_{23}^2 + s_{12}^2 s_{13}^2 s_{23}^2 - 2s_{12} s_{13} s_{23} c_{12} c_{23} \cos \delta)^2 \Delta_{21}^2 \quad (2.79)
\end{aligned}$$

where positive (negative) signs are taken for neutrino (antineutrino) oscillations respectively.

- As can be seen in the equation (2.79), the second term dominates.
- The third and the fourth are related to matter effect.
- Due to relative smallness of θ_{13} the first term is dominated in the accelerator-based long-baseline neutrino experiment and measurement with this channel is essentially sensitive to mixing angle θ_{23} and Δm_{31}^2 .

In practice, neutrino oscillation analyses take advantage of combining both appearance channel and disappearance channel in order to provide the most precise measurements of oscillation parameters and explore CP violation from constraints on δ_{CP} .

2.4 Oscillation Parameter Degeneracy

We revisit on the degeneracies between the various oscillation parameters in this section. In the context of neutrino oscillations, parameter degeneracy refers to the probability of obtaining the same value for various sets of oscillation parameters. The number of neutrino and antineutrino events that are functions of neutrino oscillation probabilities determines how sensitive an experiment is. This suggests that different sets of parameters can provide an equally good fit to the data in the

presence of degeneracies, making it challenging to determine the precise values of the parameters. Determining the unknown parameters, therefore, requires a thorough understanding of various degeneracies, their dependence on various oscillation parameters, and their resolution. When θ_{13} was unknown, three types of degeneracies have been discussed widely in the literature [19–21].

1. The intrinsic degeneracy of the $P_{\mu e}$ channel refers to the same value of probability coming from a different θ_{13} and δ_{CP} value and can be expressed as

$$P_{\mu e(\bar{\mu}\bar{e})}(\theta_{13}, \delta_{CP}) = P_{\mu e(\bar{\mu}\bar{e})}(\theta'_{13}, \delta'_{CP}) \quad (2.80)$$

2. The hierarchy- δ_{CP} degeneracy of the $P_{\mu e}$ channel leads to wrong hierarchy solutions arising due to a different value of δ_{CP} other than the true value. This degeneracy can be expressed mathematically as

$$P_{\mu e(\bar{\mu}\bar{e})}(NH, \delta_{CP}) = P_{\mu e(\bar{\mu}\bar{e})}(IH, \delta'_{CP}) \quad (2.81)$$

3. The intrinsic octant degeneracy of the $P_{\mu\mu}$ channel refers to the clone solutions occurring for θ_{23} and $\pi/2 - \theta_{23}$ and expressed as

$$P_{\mu\mu(\bar{\mu}\bar{\mu})}(\theta_{23}) = P_{\mu\mu(\bar{\mu}\bar{\mu})}(\pi/2 - \theta_{23}) \quad (2.82)$$

Summing up the above degeneracies, a system of solutions, illustrated in Figure 2-5, is given by

$$P_{\alpha\rightarrow\beta(\bar{\alpha}\rightarrow\bar{\beta})}(\theta_{13}, \delta_{CP}, NH, \theta_{23}) = P_{\alpha\rightarrow\beta(\bar{\alpha}\rightarrow\bar{\beta})}(\theta'_{13}, \delta'_{CP}, IH, \theta'_{23}) \quad (2.83)$$

where, $\alpha = \nu_{\mu}$ and $\beta = \nu_{\mu}, \nu_e$. Solving these equation gives us a true solution and additional clone solutions to form the eight fold degeneracy [22]. However, there is no intrinsic octant degeneracy in the $P_{\mu e}$ channel as the dependence of θ_{23} in the leading order term of $P_{\mu e}$ channel goes as $\sin^2 \theta_{13} \sin^2 \theta_{23}$.

At present, the measurement of the non-zero precise value of θ_{13} from the reactor experiments resolves the degeneracies associated with θ_{13} . The intrinsic

2.4. Oscillation Parameter Degeneracy

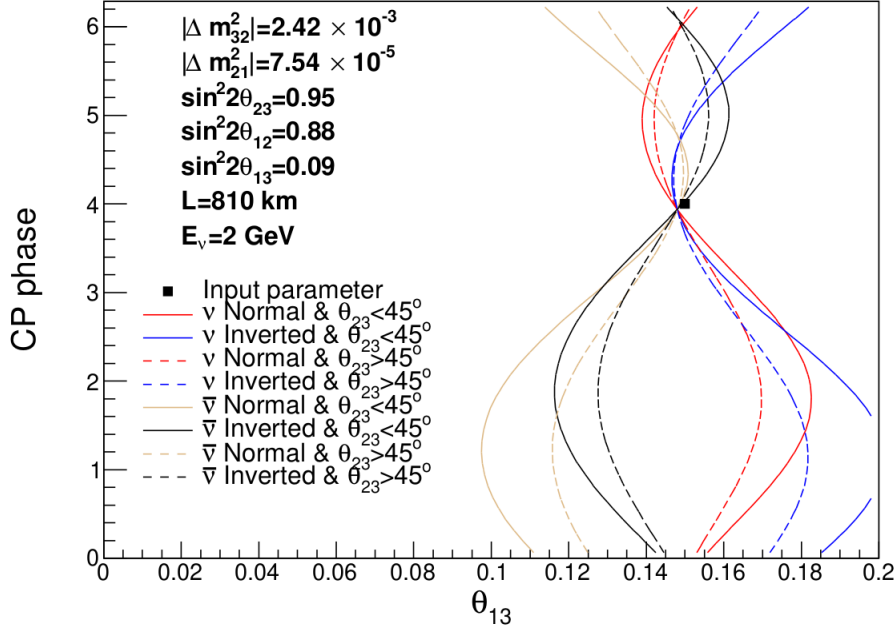


Figure 2-5: The Eight-fold degeneracy in $\nu_\mu \rightarrow \nu_e$ appearance channel for NO ν A baseline. Courtesy: Son Cao [23].

degeneracy is largely resolved and the octant sensitivity of the appearance channel has greatly improved. But due to the completely unknown value of δ_{CP} , the hierarchy- δ_{CP} degeneracy still persists and there are also degenerate solutions arising due to different values of θ_{23} and δ_{CP} . This degeneracy is referred as octant- δ_{CP} degeneracy. The degeneracy illustration are shown in Figures 2-6, 2-7 and 2-8. There are several methods discussed in the literature to break

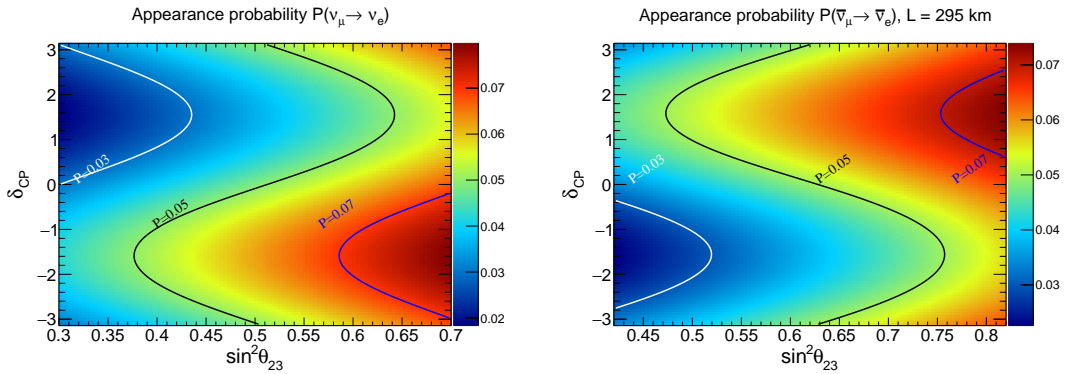


Figure 2-6: $P_{\mu e}(\theta_{23}, \delta_{CP}) = P_{\mu e}(\theta'_{23}, \delta'_{CP})$ Degeneracy at $E_\nu = 0.6$ GeV (T2K).

these degeneracies and to have a clean measurement of the neutrino oscillation parameters. They include combination of experiments at various baselines and L/E values [20, 22, 24], use of spectral information [25, 26], combination of different oscillation channels [27], and combination of experiments with varying neutrino

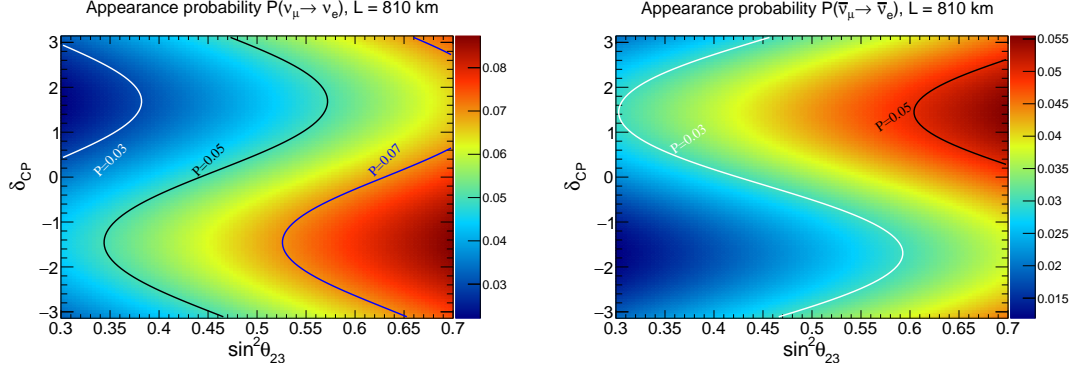


Figure 2-7: $P_{\mu e}(\theta_{23}, \delta_{CP}) = P_{\mu e}(\theta'_{23}, \delta'_{CP})$ Degeneracy at $E_\nu=2.0$ GeV (NO ν A).

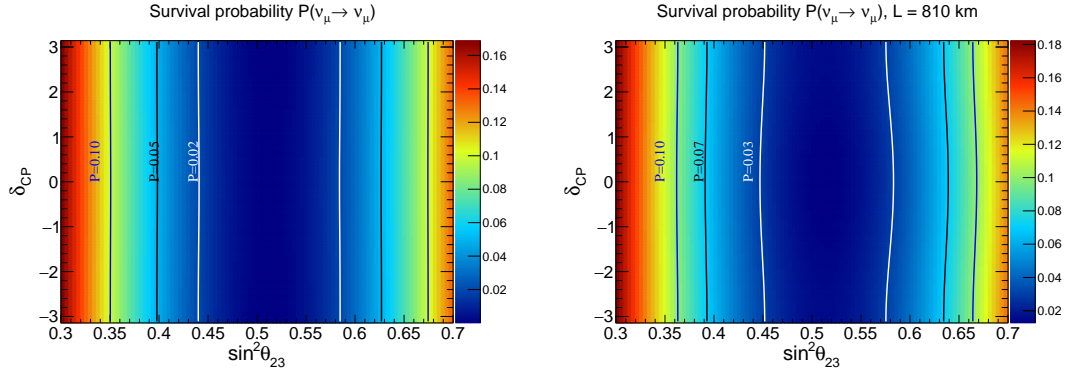


Figure 2-8: $P_{\mu\mu}(\theta_{23}) = P_{\mu\mu}(\pi/2 - \theta_{23})$ Degeneracy at $E_\nu = 0.6$ GeV for T2K(*left*) and 2.0 GeV for NO ν A(*right*).

sources, such as A-LBL and reactor-based neutrino experiments [28–32], or A-LBL with atmospheric neutrino experiments [33, 34].

2.5 Summary

This chapter forms the motivation of the thesis to adopt a framework to address the objectives. We describe the neutrino oscillation phenomena in vacuum and matter and revisited the oscillation parameter degeneracies associated with physics studies in A-LBL experiments. In the upcoming chapters, we will show how these parameter degeneracies affect the CP measurement, MH determination, and θ_{23} octant resolution capabilities of the long-baseline experiments and how adding a reactor-based oscillation experiment can be crucial to determining the present unknowns.

Bibliography

- [1] Mikheev, S. P. & Smirnov, A. Y. Resonant amplification of neutrino oscillations in matter and solar neutrino spectroscopy. *Nuovo Cim. C* **9**, 17–26, 1986.
- [2] Mikheyev, S. P. & Smirnov, A. Y. Resonance Amplification of Oscillations in Matter and Spectroscopy of Solar Neutrinos. *Sov. J. Nucl. Phys.* **42**, 913–917, 1985.
- [3] Wolfenstein, L. Neutrino Oscillations in Matter. *Phys. Rev. D* **17**, 2369–2374, 1978.
- [4] Giunti, C. & Kim, C. W. *Fundamentals of Neutrino Physics and Astrophysics*, 2007.
- [5] Gonzalez-Garcia, M. C. & Nir, Y. Neutrino Masses and Mixing: Evidence and Implications. *Rev. Mod. Phys.* **75**, 345–402, 2003. [hep-ph/0202058](#).
- [6] Linder, J. Derivation of neutrino matter potentials induced by earth , 2005. [hep-ph/0504264](#).
- [7] Langacker, P. *et al.* On the Detection of Cosmological Neutrinos by Coherent Scattering. *Phys. Rev. D* **27**, 1228, 1983.
- [8] Bethe, H. A. A Possible Explanation of the Solar Neutrino Puzzle. *Phys. Rev. Lett.* **56**, 1305, 1986.
- [9] Arafune, J. *et al.* CP violation and matter effect in long baseline neutrino oscillation experiments. *Phys. Rev. D* **56**, 3093–3099, 1997. [Erratum: *Phys.Rev.D* 60, 119905 (1999)], [hep-ph/9703351](#).
- [10] Cervera, A. *et al.* Golden measurements at a neutrino factory. *Nucl. Phys. B* **579**, 17–55, 2000. [Erratum: *Nucl.Phys.B* 593, 731–732 (2001)], [hep-ph/0002108](#).
- [11] Asano, K. & Minakata, H. Large- θ_{13} Perturbation Theory of Neutrino Oscillation for Long-Baseline Experiments. *JHEP* **06**, 022, 2011. [1103.4387](#).

- [12] Freund, M. Analytic approximations for three neutrino oscillation parameters and probabilities in matter. *Phys. Rev. D* **64**, 053003, 2001. [hep-ph/0103300](#).
- [13] Akhmedov, E. K. *et al.* Series expansions for three flavor neutrino oscillation probabilities in matter. *JHEP* **04**, 078, 2004. [hep-ph/0402175](#).
- [14] Friedland, A. & Lunardini, C. Two modes of searching for new neutrino interactions at MINOS. *Phys. Rev. D* **74**, 033012, 2006. [hep-ph/0606101](#).
- [15] Minakata, H. & Parke, S. J. Simple and Compact Expressions for Neutrino Oscillation Probabilities in Matter. *JHEP* **01**, 180, 2016. [1505.01826](#).
- [16] Denton, P. B. *et al.* Compact Perturbative Expressions For Neutrino Oscillations in Matter. *JHEP* **06**, 051, 2016. [1604.08167](#).
- [17] Denton, P. B. & Parke, S. J. Addendum to “Compact perturbative expressions for neutrino oscillations in matter” , 2018. [Addendum: *JHEP* **06**, 109 (2018)], [1801.06514](#).
- [18] Esteban, I. *et al.* The fate of hints: updated global analysis of three-flavor neutrino oscillations. *JHEP* **09**, 178, 2020. [2007.14792](#).
- [19] Burguet-Castell, J. *et al.* Superbeams plus neutrino factory: The golden path to leptonic cp violation. *Nuclear Physics B* **646** (1-2), 301–320, 2002.
- [20] Minakata, H. & Nunokawa, H. Exploring neutrino mixing with low energy superbeams. *Journal of High Energy Physics* **2001** (10), 001, 2001.
- [21] Fogli, G. L. & Lisi, E. Tests of ttexas u.hree-flavor mixing in long-baseline neutrino oscillation experiments. *Physical Review D* **54** (5), 3667, 1996.
- [22] Barger, V. *et al.* Breaking eight fold degeneracies in neutrino CP violation, mixing, and mass hierarchy. *Phys. Rev. D* **65**, 073023, 2002. [hep-ph/0112119](#).
- [23] Cao, S. V. *Study of antineutrino oscillations using accelerator and atmospheric data in MINOS*. Ph.D. thesis, Texas U., 2014.

- [24] Minakata, H. *et al.* Parameter Degeneracies in Neutrino Oscillation Measurement of Leptonic CP and T Violation. *Phys. Rev. D* **66**, 093012, 2002. [hep-ph/0208163](#).
- [25] Burguet-Castell, J. *et al.* Neutrino oscillation physics with a higher gamma beta beam. *Nucl. Phys. B* **695**, 217–240, 2004. [hep-ph/0312068](#).
- [26] Freund, M. *et al.* Systematic exploration of the neutrino factory parameter space including errors and correlations. *Nuclear Physics B* **615** (1-3), 331–357, 2001.
- [27] Donini, A. *et al.* The Silver channel at the neutrino factory. *Nucl. Phys. B* **646**, 321–349, 2002. [hep-ph/0206034](#).
- [28] Minakata, H. & Sugiyama, H. Exploring leptonic CP violation by reactor and neutrino superbeam experiments. *Phys. Lett. B* **580**, 216–228, 2004. [hep-ph/0309323](#).
- [29] Huber, P. *et al.* Prospects of accelerator and reactor neutrino oscillation experiments for the coming ten years. *Phys. Rev. D* **70**, 073014, 2004. [hep-ph/0403068](#).
- [30] Huber, P. *et al.* Reactor neutrino experiments compared to superbeams. *Nucl. Phys. B* **665**, 487–519, 2003. [hep-ph/0303232](#).
- [31] Minakata, H. *et al.* Reactor measurement of θ_{13} and its complementarity to long baseline experiments. *Phys. Rev. D* **68**, 033017, 2003. [Erratum: *Phys.Rev.D* 70, 059901 (2004)], [hep-ph/0211111](#).
- [32] McConnel Mahn, K. B. & Shaevitz, M. H. Comparisons and combinations of reactor and long-baseline neutrino oscillation measurements. *Int. J. Mod. Phys. A* **21**, 3825–3844, 2006. [hep-ex/0409028](#).
- [33] Huber, P. *et al.* Resolving parameter degeneracies in long-baseline experiments by atmospheric neutrino data. *Phys. Rev. D* **71**, 053006, 2005. [hep-ph/0501037](#).

- [34] Campagne, J.-E. *et al.* Physics potential of the CERN-MEMPHYS neutrino oscillation project. *JHEP* **04**, 003, 2007. [hep-ph/0603172](#).

Chapter 3

Experiment Specifications and Event Spectra

In section 3.1, we give an overview of T2K-II, NO ν A-II and JUNO: the terrestrial neutrino oscillation experiments considered in this thesis. In section 3.2, we introduce the simulation software GLOBES used in our statistical analysis of the experiments. We discuss the simulation technique adopted to study the physics potential of the experiments. We describe the experiments using updated information on fluxes, signal and background efficiencies, and systematic errors. We present criteria for the signal and background event selection procedures. Finally, in section 3.3, we present our results on the event spectra for the selected ν_e ($\bar{\nu}_e$) appearance and ν_μ ($\bar{\nu}_\mu$) disappearance channels for A-LBL experiments T2K-II and NO ν A-II, as well as $\bar{\nu}_e$ disappearance channel of R-MBL experiment JUNO.

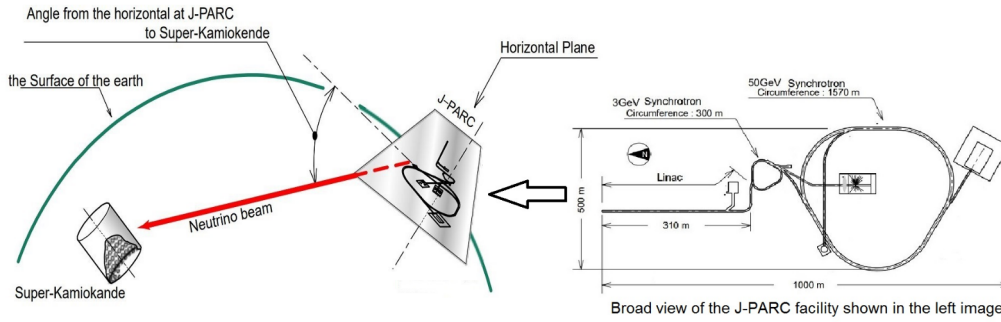


Figure 3-1: A Schematic diagram of J-PARC, Tokai to Super-K detector, Kamioka. Images taken from Mishima K, et al. 9th International Workshop on Accelerator Alignment, September 26-29, 2006.

3.1 Specifications of the Terrestrial Neutrino Oscillation Experiments

3.1.1 T2K-II

Tokai-To-Kamioka (T2K) [1] is the second generation of accelerator-based long-baseline (A-LBL) neutrino oscillation experiments located in Japan. T2K-II [2] is a proposal to extend the T2K run until 2026 before Hyper-Kamiokande (HK) [3] starts operation. At the Japan Proton Accelerator Research Centre (J-PARC), protons of 3 GeV energy are accelerated to 30 GeV to produce a powerful beam intensity of about 0.77 MW. Pions and kaons are produced at the interaction of the 30 GeV proton beam from the (See Figure 3-1) Main Ring (MR) with a graphite target, 91.4 cm long and 2.6 cm in diameter, with a density of 1.8 g/cm^3 . Pions are focused by three magnetic horns to increase the neutrino beam's intensity. A muon neutrino beam is produced from the decay products of pions and kaons. The properties of the neutrinos are measured at near detectors placed 280 m from the target, and the oscillation analysis is performed at the far detector, Super-Kamiokande (SK), which is located 295 km away.

The off-axis beam method is used to generate a narrow-band neutrino beam, as per Equations 1.12 and 1.13. The beam axis is slightly shifted away at an average angle of 2.5° w.r.t the direction of the proton beam in order for SK to receive a neutrino beam with a peak energy of 0.6 GeV, close to the first oscillation maxima.

3.1. Specifications of the Terrestrial Neutrino Oscillation Experiments

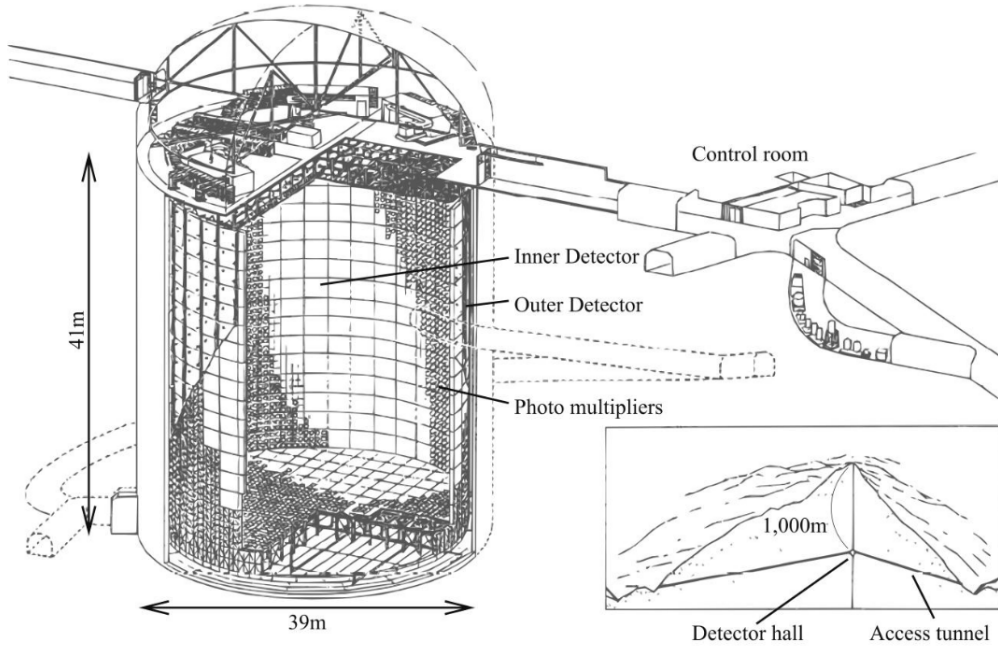


Figure 3-2: Schematic of T2K far neutrino detector: Super Kamiokande [8].

This technique increases the the fraction of CCQE events in energy range less than 1 GeV. For the event selection and energy reconstruction at SK, the CCQE events are signals while other CC events are background.

T2K Near and Far Detectors The T2K near neutrino detectors are composed of the neutrino beam monitor (INGRID) [4] and the neutrino spectrometer (ND280) [1, 5, 6]. These detectors are set in a pit inside the ND280 hall. The pit has a diameter of 17.5 m and a depth of 37 m. The ND280 detector measures the off-axis neutrino flux and energy spectrum at a baseline of 280 m. The off-axis angle to ND280 from the target position is 2.04° . This angle was chosen to make the neutrino spectrum at ND280 as similar as possible to the spectrum at SK. The neutrino beam intensity and direction are monitored directly by measuring the profile of neutrinos at the INGRID detector [7], located 280 m away from the target.

Super-Kamiokande is the far detector and an upgrade of the previous Kamiokande detector, and it measures the event rate and energy spectrum in the off-axis direction at a baseline of 295 km. The detector lies under the peak of Mt. Ikenoyama, with 1000 metres of rock overburden at geographical co-ordinates

$36^{\circ}25'32.6''\text{N}$ and $137^{\circ}18'37.1''\text{E}$. The water Cherenkov detector consists of a welded stainless steel tank of 39m diameter and 42m tall with nominal capacity of 50ktons supported by an array of 11,146 50cm-diameter hemispherical inward-facing and 1885 outward facing 20cm-diameter hemispherical PMTs [9]. Neutrinos are detected with the PMTs by measuring the Cherenkov lights emitted by charged particles from the neutrino interactions in the water. The particle's vertex, energies, and directions are reconstructed from the timing and position of the Cherenkov lights. The particle identification (muon/electron separation) is performed based on the edge of the Cherenkov lights: the Cherenkov lights produced by muons have a sharp outer ring edge, while the Cherenkov lights produced by electrons have characteristically fuzzy edges due to electromagnetic showers. More details of SK are described in [10, 11].

SK provides excellent performance in reconstructing the neutrino energy and the neutrino flavor classification. This capability allows T2K(-II) to measure simultaneously the disappearance of muon (anti-)neutrinos and the appearance of electron (anti-)neutrinos from the flux of almost pure muon (anti-)neutrinos. While the data samples of the ν_{μ} ($\bar{\nu}_{\mu}$) disappearance provide a precise measurement of the atmospheric neutrino parameters, $\sin^2 2\theta_{23}$ and Δm_{31}^2 , the ν_e ($\bar{\nu}_e$) appearance rates are driven by $\sin^2 2\theta_{13}$ and sensitive to δ_{CP} and MH. T2K made an observation of electron neutrinos appearing from a muon neutrino beam [12] and presented an indication of CPV in the neutrino oscillation [13]. T2K originally planned to take data equivalent to 7.8×10^{21} protons-on-target (POT) exposure. In Neutrino 2020 conference, T2K [14] reported a collected data sample from 3.6×10^{21} POT exposure. In Ref. [2], T2K proposes to extend the run until 2026 and collect 20×10^{21} POT, allowing T2K to explore CPV with a confidence level (C.L.) of 3σ or higher if δ_{CP} is close to $-\pi/2$ and make precision measurements of θ_{23} and $|\Delta m_{31}^2|$.

3.1. Specifications of the Terrestrial Neutrino Oscillation Experiments

3.1.2 $\text{NO}\nu\text{A-II}$

NuMI Off-axis ν_e Appearance ($\text{NO}\nu\text{A}$) [15] is also the 2nd generation of A-LBL neutrino experiments placed in the US with a baseline of 810 km between the production source and the far detector. $\text{NO}\nu\text{A}$, similar to T2K(-II), adopts the off-axis technique such that the far detector is placed at an angle of 14 mrad to the averaged direction of the neutrino beam, with the oscillation maxima at about 2 GeV. The experiment aims to answer the same questions, but with different sensitivities to different parameters, depending on the baseline and the range of beam energies [16].

3.1.2.1 The NuMI beam

The NuMI beam at Fermilab [17] is designed to produce neutrinos and antineutrinos at high intensity by colliding a proton beam onto a fixed target. The proton beam is first accelerated to 8 GeV in a rapid cycling synchrotron called the Booster and then delivered to the Main Injector ring. The Main Injector accelerates the protons to 120 GeV that hit the 1.2 m graphite target. Operating at around 742 kW, the Main Injector is able to deliver $\sim 6 \times 10^{20}$ POT every year. The schematic diagram of the proton accelerator is shown in Figure 1-6. The production of mesons is similar to that of T2K(-II), the decay of which produces the neutrinos and antineutrinos when the magnetic horns with a current of 200kA defocus the mesons into a 675m long decay pipe. The neutrino energy range for oscillation analysis is 1-5 GeV for the experiment.

3.1.2.2 $\text{NO}\nu\text{A}$ detectors

$\text{NO}\nu\text{A}$ uses a near detector [18], located 1 km away from the production target, to characterize the unoscillated neutrino flux. The $\text{NO}\nu\text{A}$ far detector is filled with liquid scintillator contained in PVC cells, totally weighted up 14 ktons with 63% active materials. Both the ND and FD are functionally identical, differing primarily in their sizes with the ND being 290 tons. The schematic diagram of

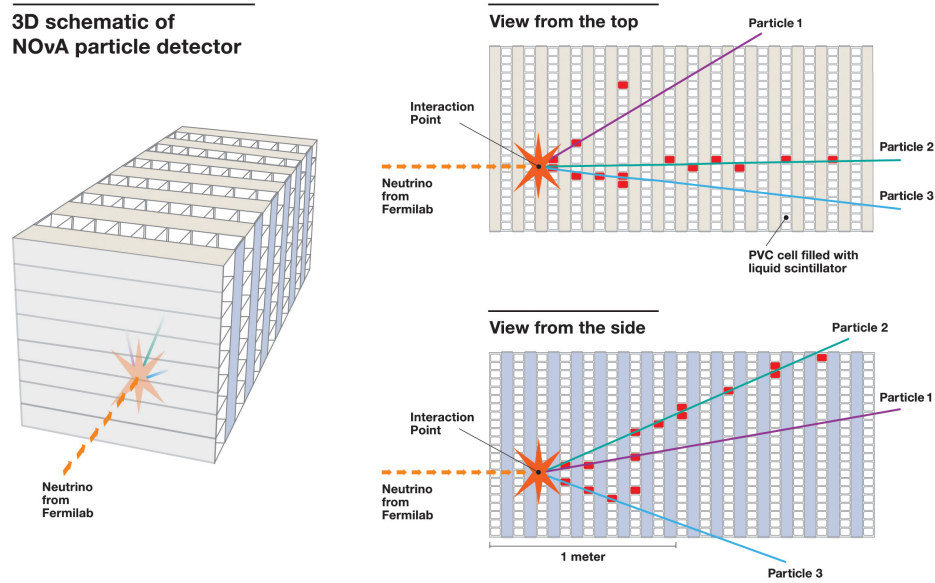


Figure 3-3: A graphic representation of one of the first neutrino interactions captured at the NOvA far detector in northern Minnesota. The dotted red line represents the neutrino beam, generated at Fermilab in Illinois and sent through 500 miles of earth to the far detector. The image on the left is a simplified 3-D view of the detector, the top right view shows the interaction from the top of the detector, and the bottom right view shows the interaction from the side of the detector. The information is reproduced from <https://vms.fnal.gov/asset>.

the NOvA detector is shown in Figure 3-3. The Far Detector has a dimension of $15.8m \times 15.8m \times 60m$, while the ND is of dimensions $3.8m \times 3.8m \times 15.9m$. The Far Detector is placed on surface in a detector hall with a modest overburden of 1.2 m concrete and 15 cm barite. It collects an enormous number of cosmic rays, the fundamental background to the oscillation analysis. The Near Detector is placed 100 m underground, where cosmic rays are negligible. NOvA takes advantage of machine learning for particle classification to enhance the event selection performance.

The event reconstruction of interactions in the detector deals with clustering calibrated hits, which characterize the topology of the interaction and thereby, identify the neutrino flavor and the incoming neutrino energy. The major interaction types that are relevant for the oscillation analysis are $CC\nu_\mu$, $CC\nu_e$, NC and Cosmic muons. $CC\nu_\mu$ events are identifiable by a long and straight muon track made up of minimum ionizing hits. $CC\nu_e$ events are characterized by an electron in the final state which produces a roughly conical shower cascade

3.1. Specifications of the Terrestrial Neutrino Oscillation Experiments

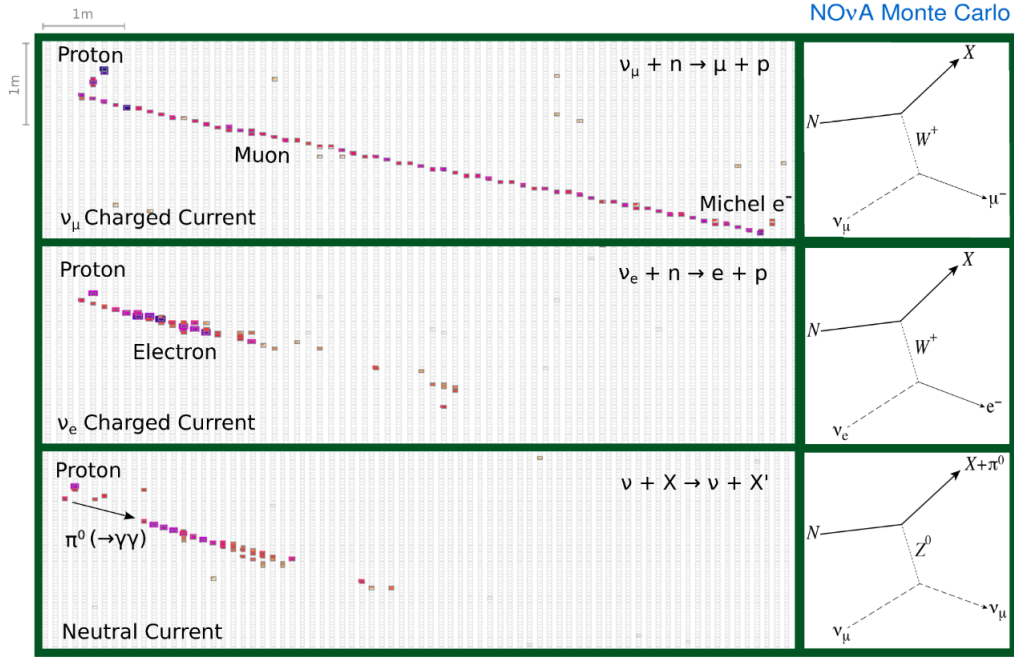


Figure 3-4: Interaction topologies for $CC\nu_\mu$ (*top*), $CC\nu_e$ (*middle*) and NC (*bottom*) neutrino interactions [18].

driven by pair production as the electron interacts with the dense material. It is difficult to separate oscillated $CC\nu_e$ events and events coming from the intrinsic beam contamination. As a result, the beam $CC\nu_e$ component is an irreducible background to the appearance channel. NC events are flavor independent interactions where the observed final state particles are only the hadronic component, as the neutrino just scatters off the nuclei and can't be observed. If the hadronic component involves a π^0 , then, the decay can mimic $CC\nu_e$ events at typical energies. Charged pions can also be produced resulting in track like topologies, which can be misidentified as short muon tracks and thus $CC\nu_\mu$ events. Hence, these events are important backgrounds to both oscillation channels. Charged Muons from cosmic ray interactions are also important backgrounds. Most of them are long muon tracks coming in from the top of the detector and can be differentiated by their directions from a $CC\nu_\mu$ event. Some of them can also emit bremsstrahlung radiation at a variety of angles, which is sufficiently energetic to mimic $CC\nu_e$ events. Examples of interaction topologies seen at the NOvA detectors for different types of neutrino interactions are shown in Figure 3-4.

In 2018 [19], NOvA provided more than 4σ C.L. evidence of electron anti-neutrino

appearance from a beam of muon anti-neutrinos. In Neutrino 2020 conference, NO ν A [20] reported a collected data sample from 2.6×10^{21} POT exposure. In [21], NO ν A offers the possibility of extending the run through 2024, hereby called NO ν A-II, in order to get 3σ C.L. or higher sensitivity to the MH in case the MH is *normal* and δ_{CP} is close to $-\pi/2$, and more than 2σ C.L. sensitivity to CPV.

3.1.3 JUNO



Figure 3-5: Location of JUNO site [22].

Jiangmen Underground Neutrino Observatory (JUNO) [22] is a reactor-based medium-baseline neutrino experiment, based in China. It is located in Jinji town, Kaiping city, Jiangmen city, Guangdong province. The geographic location is $112^{\circ}31'05''$ longitude east and $22^{\circ}07'05''$ latitude north, as shown in Figure 3-5. JUNO has an average baseline of 52.5 km and houses a 20 kton large liquid scintillator detector for detecting the electron anti-neutrinos ($\bar{\nu}_e$) from the Yangjiang (YJ) and Taishan (TS) nuclear power plants (NPPs) with an average baseline of 52.5 km. In JUNO, the electron antineutrino $\bar{\nu}_e$ flux comes mainly from four radioactive isotopes [23] ^{235}U , ^{238}U , ^{239}Pu , and ^{241}Pu , located at the reactor cores with an assumed detection efficiency of 73%. Each of the six cores at YJ nuclear plant will produce a power of 2.9 GW and the four cores at TS NPP will generate 4.6 GW each. They are combined to give 36 GW thermal power.

3.1. Specifications of the Terrestrial Neutrino Oscillation Experiments

Table 3.1: Summary of the thermal power and baseline to the JUNO detector for the Yangjiang (YJ) reactor cores .

Cores	YJ-C1	YJ-C2	YJ-C3	YJ-C4	YJ-C5	YJ-C6
Power (GW)	2.9	2.9	2.9	2.9	2.9	2.9
Baseline (km)	52.75	52.84	52.42	52.51	52.12	52.21

Table 3.2: Summary of the thermal power and baseline to the JUNO detector for the Taishan (TS) reactor cores.

Cores	TS-C1	TS-C2	TS-C3	TS-C4
Power (GW)	4.6	4.6	4.6	4.6
Baseline (km)	52.76	52.63	52.32	52.20

The thermal power of all cores and the baselines are listed in Table 3.1 and 3.2.

3.1.3.1 JUNO Detector

The JUNO detector [22] consists of a central detector, a water Cherenkov detector and a muon tracker. The central detector is a liquid scintillator (LS) detector of 20 kton fiducial mass with an designed energy resolution of 3%/ E(MeV). The central detector is submerged in a water pool to be shielded from natural radioactivity from the surrounding rock and air. The water pool is equipped with Photomultiplier Tubes (PMTs) to detect the Cherenkov light from cosmic muons, acting as a veto detector. On top of the water pool, there is another muon detector to accurately measure the muon tracks. A schematic view of the JUNO detector is shown in Figure 3-6.

To realize practically the capability of mass hierarchy resolution, JUNO must achieve a very good neutrino energy resolution, which has been demonstrated recently in Ref. [24], and collect a huge amount of data. With six years of operation, JUNO can reach 3σ C.L. or higher sensitivity to the MH and achieve better than 1% precision on the solar neutrino parameters and the atmospheric neutrino mass-squared splitting $|\Delta m_{31}^2|$.

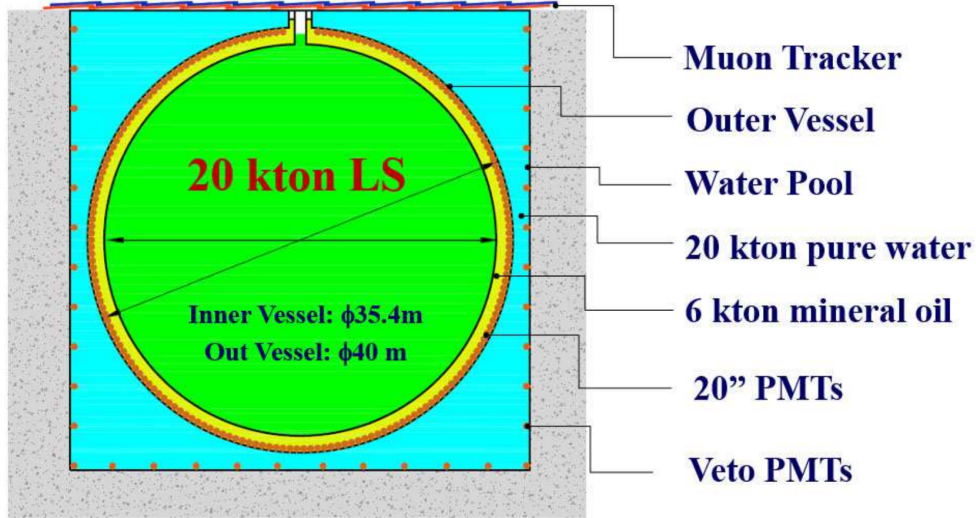


Figure 3-6: A schematic view of the JUNO detector [22] .

3.2 Simulation Technique

Although T2K and $\text{NO}\nu\text{A}$ experiments have already collected with 18% and 36% of the total proton exposure assumed in this study, respectively, we do not directly use their experimental data to estimate their final reaches. The main reason is that measurements of the CP violation, the mass hierarchy, and the mixing angle θ_{23} , so far been statistically limited, except for a specific set of oscillation parameters. We thus carry out the study with the assumption that all values of δ_{CP} and two scenarios of the neutrino mass hierarchy are still possible, and mixing angle θ_{23} is explored in a range close to 45° .

Reaching the three above mentioned *unknowns* depends on the ability to resolve the parameter degeneracies among δ_{CP} , the sign of Δm_{31}^2 , θ_{13} , and θ_{23} [25]. Combining the data samples of the A-LBL experiments (T2K-II and $\text{NO}\nu\text{A-II}$) and JUNO would enhance the CPV search and MH determination since the JUNO sensitivity to MH has no ambiguity to δ_{CP} . To further enhance the CPV search, one can break the $\delta_{\text{CP}}\text{-}\theta_{13}$ degeneracy by using the constraint of θ_{13} from reactor-based short-baseline (R-SBL) neutrino experiments such as Daya Bay [26], Double Chooz [27], and RENO [28]. This combination also helps to solve the θ_{23} octant in cases of non-maximal mixing.

3.2. Simulation Technique

3.2.1 GLoBES package

The General Long Baseline Experiment Simulator (GLoBES) [29, 30] is used for simulating the experiments and calculating the statistical significance. GLoBES is a software package to simulate A-LBL and reactor-based neutrino experiments. It is unable to describe solar and atmospheric neutrino experiments because in these experiments, one cannot assume the production of neutrinos to be stationary point sources. Within GLoBES, we define the experiments in a comprehensive Abstract Experiment Definition Language (AEDL). The AEDL file contains the externally feeded neutrino/antineutrino flux information and cross-section files of relevant neutrino interactions, run-time in neutrino/antineutrino mode, proton beam power, baseline, matter density profile, energy resolution functions, constant and variable energy bin widths, oscillation channels and energy-dependent detection efficiencies for a particular experiment that we want to simulate. For the systematics, energy normalization and calibration errors can be simulated in a straightforward way. It is then loaded in the user interface which is a C-library. Using GLoBES, we can compute the neutrino oscillation probabilities and the signal and background event rates. It allows to extract information in the level of event spectra and calculate the corresponding χ^2 values for different oscillation channels of an experiment or a combination of upto 32 experiments.

In this simulator, number of expected events of ν_j from ν_i oscillation in the n -th energy bin of the detector in a given experiment is calculated as

$$R_n(\nu_i \rightarrow \nu_j) = \frac{N}{L^2} \int_{E_n - \frac{\Delta E_n}{2}}^{E_n + \frac{\Delta E_n}{2}} dE_r \times \int dE_t \Phi_i(E_t) \sigma_{\nu_j} R_j(E_t, E_r) \epsilon_j(E_r) P_{\nu_i \rightarrow \nu_j}(E_t) \quad (3.1)$$

where,

- i, j are the charged lepton(s) associated with the initial and final flavor(s) of the neutrinos,
- Φ_i is the flux of the initial flavor at the source,
- σ_{ν_j} is the cross-section for the final flavor f ,

- L is the baseline length,
- E_t and E_r are the incident and reconstructed neutrino energy, respectively,
- $\epsilon_j(E_r)$ is the detection efficiency of final flavor f , and
- N is the normalization factor for standard units in GLOBES.

$R_j(E_t, E_r)$ in the energy resolution function *i.e.* the probability to observe a reconstructed neutrino energy E_r , if the true neutrino energy is E_t . We consider a gaussian, given by

$$R_j(E_t, E_r) = \frac{1}{\sqrt{2\pi\sigma^2(E)}} e^{-\frac{(E_t - E_r)^2}{2\sigma^2(E)}} \quad (3.2)$$

with mean E_r and standard deviation $\sigma(E)$. We define the energy resolution function as follow:

For A-LBL,

$$\sigma(E) = p.E + q.\sqrt{E} + r \quad (3.3)$$

For R-MBL (relevant for inverse beta decay process),

$$\sigma(E) = \begin{cases} p.\sqrt{1000}^{-1} \sqrt{(x-8).10^{-4}}, & \text{for } x > 1.8 \times 10^{-3} \\ p.10^{-3}, & \text{for } x \leq 1.8 \times 10^{-3} \end{cases} \quad (3.4)$$

where the parameters p , q and r are provided by the user. For T2K-II, input parameters are $p = 0$, $q = 3\%$ and $r = 8.5\%$ for both ν_μ ($\bar{\nu}_\mu$) and ν_e ($\bar{\nu}_e$) event reconstruction. For NO ν A, the the definition of energy resolution function varies for different events which are given in Table 3.4. For JUNO, we define $p = 3\%$.

The latest results from the T2K and NO ν A experiments on $\nu_\mu \rightarrow \nu_e$ ($\bar{\nu}_\mu \rightarrow \bar{\nu}_e$) appearances and $\nu_\mu \rightarrow \nu_\mu$ ($\bar{\nu}_\mu \rightarrow \bar{\nu}_\mu$) disappearance are given in Figure 3-7 and 3-8. The event spectra presented here for T2K are for Runs 1-9, from June, 2010 to May, 2018. That corresponds to an exposure of 14.94×10^{20} protons-on-target (POT) in ν -mode and 16.35×10^{20} POT in $\bar{\nu}$ -mode. For NO ν A, data taken in neutrino mode beam exposure of 13.6×10^{20} POT for a period from February, 2014 to March, 2020 and in antineutrino mode from June 29, 2016 to

3.2. Simulation Technique

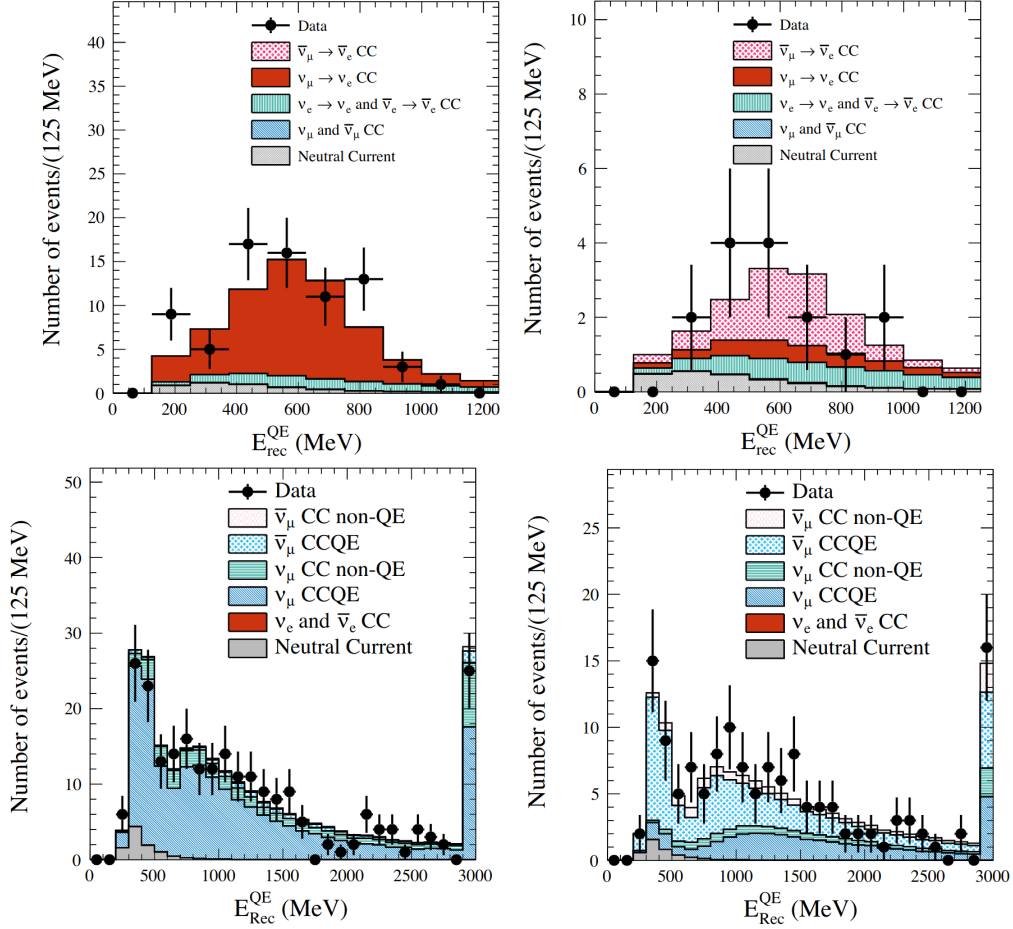


Figure 3-7: Recent results of T2K experiment. The *top* figures show the reconstructed energy distribution for ν_e appearance and the *bottom* figures represent the ν_μ disappearance events. The left (right) plot shows the events in neutrino (antineutrino) mode [31].

February 26, 2019 is taken with an exposure of 12.5×10^{20} POT. During these periods, the proton beam was operated with an average power of 650 kW, with a peak at 756kW.

3.2.2 Neutrino Flux for T2K-II and NO ν A-II

The flux predictions for the T2K SK far detector are provided in Figure 3-9. The original description of the flux predictions is published in [33]. Since the publication, the flux prediction has been updated with new thin target data from the NA61/SHINE experiment, and flux predictions for antineutrino enhanced beam operation have been produced. The NA61/SHINE thin target measurements of $\pi^\pm, K^\pm, K_S^0, \Lambda$ and p production are published in [34]. The updated flux

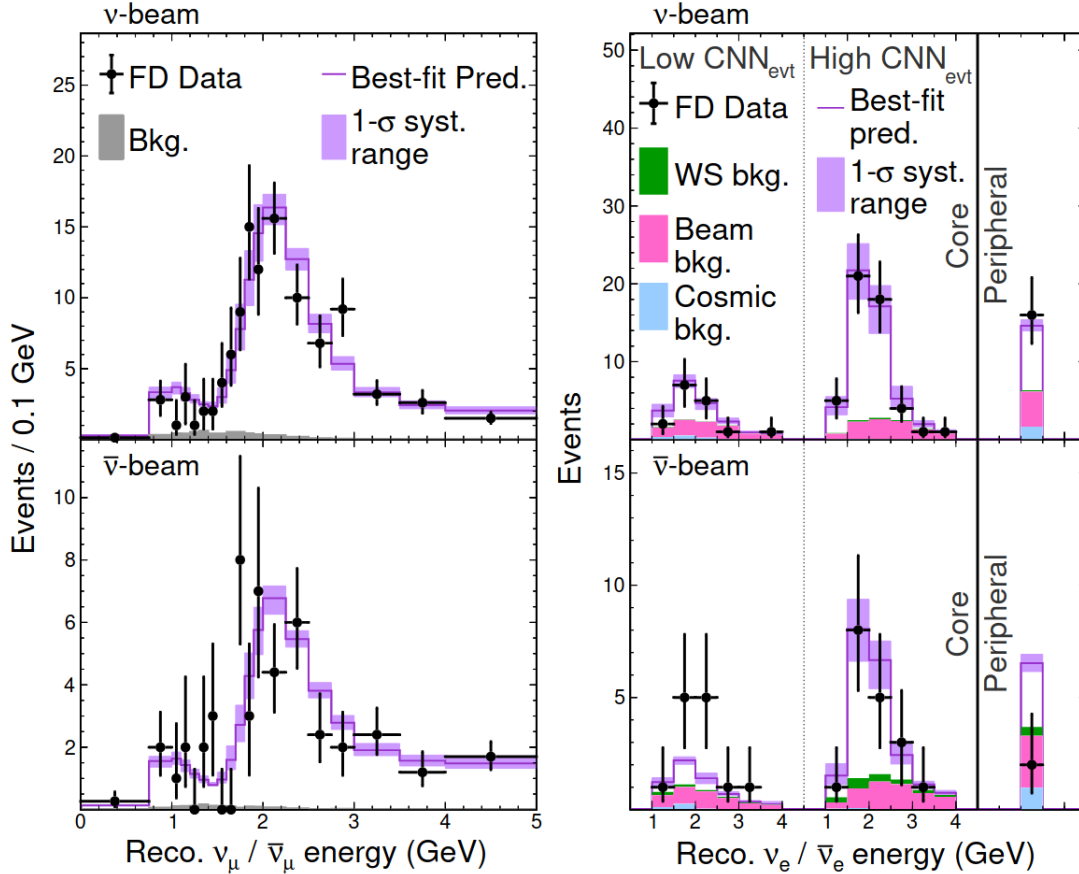


Figure 3-8: Reconstructed neutrino energy spectra for the NO ν A FD. The *left* figures show the reconstructed energy distribution for ν_{μ} disappearance and the *right* figures represent the ν_e appearance events. The top (bottom) plot shows the events in neutrino (antineutrino) mode. The appearance events are classified in three bins from lowest to highest purity: “Peripheral”, “Low PID”, and “High PID” [32].

prediction is described in [35]. The provided flux predictions include no neutrino oscillations. The SK flux is calculated for an infinitesimal angular range in a direction that is offset by 2.506° from the beam direction. The SK flux is calculated at a distance of 295.3 km from the center of the production target. Fluxes are provided for both +250 kA (neutrino enhanced beam) and -250 kA (antineutrino enhanced beam) operation of the T2K magnetic horns. The flux is given in 50 MeV wide bins of neutrino energy from 0 to 10 GeV neutrino energy. Above 10 GeV, the bins are 1 GeV wide, and are normalized to show the flux per 50 MeV. All flux predictions are normalized to 10^{21} protons delivered to the T2K production target. Figure 3-9 shows the flux distribution for the energy range 1-10 GeV in both neutrino and antineutrino modes.

3.2. Simulation Technique

For NO ν A-II, we use the event spectra of [36] to construct the simulated experiment. The Monte Carlo information is available for 8.85×10^{20} POTs and 12.33×10^{20} POTs for neutrino and anti-neutrino respectively. We downloaded the ND flux files from the NO ν A webpage [37] and reproduced as in Figure 3-10. The units of the files are in neutrinos/ m^2 /GeV/1M POT per year. We obtained the Far Detector fluxes corresponding to 10^{20} POT per year by scaling the ND fluxes with a factor of $1e14 \times \left[\frac{\text{ND baseline}}{\text{FD baseline}} \right]^2 = 1e14 \times \left(\frac{1km}{810km} \right)^2$. The flux distribution for the FD is shown in Figure 3-11.

We describe the experiments using updated information of fluxes, signal and background efficiencies, and systematic errors. Remaining differences between the energy spectra of the simulated data sample at the reconstruction level obtained by GLOBES and the real experiment simulation can be due to the effects of the neutrino interaction model, the detector acceptance, detection efficiency variation as a function of energy, etc.. These differences are then treated quantitatively using post-smearing efficiencies, consequently allowing us to match our simulation with the published spectra of each simulated sample from each experiment.

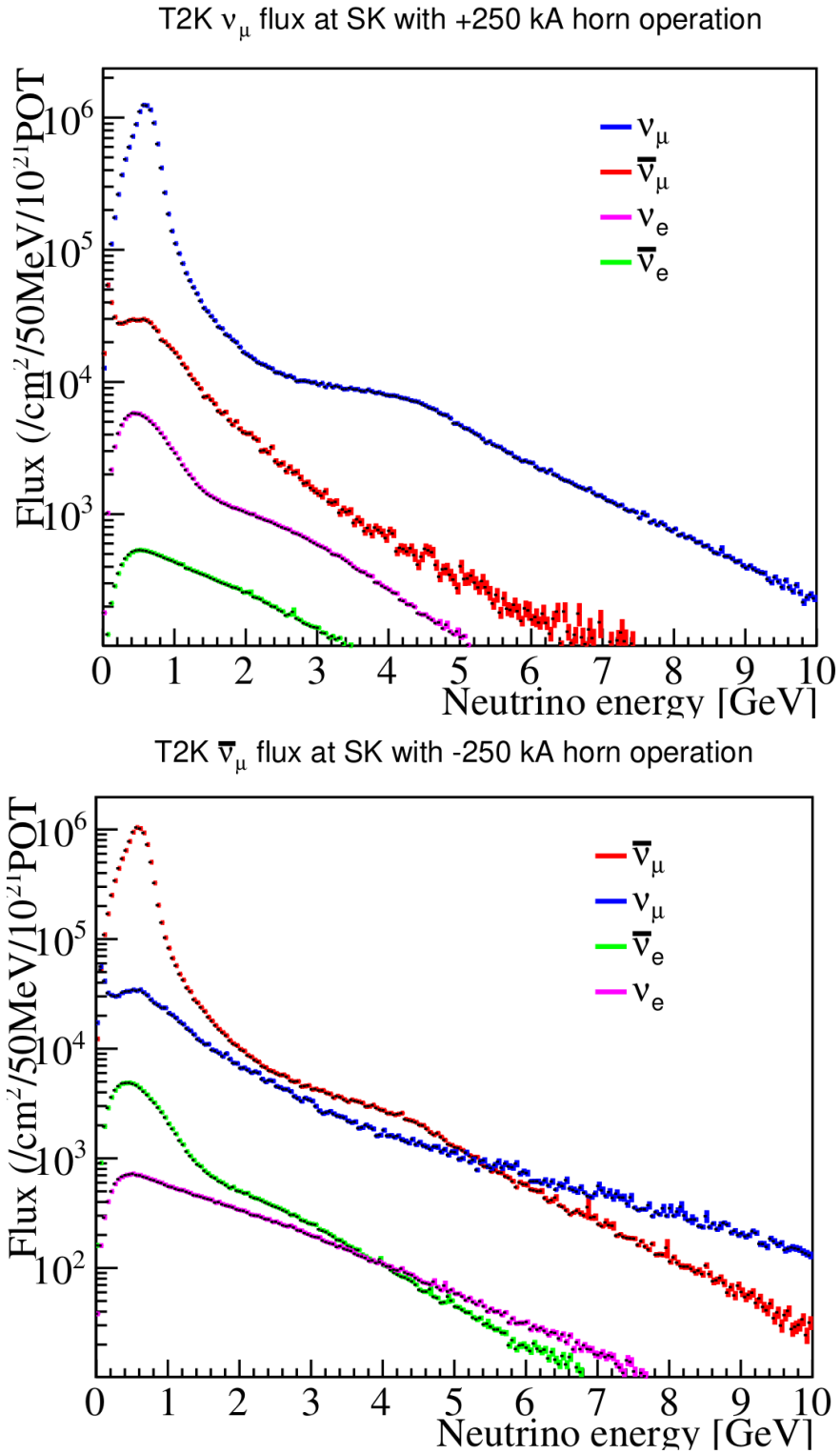


Figure 3-9: T2K flux at far detector for antineutrino mode (left panel) and neutrino mode (right panel), updated in 2016.

3.2. Simulation Technique

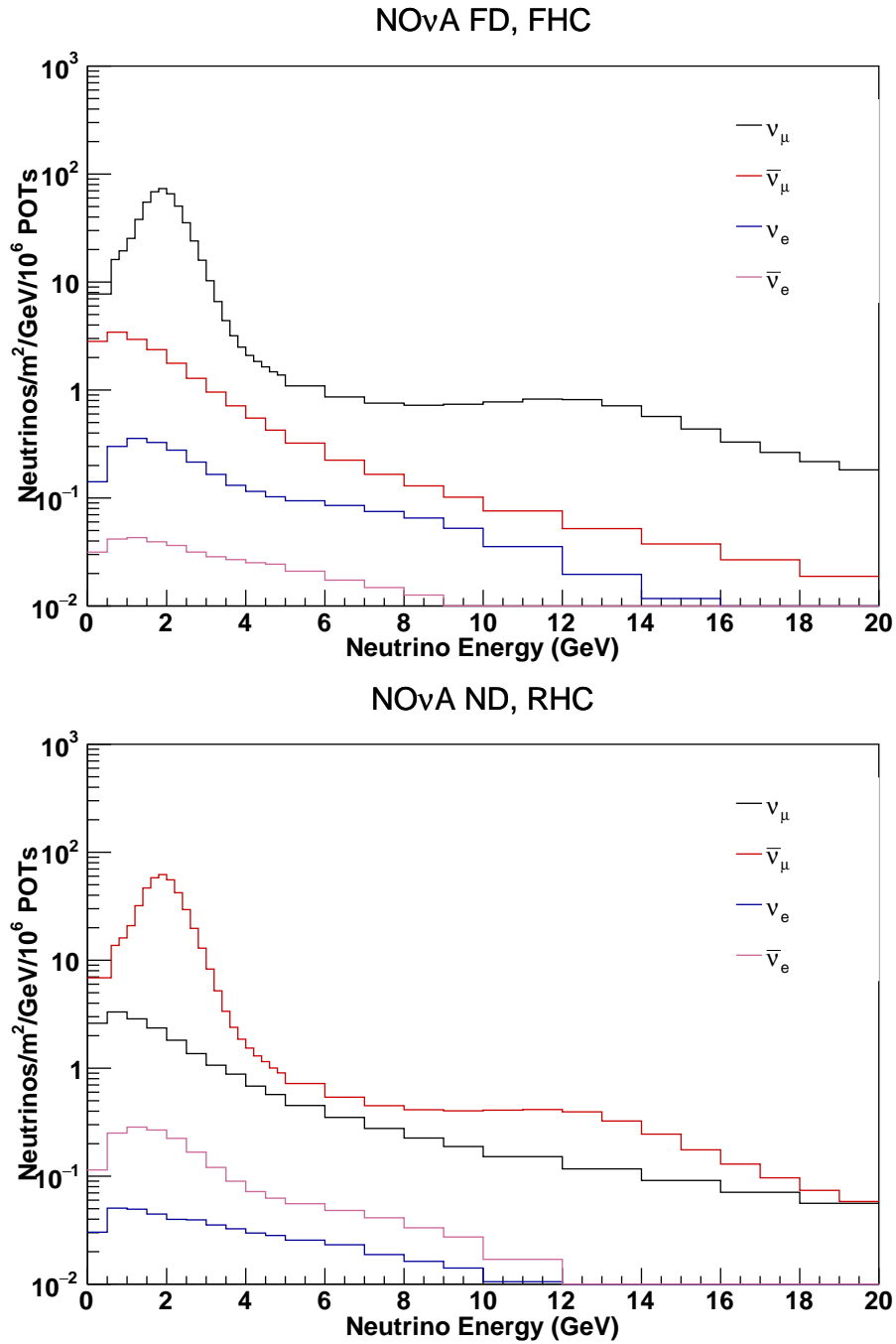


Figure 3-10: NO ν A Near Detector Flux.

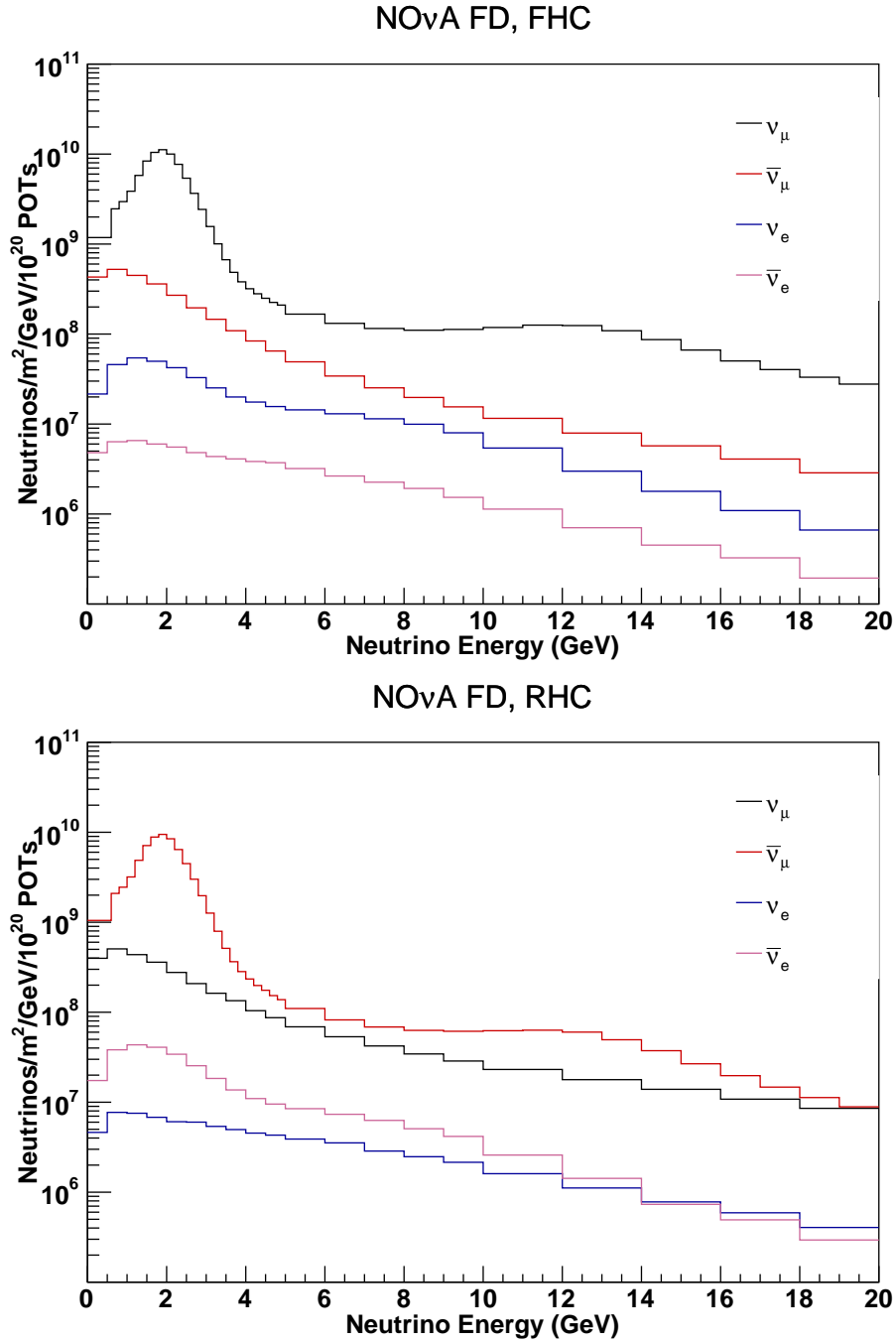


Figure 3-11: NO ν A Far Detector Flux normalized to 10^{20} POTs per year.

3.3 Event Spectra

Each experimental setup is validated at the event rate level and sensitivity level to ensure that physics reaches of the simulated data samples we obtain are in relatively good agreement with the real experimental setup.

3.3.1 T2K-II and NO ν A

For each of T2K-II and NO ν A-II, four simulated data samples per each experiment are used: $\nu_\mu(\bar{\nu}_\mu)$ disappearance and $\nu_e(\bar{\nu}_e)$ appearance in both ν -mode and $\bar{\nu}$ -mode. The experimental specifications of these two experiments are shown in Tables 3.3 and 3.4.

In T2K(-II), neutrino events are dominated by the Charged Current Quasi-Elastic (CCQE) interactions. Thus, for appearance (disappearance) in ν -mode and $\bar{\nu}$ -mode, the signal events are obtained from the $\nu_\mu \rightarrow \nu_e$ ($\nu_\mu \rightarrow \nu_\mu$) CCQE events and $\bar{\nu}_\mu \rightarrow \bar{\nu}_e$ ($\bar{\nu}_\mu \rightarrow \bar{\nu}_\mu$) CCQE events, respectively.

Table 3.3: Experimental specifications of the A-LBL experiment T2K-II.

Characteristics	T2K-II[2, 38]
Baseline	295 km
Matter density [39]	2.6 gcc^{-1}
Total Exposure	20×10^{21} POT
Detector fiducial mass	22.5 kton
Systematics ¹	3% (0.01%)
Energy resolution	$0.03 \times \sqrt{E(\text{GeV})}$
Energy window	0.1-1.3 GeV (<i>APP</i> ²), 0.2-5.05 GeV (<i>DIS</i> ³)
Bin Width	0.125 GeV/bin (<i>APP</i>), 0.1 GeV/bin (<i>DIS</i>)

¹normalization (calibration) error for both signals and backgrounds.

²shortened for the appearance sample.

³shortened for the disappearance sample.

Table 3.4: Experimental specifications of the A-LBL experiment NO ν A-II.

Characteristics	NO ν A-II [19, 21]
Baseline	810 km
Matter density	2.84 gcc^{-1}
Total Exposure	72×10^{20} POT
Detector fiducial mass	14 kton
Systematics	5% (2.5%)
Energy resolution	$x \times \sqrt{E(\text{GeV})}^1$
Energy window	0.0-4.0 GeV (<i>APP</i>), 0.0-5.0 GeV (<i>DIS</i>)
Bin Width	0.5 GeV/bin (<i>APP</i>), variable ² (<i>DIS</i>)

¹ $x = 0.107, 0.091, 0.088$ and 0.081 for $\nu_e, \nu_\mu, \bar{\nu}_e$ and $\bar{\nu}_\mu$ respectively.

²used the binning as in[19].

In the appearance samples, the intrinsic $\nu_e/\bar{\nu}_e$ contamination from the beam, the *wrong-sign* components i.e $\bar{\nu}_\mu \rightarrow \bar{\nu}_e$ ($\nu_\mu \rightarrow \nu_e$) in ν -mode ($\bar{\nu}$ -mode) respectively, and the neutral current (NC) events constitute the backgrounds.

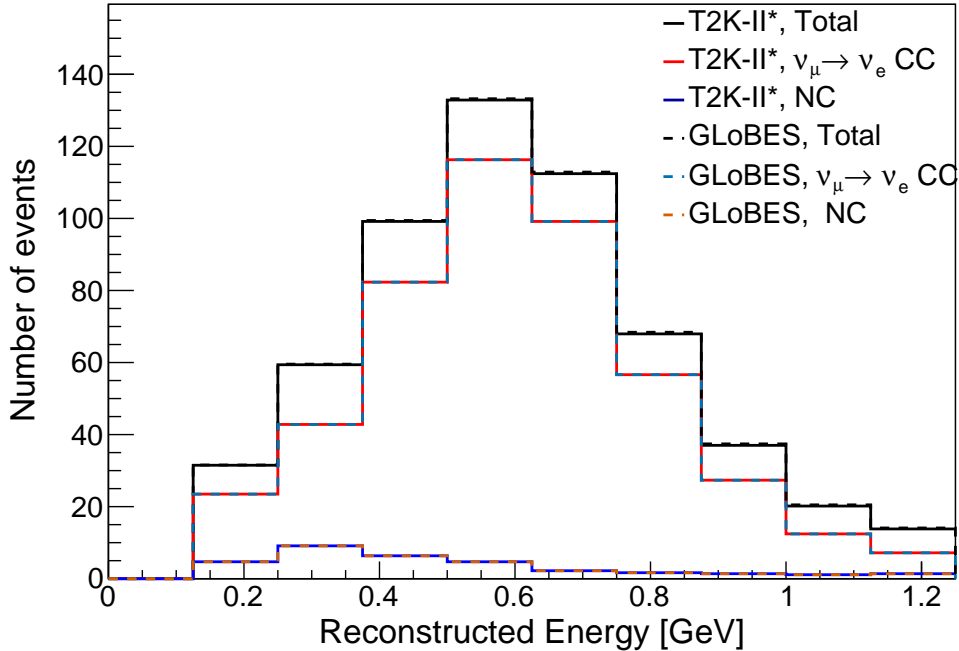
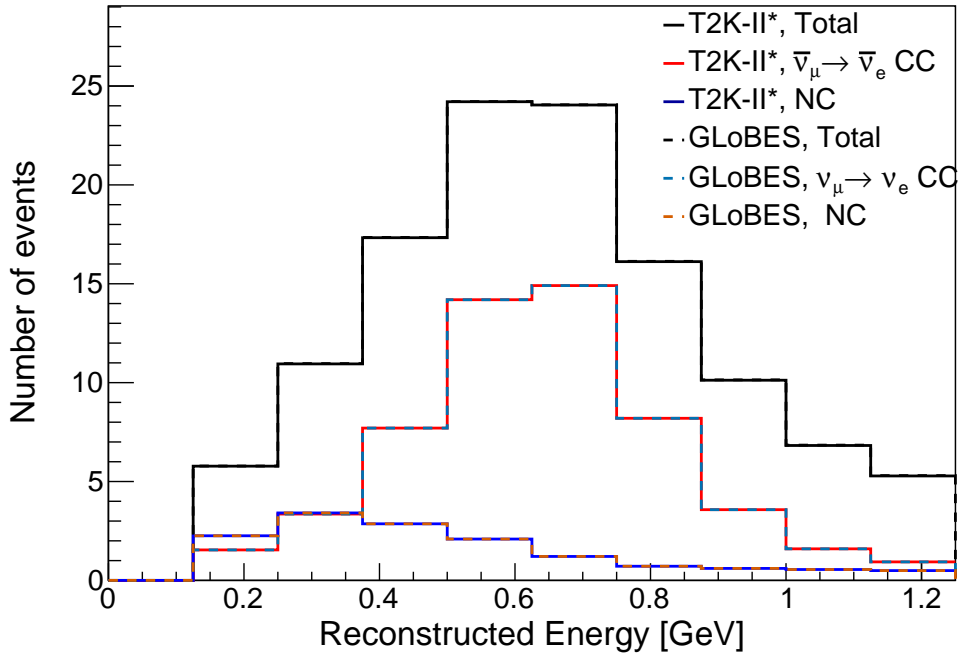


Figure 3-12: Expected event spectra of the signal and background as a function of reconstructed neutrino energy for T2K-II for appearance sample. The spectra are for ν -mode. Same oscillation parameters as Ref. [38] are used.


 Figure 3-13: Same as Figure 3-12, but for $\bar{\nu}$ -mode.

In the disappearance samples, the backgrounds come from ν_μ , $\bar{\nu}_\mu$ CC interaction excluding CCQE, hereby called CC-nonQE, and NC interactions. We use the updated T2K flux released along with Ref. [35]. In simulation, the cross section for low and high energy regions are taken from Ref. [40] and Ref. [41] respectively. In our T2K-II set-up, an exposure of 20×10^{21} POT equally divided among the ν -mode and the $\bar{\nu}$ -mode is considered along with a 50% effectively statistic improvement as presented in Ref. [2]. The signal and background efficiencies and the spectral information for T2K-II are obtained by scaling the T2K analysis reported in Ref. [38] to same exposure as the T2K-II proposal. In Fig. 3-12 and 3-13, the T2K-II expected spectra of the signal and background events of

Table 3.5: Detection efficiencies(%)^a of signal and background events in appearance samples. Normal mass hierarchy and $\delta_{CP} = 0$ are assumed.

		$\nu_\mu \rightarrow \nu_e$	$\bar{\nu}_\mu \rightarrow \bar{\nu}_e$	ν_μ CC	$\bar{\nu}_\mu$ CC	ν_e CC	$\bar{\nu}_e$ CC	NC
T2K-II	ν mode	65.5	46.2	0.02	0.02	19.8	19.8	0.41
	$\bar{\nu}$ mode	45.8	70.7	0.01	0.01	17.5	17.5	0.45
NOνA-II	ν mode	62.0	38.0	0.15	–	79.0	69.0	0.87
	$\bar{\nu}$ mode	25.0	67.0	0.14	0.05	20.7	40.7	0.51

^adefined per each interaction channel as the ratio of selected events in the data sample to the totally simulated interaction supposed to happen in the detector.

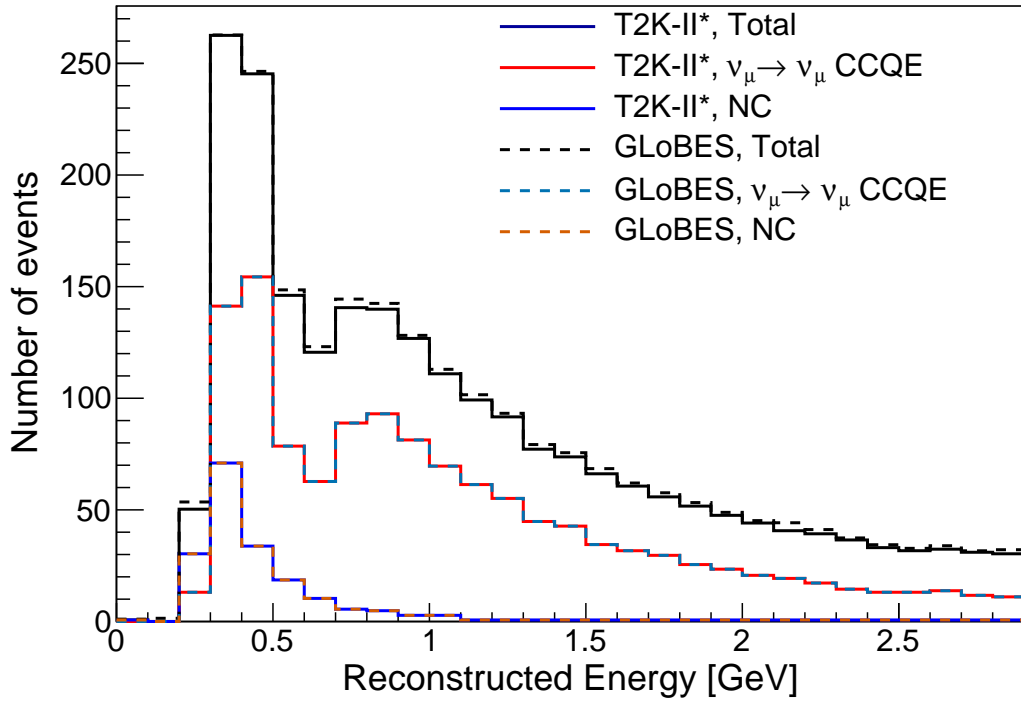


Figure 3-14: Expected event spectra of the signal and background as a function of reconstructed neutrino energy for T2K-II disappearance sample. The spectra are for ν -mode. Same oscillation parameters as Ref. [38] are used.

appearance samples as a function of reconstructed neutrino and antineutrino energy, respectively obtained with GLoBES are compared to those of Monte-Carlo simulation scaled from Ref. [2]. A 3% error is assigned for both the energy resolution and the normalization uncertainties of the signal and background in all simulated samples. Fig. 3-14 and 3-15 show the T2K-II expected spectra of the signal and background events of disappearance samples as a function of reconstructed neutrino energy.

For NO ν A-II, we consider a total exposure of 72×10^{20} POT equally divided among ν -mode and $\bar{\nu}$ -mode [21]. We predict the neutrino fluxes at the NO ν A far detector by using the flux information from the near detector given in Ref. [37] and

Table 3.6: Detection efficiencies(%) of signal and background events in disappearance samples. Normal mass hierarchy is assumed .

		ν_μ CCQE	ν_μ CC non-QE	$\bar{\nu}_\mu$ CCQE	$\bar{\nu}_\mu$ CC non-QE	$(\nu_e + \bar{\nu}_e)$ CC	NC	$\nu_\mu \rightarrow \nu_e$
T2K-II	ν mode	71.2	20.4	71.8	20.4	0.84	2.7	0.84
	$\bar{\nu}$ mode	65.8	24.5	77.5	24.5	0.58	2.5	0.58
NOνA-II	ν mode	31.2 ^b		27.2		–	0.44	–
	$\bar{\nu}$ mode	33.9		20.5		–	0.33	–

^bthe efficiencies for CCQE and CC non-QE interactions are considered equal.

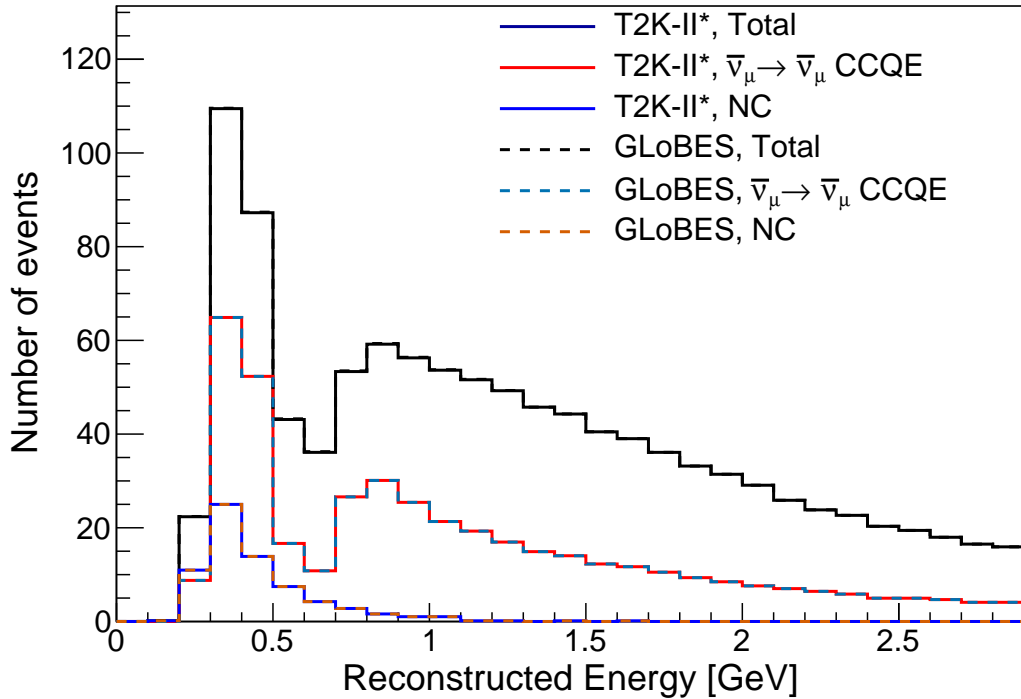


Figure 3-15: Same as Figure 3-14, but for $\bar{\nu}$ -mode.

normalizing it with the square of their baseline ratio. A 5% systematic error for all samples and 8-10% sample-dependent energy resolutions are assigned. Significant background events in the appearance samples stem from the intrinsic beam $\nu_e/\bar{\nu}_e$, NC components, and cosmic muons. In the appearance sample of the $\bar{\nu}$ -mode, *wrong-sign* events from ν_e appearance events are included as the backgrounds in the simulation. We use the reconstructed energy spectra of the NO ν A far detector simulated sample reported in Ref. [42] to tune our GLoBES simulation. The low- and high-particle identification (PID) score samples are used but not the peripheral sample since the reconstructed energy information is not available. In the disappearance samples of both ν -mode and $\bar{\nu}$ -mode, events from both CC ν_μ and $\bar{\nu}_\mu$ interactions are considered as signal events, which is tuned to match with the NO ν A far detector simulated signal given an identical exposure. Background from the NC ν_μ ($\bar{\nu}_\mu$) interactions is taken into consideration and weighted such that the rate at a predefined exposure is matched to a combination of the reported NC and cosmic muon backgrounds in Ref. [42]. Fig. 3-16 and 3-17 show the simulated NO ν A-II event spectra for ν_e appearance as a function of reconstructed neutrino energy, in both ν -mode and $\bar{\nu}$ -mode, where *normal* MH is assumed, δ_{CP}

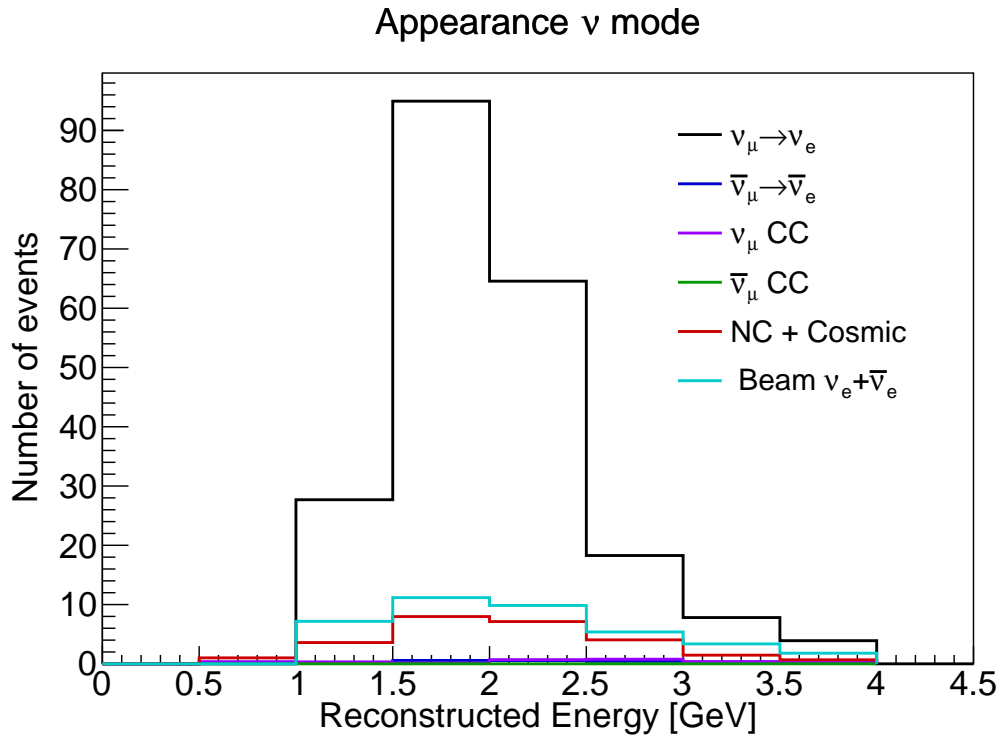


Figure 3-16: Expected event spectra of the signal and background as a function of reconstructed neutrino energy for NO ν A-II for the appearance channel. The spectra are for ν -mode. *Normal* MH, $\delta_{CP} = 0$, and other oscillation parameters given in Tab. 2.1 are assumed.

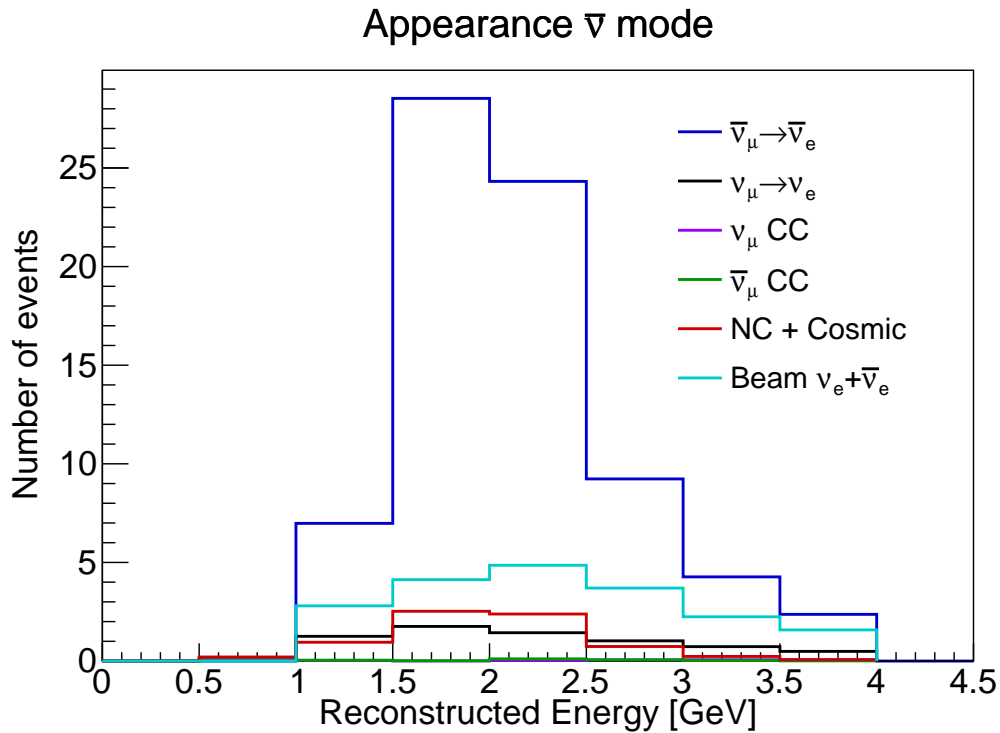


Figure 3-17: Same as Figure 3-16, but for $\bar{\nu}$ -mode.

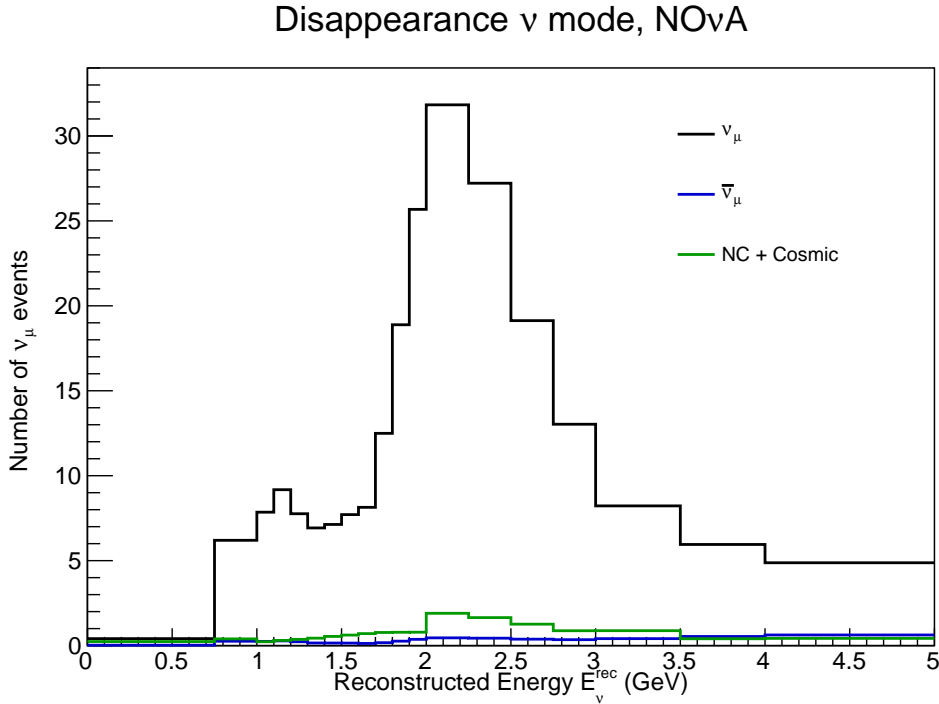


Figure 3-18: Expected event spectra of the signal and background as a function of reconstructed neutrino energy for NO ν A-II for disappearance channel. The spectra are for ν -mode. *Normal* MH, $\delta_{CP} = 0$, and other oscillation parameters given in Tab. 2.1 are assumed.

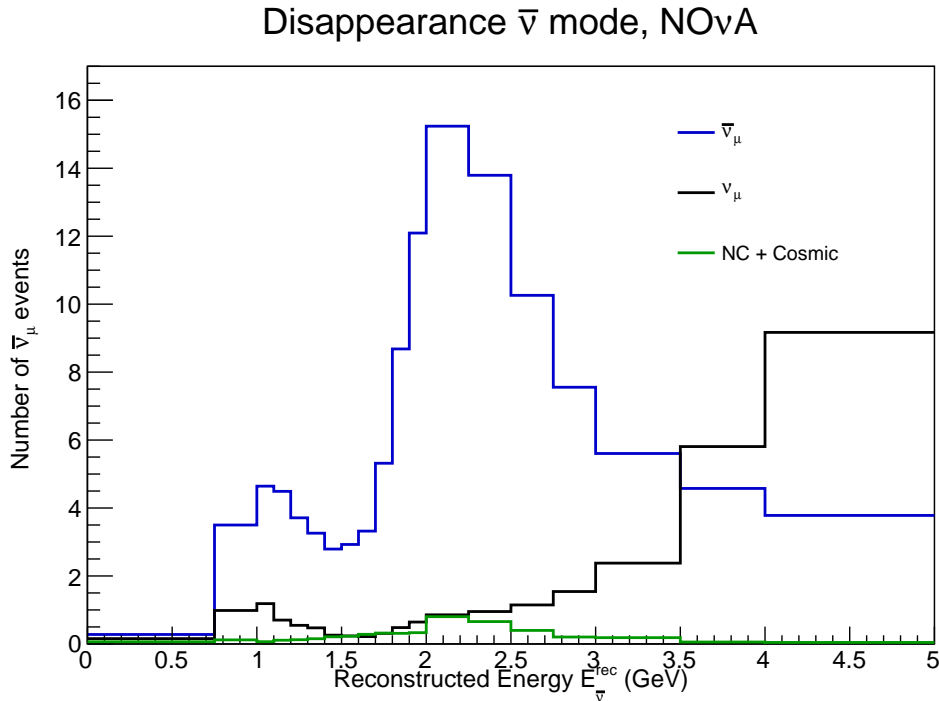


Figure 3-19: Same as Figure 3-18, but for $\bar{\nu}$ -mode.

is fixed at 0° , and other parameters are given in Table 2.1. The event spectra for ν_μ disappearance channels in neutrino and antineutrino mode are presented in Figures 3-18 and 3-19, respectively. Tables 3.5 and Table 3.6 detail our calculated signal and background detection efficiencies for the electron (anti-)neutrino appearance and muon (anti-)neutrino disappearance respectively in T2K and NO ν A.

3.3.2 JUNO

In JUNO, the electron anti-neutrino $\bar{\nu}_e$ flux, which is produced mainly from four radioactive isotopes ^{235}U , ^{238}U , ^{239}Pu , and ^{241}Pu [23], is simulated with an assumed detection efficiency of 73%. The backgrounds, which have a marginal effect on the MH sensitivity, are not included in our simulation. In our setup, to speed up the calculation, we consider one core of 36 GW thermal power with an average baseline of 52.5 km instead of the true distribution of the reactor cores, baselines, and powers. The simulated JUNO specification is listed in Table 3.7.

For systematic errors, we use 1% commonly for the errors associated with the uncertainties of the normalization of the $\bar{\nu}_e$ flux produced from the reactor core, the normalization of the detector mass, the spectral normalization of the signal, the detector response to the energy scale, the isotopic abundance, and the bin-to-bin reconstructed energy shape.

Table 3.7: JUNO simulated specifications

Characteristics	Inputs
Baseline	52.5 km
Density	2.8 gcc^{-1} [43]
Detector type	Liquid Scintillator
Detector mass	20 kton
$\bar{\nu}_e$ Detection Efficiency	73%
Running time	6 years
Thermal power	36 GW
Energy resolution	3% / \sqrt{E} (MeV)
Energy window	1.8-9 MeV
Number of bins	200

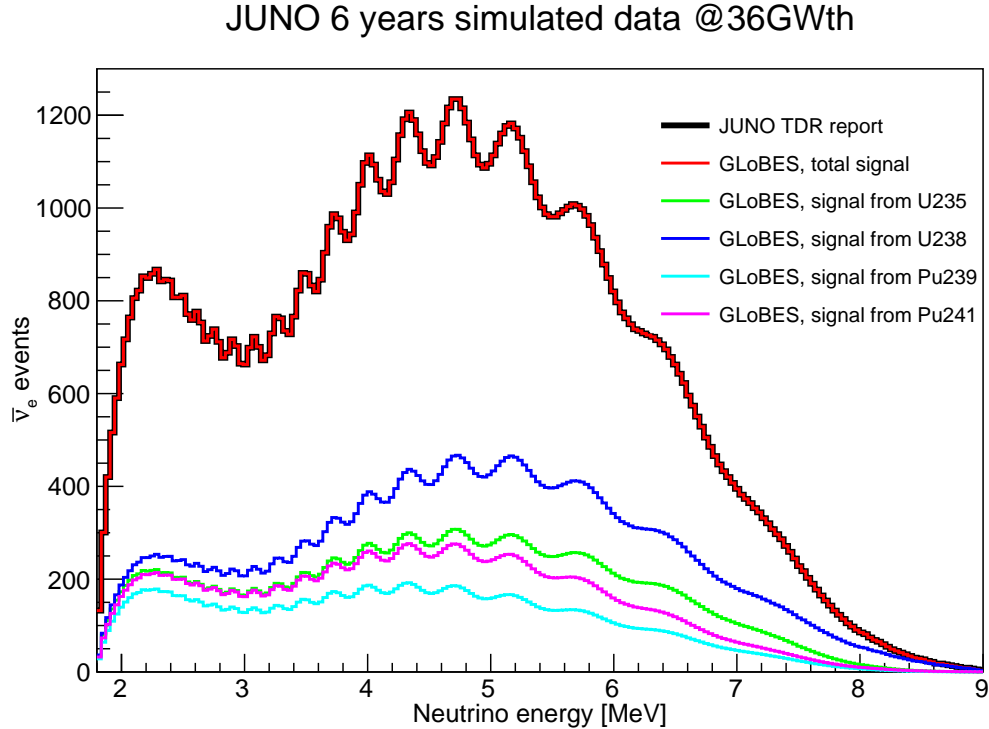


Figure 3-20: JUNO event rate calculated at same oscillation parameters as Ref. [22]

3.4 Discussion

The two neutrino experiments T2K-II and NO ν A-II reach a relatively similar performance for selecting the electron (anti-)neutrino appearance samples. While T2K-II gains to the excellent separation of muons and electrons with the water Cherenkov detector, NO ν A-II boosts the selection performance with the striking features of the liquid scintillator and the powerful deep learning. For selecting the disappearance samples, T2K outperforms since the T2K far detector is placed deep underground while the NO ν A far detector is on the surface and suffers a much higher rate of cosmic ray muons. Besides T2K-II, NO ν A-II, and JUNO, we implement a R-SBL neutrino experiment to constrain $\sin^2 \theta_{13}$ at 3% uncertainty, which is reachable as prospected in Ref. [44]. This constraint is important to break the parameter degeneracy between $\delta_{\text{CP}}-\theta_{13}$, which is inherent from the measurement with the electron (anti-)neutrino appearance samples in the A-LBL experiments.

Bibliography

- [1] **T2K Collaboration** *et al.* The T2K experiment. *Nuclear Instruments and Methods in Physics Research Section A: Accelerators, Spectrometers, Detectors and Associated Equipment* **659**, 106–135, 2011. [1106.1238](#).
- [2] **T2K Collaboration** *et al.* Sensitivity of the T2K accelerator-based neutrino experiment with an extended run to 20×10^{21} POTs , 2016. [1607.08004](#).
- [3] **Hyper-Kamiokande Proto-Collaboration** *et al.* Hyper-Kamiokande Design Report , 2018. [1805.04163](#).
- [4] Otani, M. *et al.* Design and construction of INGRID neutrino beam monitor for T2K neutrino experiment. *Nucl. Instrum. Meth. A* **623**, 368–370, 2010.
- [5] Abgrall, N. *et al.* Time Projection Chambers for the T2K Near Detectors. *Nucl. Instrum. Meth. A* **637**, 25–46, 2011. [1012.0865](#).
- [6] Amaudruz, P. A. *et al.* The T2K Fine-Grained Detectors. *Nucl. Instrum. Meth. A* **696**, 1–31, 2012. [1204.3666](#).
- [7] Abe, K. *et al.* Measurements of the T2K neutrino beam properties using the INGRID on-axis near detector. *Nucl. Instrum. Meth. A* **694**, 211–223, 2012. [1111.3119](#).
- [8] Itow, Y. *et al.* The JHF-Kamioka neutrino project. In *3rd Workshop on Neutrino Oscillations and Their Origin (NOON 2001)*. 239–248, 2001. [hep-ex/0106019](#).
- [9] Fukuda, Y. *et al.* Measurements of the solar neutrino flux from super-kamiokande’s first 300 days. *Physical review letters* **81** (6), 1158, 1998.
- [10] Abe, K. *et al.* The T2K experiment. *Nuclear Instruments and Methods in Physics Research Section A: Accelerators, Spectrometers, Detectors and Associated Equipment* **659** (1), 106–135, 2011.
- [11] Fukuda, Y. *et al.* The Super-Kamiokande detector. *Nucl. Instrum. Meth. A* **501**, 418–462, 2003.

- [12] **T2K Collaboration** *et al.* Observation of electron neutrino appearance in a muon neutrino beam. *Physical Review Letters* **112**, 061802, 2014. [1311.4750](#).
- [13] **T2K Collaboration** *et al.* Constraint on the matter-antimatter symmetry-violating phase in neutrino oscillations. *Nature* **580** (7803), 339–344, 2020. [Erratum: *Nature* 583, E16 (2020)], [1910.03887](#).
- [14] Dunne, P. Latest neutrino oscillation results from T2K, 2020. URL <https://doi.org/10.5281/zenodo.4154355>.
- [15] **NO ν A Collaboration** *et al.* The NO ν A Technical Design Report , 2007.
- [16] Kafka, T. MINOS Experiment at Fermilab. *Prog. Part. Nucl. Phys.* **64**, 184–186, 2010.
- [17] Adamson, P. *et al.* The NuMI Neutrino Beam. *Nucl. Instrum. Meth. A* **806**, 279–306, 2016. [1507.06690](#).
- [18] Nayak, N. *A Joint Measurement of ν_{μ} -Disappearance and ν_e -Appearance in the NuMI beam using the NO ν A Experiment*. Ph.D. thesis, UC, Irvine (main), UC, Irvine, 2021.
- [19] **NO ν A Collaboration** *et al.* First measurement of neutrino oscillation parameters using neutrinos and anti-neutrinos by NO ν A. *Physical Review Letters* **123** (15), 151803, 2019. [1906.04907](#).
- [20] Himmel, A. New oscillation results from the nova experiment, 2020. URL <https://doi.org/10.5281/zenodo.4142045>.
- [21] **NO ν A Collaboration**, M. Sanchez. NO ν A results and prospects. *XXVIII International Conference on Neutrino Physics and Astrophysics* , 2018.
- [22] **JUNO Collaboration** *et al.* JUNO Conceptual Design Report , 2015. [1508.07166](#).
- [23] Huber, P. & Schwetz, T. Precision spectroscopy with reactor anti-neutrinos. *Physical Review D* **70** (5), 053011, 2004. [0407026](#).

- [24] Abusleme, A. *et al.* Calibration Strategy of the JUNO Experiment , 2020. [2011.06405](#).
- [25] Barger, V. *et al.* Breaking eight fold degeneracies in neutrino CP violation, mixing, and mass hierarchy. *Phys. Rev. D* **65**, 073023, 2002. [hep-ph/0112119](#).
- [26] **Daya Bay Collaboration** *et al.* A Precision measurement of the neutrino mixing angle θ_{13} using reactor antineutrinos at Daya-Bay , 2007. [0701029](#).
- [27] **Double Chooz Collaboration** *et al.* Double Chooz: A Search for the neutrino mixing angle $\theta(13)$, 2006. [0606025](#).
- [28] **RENO Collaboration** *et al.* RENO: An Experiment for Neutrino Oscillation Parameter θ_{13} Using Reactor Neutrinos at Yonggwang , 2010. [1003.1391](#).
- [29] Huber, P. *et al.* Simulation of long-baseline neutrino oscillation experiments with GLoBES (General Long Baseline Experiment Simulator). *Computer Physics Communications* **167**, 195, 2005. [0407333](#).
- [30] Huber, P. *et al.* New features in the simulation of neutrino oscillation experiments with GLoBES 3.0. *Computer Physics Communications* **177** (5), 432–438, 2007. [hep-ph/0701187](#).
- [31] Abe, K. *et al.* Improved constraints on neutrino mixing from the T2K experiment with 3.13×10^{21} protons on target. *Phys. Rev. D* **103** (11), 112008, 2021. [2101.03779](#).
- [32] Acero, M. A. *et al.* An Improved Measurement of Neutrino Oscillation Parameters by the NOvA Experiment , 2021. [2108.08219](#).
- [33] Abe, K. *et al.* T2K neutrino flux prediction. *Phys. Rev. D* **87** (1), 012001, 2013. [Addendum: *Phys.Rev.D* 87, 019902 (2013)], [1211.0469](#).
- [34] Abgrall, N. *et al.* Measurements of π^\pm , K^\pm , K_S^0 , Λ and proton production in proton–carbon interactions at 31 GeV/c with the NA61/SHINE spectrometer at the CERN SPS. *Eur. Phys. J. C* **76** (2), 84, 2016. [1510.02703](#).

- [35] Abe, K. *et al.* Measurements of neutrino oscillation in appearance and disappearance channels by the T2K experiment with 6.6×10^{20} protons on target. *Phys. Rev. D* **91** (7), 072010, 2015. [1502.01550](#).
- [36] **NO ν A Collaboration**, A. Himmel. *New Oscillation Results from the NO ν A Experiment*. In *XXIX International Conference on Neutrino Physics and Astrophysics*, 2020.
- [37] Soplin, L. A. & Cremonesi, L. NO ν A near detector fluxes. <https://nova-docdb.fnal.gov/cgi-bin/ShowDocument?docid=25266>, 2018.
- [38] **T2K Collaboration** *et al.* Measurement of neutrino and antineutrino oscillations by the T2K experiment including a new additional sample of ν_e interactions at the far detector. *Physical Review D* **96** (9), 092006, 2017. [Erratum: *Phys.Rev.D* 98, 019902 (2018)], [1707.01048](#).
- [39] Dziewonski, A. M. & Anderson, D. L. Preliminary reference earth model (PREM). *Physics of the earth and planetary interiors* **25** (4), 297–356, 1981.
- [40] Messier, M. D. *Evidence for neutrino mass from observations of atmospheric neutrinos with Super-Kamiokande*. Ph.D. thesis, Boston University, 1999. UMI-99-23965.
- [41] Paschos, E. A. & Yu, J. Y. Neutrino interactions in oscillation experiments. *Physical Review D* **65**, 033002, 2002. [hep-ph/0107261](#).
- [42] **NO ν A Collaboration** *et al.* New constraints on oscillation parameters from ν_e appearance and ν_μ disappearance in the NO ν A experiment. *Physical Review D* **98** (3), 032012, 2018. [1806.00096](#).
- [43] Khan, A. N. *et al.* Why matter effects matter for JUNO? *Physics Letters B* **803**, 135354, 2020. [1910.12900](#).
- [44] Cao, J. & Luk, K.-B. An overview of the Daya Bay Reactor Neutrino Experiment. *Nucl. Phys. B* **908**, 62–73, 2016. [1605.01502](#).

Chapter 4

Leptonic CP Violation and Mass-Hierarchy in T2K-II, NO ν A-II and JUNO

4.1 Introduction

The sensitivity of the A-LBL experiments such as T2K and NO ν A to δ_{CP} and MH can be understood via the following expression of the so-called CP asymmetry [1] presenting a relative difference between $P_{(\nu_\mu \rightarrow \nu_e)}$ and $P_{(\bar{\nu}_\mu \rightarrow \bar{\nu}_e)}$ near the oscillation maximum, corresponding to $\frac{|\Delta m_{31}^2|L}{4E_\nu} = \pi/2$.

$$A_{CP} \left(\frac{|\Delta m_{31}^2|L}{4E_\nu} = \pi/2 \right) = \frac{P_{(\nu_\mu \rightarrow \nu_e)} - P_{(\bar{\nu}_\mu \rightarrow \bar{\nu}_e)}}{P_{(\nu_\mu \rightarrow \nu_e)} + P_{(\bar{\nu}_\mu \rightarrow \bar{\nu}_e)}} \sim -\frac{\pi \sin 2\theta_{12}}{\tan \theta_{23} \sin 2\theta_{13}} \frac{\Delta m_{21}^2}{|\Delta m_{31}^2|} \sin \delta_{CP} \pm \frac{L}{2800km}, \quad (4.1)$$

where $+$ ($-$) sign is taken for the *normal* (*inverted*) MH respectively. The relation shows that the matter effect due to the baseline (L), in the second term, produces a fake asymmetry along with the intrinsic CP violation asymmetry due to δ_{CP} . With longer baselines the asymmetry due to matter effects dominates over that of δ_{CP} . Figure 4-1 shows the baseline dependence of A_{CP} with matter effect. It is inevitable to remove the effect of the fake asymmetry caused by matter effect unless the baseline is very short. This will be the window to measure $\sin \delta_{CP}$.

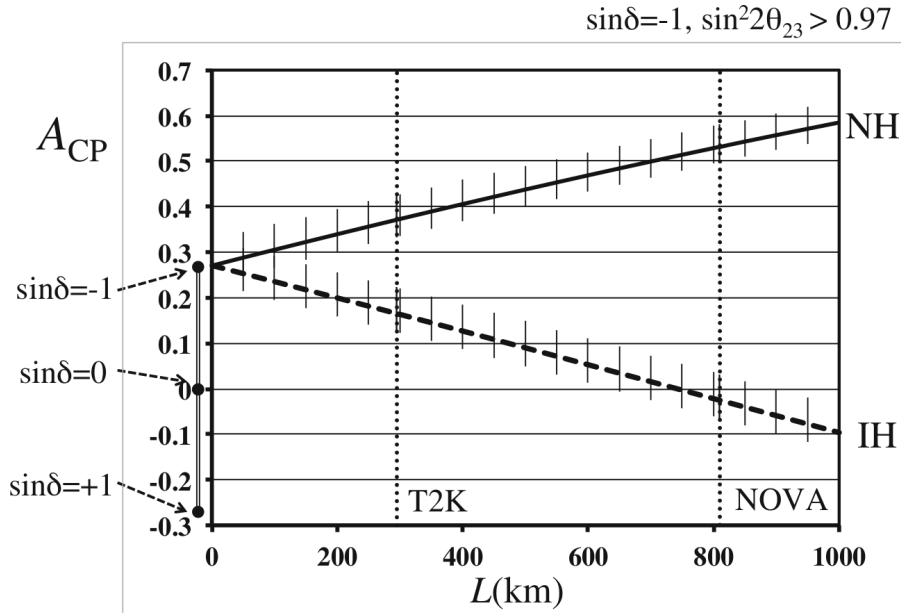


Figure 4-1: Baseline dependence on A_{CP} . The thin vertical lines show the ambiguity from the θ_{23} octant degeneracy. The positions of the intercept at $L = 0$ for $\sin \delta_{CP} = 0, \pm 1$ are shown [1].

By combining experiments at different baselines, it is possible to know the mass hierarchy and obtain the genuine CP asymmetry. Moreover, the antineutrino-nucleus cross-sections are one-third of the neutrino-nucleus cross-sections, and as such, three times antineutrino flux is necessary to obtain equivalent statistical uncertainties for the ν_e event detection. Therefore, a very high neutrino flux and a large detector mass are necessary to measure the CP violation. Upcoming experiment T2HK is considering the method to emphasize on the problem.

Determining the Δm_{31}^2 mass hierarchy is an important next experimental target, not only for the CP asymmetry measurement, but because it is related to the lower limit of the absolute neutrino masses. With values listed in Table 2.1, Equation 4.1 gives $\frac{\pi \sin 2\theta_{12}}{\tan \theta_{23} \sin 2\theta_{13}} \frac{\Delta m_{21}^2}{|\Delta m_{31}^2|} \sim 0.256$, which means the CP violation effect can be observed somewhat between -25.6% and $+25.6\%$. For a 295 km baseline of the T2K experiment, mass hierarchy effect is subdominant with $\sim 10.5\%$. T2K uses a near detector complex, situated 280 m from the production target to constrain the neutrino flux and the neutrino interaction model.

A longer baseline allows NO ν A to explore the MH with high sensitivity via the matter effect on the (anti-)neutrino interactions. From Eq. 4.1, it can be estimated that the matter effect in NO ν A is $\sim 28.9\%$, which is slightly higher than the CP

violation effect. However, these two effects, along with the ambiguity of the θ_{23} octant, are largely entangled. In other words, NO ν A sensitivity on the neutrino MH depends on the value of δ_{CP} . From Figure 2-4, we observe that the separation between NH and IH of NO ν A is larger compared to T2K. This is a manifestation of the increased matter effect because of the longer baseline in NO ν A.

NO ν A's recent data [2] does not provide as much preference to the neutrino mass hierarchy as T2K [3] does since NO ν A data shows no indication of the CP violation. As in NuFIT 5.0 data, the best fit in the global analysis remains for the normal mass hierarchy. Without the atmospheric experiment SK, IH rejection is poor with a value of $\Delta\chi^2 = 2.7$ only, which is equivalent to 1.6σ C.L. The result is driven by the updated data from A-LBL T2K and NO ν A. However, driven by the better compatibility between the $\Delta m_{31(2)}^2$ determined in ν_μ ($\bar{\nu}_\mu$) disappearance at A-LBL experiments and $\bar{\nu}_e$ disappearance at reactors, the combined global analysis favours NH. If atmospheric data from SK is considered in the global analysis, IH is rejected with an improved sensitivity of $\Delta\chi^2 = 7.3$, which is equivalent to 2.7σ C.L..

The measurement of δ_{CP} mostly comes from the A-LBL experiments. The best fit for the CP violating phase is now favoured at $\delta_{CP} = 195^\circ$. Compared to NuFIT 4.1, the allowed range of δ_{CP} has moved towards CP conserving value. The CP conserving value is now favoured at 0.6σ irrespective of the SK data. If we restrict the mass hierarchy to IO, the best fit of δ_{CP} remains close to $\frac{3\pi}{2}$, CP symmetry being maximally violated. In such case, CP conserving values are rejected at about 3σ .

Unlike the methods exploited by accelerator experiments, a different technique of resolving the MH can give a better resolution to the leptonic CP violation measurement.

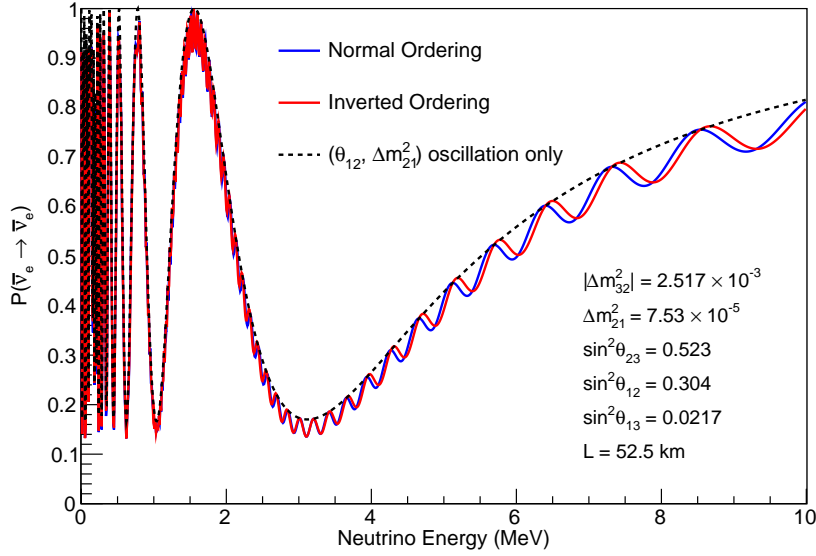


Figure 4-2: Electron antineutrino disappearance probability for JUNO.

4.1.1 Importance of JUNO

There is another method to determine the mass hierarchy by reactor based experiments. The reactor-based medium baseline experiment JUNO primarily aims to determine the MH by measuring the surviving $\bar{\nu}_e$ spectrum, which uniquely displays the oscillation patterns driven by both solar and atmospheric neutrino mass-squared splittings [4]. This feature can be understood via the $\bar{\nu}_e$ disappearance probability in vacuum expressed as follow:

$$P_{(\bar{\nu}_e \rightarrow \bar{\nu}_e)} = 1 - \cos^4 \theta_{13} \sin^2 2\theta_{12} \sin^2 \Phi_{21} - \sin^2 2\theta_{13} (\cos^2 \theta_{12} \sin^2 \Phi_{31} + \sin^2 \theta_{12} \sin^2 \Phi_{32}) \quad (4.2)$$

where $\Phi_{ij} = \frac{\Delta m_{ij}^2 L}{4E_\nu}$. An averaged 52.5 km baseline of the JUNO experiment is to obtain the maximum oscillation corresponding to $\Phi_{21} = \pi/2$ around 3 MeV, and relatively enhances the oscillation patterns driven by Φ_{31} and Φ_{32} terms. If the energy spectrum is analyzed the Fourier analysis with a parameter $1/E_\nu$, three peaks at $|\Delta m_{21}^2|$, $|\Delta m_{31}^2|$ and $|\Delta m_{32}^2|$ are observed in the frequency space. The Δm_{21}^2 peak locates much lower than the Δm_{31}^2 and Δm_{32}^2 peaks in the frequency and be distinguished very easily. Since, $\sin^2 \theta_{12} \sim 0.3$ and $\sin^2 \theta_{12} < \cos^2 \theta_{12}$, the amplitude of the terms containing $\sin \Phi_{31}$ is larger than that of $\sin \Phi_{32}$. This means the larger peak corresponds to $|\Delta m_{31}^2|$ and the smaller peak corresponds to $|\Delta m_{32}^2|$.

If the higher frequency peak is larger than that of the lower frequency peak, it means $|\Delta m_{31}^2| > |\Delta m_{32}^2|$, it corresponds to the normal hierarchy, and vice versa. To attain it, a very good resolution is still required for the neutrino detector. The oscillation behaviour of JUNO to $\bar{\nu}_e$ disappearance is shown in Figure 4-2.

4.2 Method of χ^2 analysis

We use the following χ^2 function for LBNEs in our analysis.

$$\chi^2 = \text{Min}_{\zeta_s, \zeta_b} \left[2 \sum_{i=1}^n (N_i^{\text{test}} - N_i^{\text{true}} - N_i^{\text{true}} \ln \frac{N_i^{\text{test}}}{N_i^{\text{true}}}) + \zeta_s^2 + \zeta_b^2 \right] \quad (4.3)$$

$$N_i^{\text{test}}(\zeta_s, \zeta_b) = N_i^{\text{pr}}[1 + s^s] + N_i^b[1 + s^b] \text{ and } N_i^{\text{true}} = N_i^{\text{ex}} + N_i^b \quad (4.4)$$

where,

- N_i^{pr} is the predicted no. of signal events in the i -th bin for a set of oscillation parameters.
- N_i^b is the no. of charged current backgrounds and NC backgrounds do not depend on the oscillation parameters.
- N_i^{ex} is the no. of observed current signal events in the i -th bin.
- The quantities s^s and s^b are the systematic (normalisation) errors on the signal and background respectively.
- The quantities ζ_s and ζ_b are the ‘‘pulls’’ due to systematic error on signal and background respectively.
- The minimization is performed independently for all the pulls of a particular oscillation channel. The total χ^2 for the considered experiment is obtained by repeating the process for all the oscillation channels and their χ^2 values.
- The appearance and disappearance oscillation channels and the respective signal and background events selected for the T2K-II, NO ν A-II experiments are given in Tables 3.5 and 3.6, respectively.

4.2. Method of χ^2 analysis

- To estimate the total χ^2 , we sum up its contribution from all the relevant simulated data samples in an experiment and minimize over the nuisance parameters.

$$\chi_{T2K-II(NO\nu A-II)}^2 = \text{Min}_{\zeta_s, \zeta_b} [\chi_{\mu e}^2 + \chi_{\mu\mu}^2 + \chi_{\bar{\mu}e}^2 + \chi_{\bar{\mu}\mu}^2]$$

For reactor neutrinos from JUNO, we use a Gaussian formula to obtain the value of χ^2 for electron anti-neutrino disappearance channel, given by

$$\chi_{\bar{e}e}^2 = \sum_{i=1}^{bins} \left(\frac{(N_i^{true} - (1 + a_R + a_D)N_i^{test})^2}{N_i^{true}} + \sum_{j=1}^{R,D} \frac{a_j^2}{\sigma_j^2} \right) \quad (4.5)$$

- a_R and a_D are the small uncertainties in the reactor flux and the fiducial mass of the detector, and their respective standard deviations are σ_R and σ_D . To obtain the χ^2 for JUNO, the $\chi_{\bar{e}e}^2$ is summed over four isotopes.
- $\chi_{total}^2 = \chi_{T2K-II}^2 + \chi_{NO\nu A-II}^2 + \chi_{JUNO}^2$ is then minimized over the marginalized oscillation parameters (See Table 4.1) in addition to the systematic parameters (See Table 4.2 and 4.3) to obtain the statistical significance on the hyperplane of parameters of interest.

Table 4.1: Varying $\theta_{13}, \theta_{23}, \delta_{CP}, \Delta m_{31}^2$ for the marginalisation procedure .

Parameter	Range
$\sin^2 \theta_{12}$	Fixed
$\sin^2 \theta_{13} (\times 10^{-2})$	[0.02034, 0.02430]
$\sin^2 \theta_{23}$	[0.4, 0.6]
$\delta_{CP} (^\circ)$	[0, 2π]
$\Delta m_{21}^2 (10^{-5} \text{eV}^2/c^4)$	Fixed
$\Delta m_{31}^2 (10^{-3} \text{eV}^2/c^4)$	[2.4e-3-2.6e-3 eV^2]

Table 4.2: Systematics of $\nu_\mu (\bar{\nu}_\mu)$ disappearance and $\nu_e (\bar{\nu}_e)$ appearance channels at the FD in T2K-II and NO ν A.

Experiments	Signal/BG Normalization error	Calibration Error
T2K-II	3%	0.01%
NO ν A-II	5%	2.5%

Table 4.3: Systematics of $\bar{\nu}_e$ disappearance channel in JUNO.

Parameters	Error
Detector norm error	1%
Overall normalization error	1%
Energy scale	1%
Isotopic abundance error	1%

4.3 Mass Hierarchy

The following χ^2 definition are used to study Mass Hierarchy sensitivity studies in this thesis:

$$\chi^2(\delta_{true}) \sim \text{Min}(\theta_{23}, \Delta m_{31}^2, \delta_{test}) \sum \left(\chi_{\mu e}^2 + \chi_{\mu\mu}^2 + \chi_{\bar{\mu}e}^2 + \chi_{\bar{\mu}\mu}^2 + \chi_{ee}^2 \right) \quad (4.6)$$

Significance level, $\sigma = \sqrt{\Delta\chi^2} = \sqrt{\chi_{NH}^2 - \chi_{IH}^2}$ for true hierarchy as normal. (4.7)

- To estimate quantitatively the sensitivity of the experiment(s) to the MH determination, we calculate the statistical significance $\sqrt{\Delta\chi^2}$ to exclude the *inverted* MH given the null hypothesis is a *normal* MH.
- The sensitivity is calculated as a function of *true* δ_{CP} since for the A-LBL experiments, the capability to determine the MH depends on the values of the CP-violating phase.
- Technically, for each *true* value of δ_{CP} with *normal* MH assumed, marginalized χ^2 is calculated for each *test* value of δ_{CP} with the MH fixed *to inverted*.
- Then for each *true* value of δ_{CP} the minimum value of χ^2 , which is also equivalent to $\Delta\chi^2$ since the *test* value with *normal* MH assumed would give a minimum χ^2 close to zero, is obtained.

The results, in which we assume $\sin^2 \theta_{23} = 0.5$, are shown in Fig. 4-3 for different experimental setups: (i) JUNO only; (ii) NO ν A-II only; (iii) a joint of JUNO and NO ν A-II; and (iv) a joint of JUNO, NO ν A-II, T2K-II and R-SBL experiment. It

4.3. Mass Hierarchy

is expected that the MH sensitivity of JUNO is more than 3σ C.L. and does not depend on δ_{CP} . On the other hand, the $\text{NO}\nu\text{A-II}$ sensitivity to the MH depends strongly on the *true* value of δ_{CP} . A joint analysis of JUNO with the A-LBL experiments, $\text{NO}\nu\text{A-II}$ and T2K-II, shows a great boost in the MH determination. This is expected since a joint analysis will break the parameter degeneracy between δ_{CP} and the sign of Δm_{31}^2 . Due to the parameter degeneracy among δ_{CP} , the sign of Δm_{31}^2 , θ_{13} , and θ_{23} in the measurement with the A-LBL experiments, we also expect that the MH determination depends on the value of θ_{23} .

The combined sensitivity of all considered experiments at different values of θ_{23} : (i) maximal mixing at 45° ($\sin^2 \theta_{23} = 0.50$), (ii) LO at 41° ($\sin^2 \theta_{23} = 0.43$), and (iii) HO at 51° ($\sin^2 \theta_{23} = 0.60$), is shown in Fig. 4-4. In Fig. 4-5, we compare the MH sensitivity for two hypotheses: MH is *normal* and MH is *inverted*. The result reflects what we expect: (i) the MH resolving with JUNO is less sensitive to its truth since the dominant factor is the separation power between two oscillation frequencies driven by $|\Delta m_{31}^2|$ and $|\Delta m_{32}^2|$ shown in Eq. 4.2 and relatively large mixing angle θ_{12} ; and (ii) for the A-LBL experiment like T2K and $\text{NO}\nu\text{A}$, the MH is determined through the MH- δ_{CP} degeneracy resolving as concisely described in Eq. 4.1. The A_{CP} amplitude is almost unchanged when one switch from *normal* MH to *inverted* MH and simultaneously flip the sign of δ_{CP} . Those results conclude that the *wrong* mass hierarchy can be excluded at greater than 5σ C.L. for all the *true* values of δ_{CP} and for any value of θ_{23} in the range constrained by experiments. In the other words, the MH can be determined conclusively by a joint analysis of JUNO with the A-LBL experiments, $\text{NO}\nu\text{A-II}$ and T2K-II.

As pointed out in Ref. [1], the CPV sensitivity with the A-LBL neutrino experiments does not depend on the the true value of θ_{13} . However this is not the case for the MH sensitivity since the $\bar{\nu}_e$ disappearance rate in JUNO is proportional to $\sin^2 2\theta_{13}$ as shown in Eq. 4.2. This feature is presented in Fig. 4-6 where sensitivity of the neutrino MH are studied with three different values of $\sin^2 \theta_{13}$: $\sin^2 \theta_{13} = 0.02241$ is the best fit obtained with NuFIT 4.1 [5], $\sin^2 \theta_{13} = 0.02221$ is with NuFIT 5.0 [6], and $\sin^2 \theta_{13} = 0.02034$ is 3σ C.L. lower limit. Although the neutrino MH sensitivity is slightly reduced with smaller values of $\sin^2 \theta_{13}$, the MH

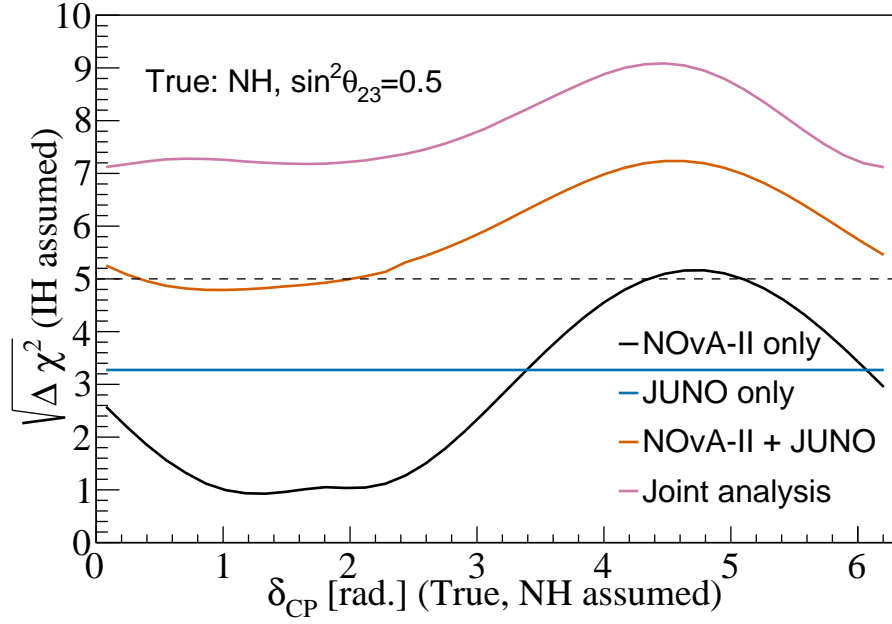


Figure 4-3: MH sensitivities as a function of *true* δ_{CP} calculated for various experimental setups. $\sin^2 \theta_{23} = 0.5$ is assumed to be true.

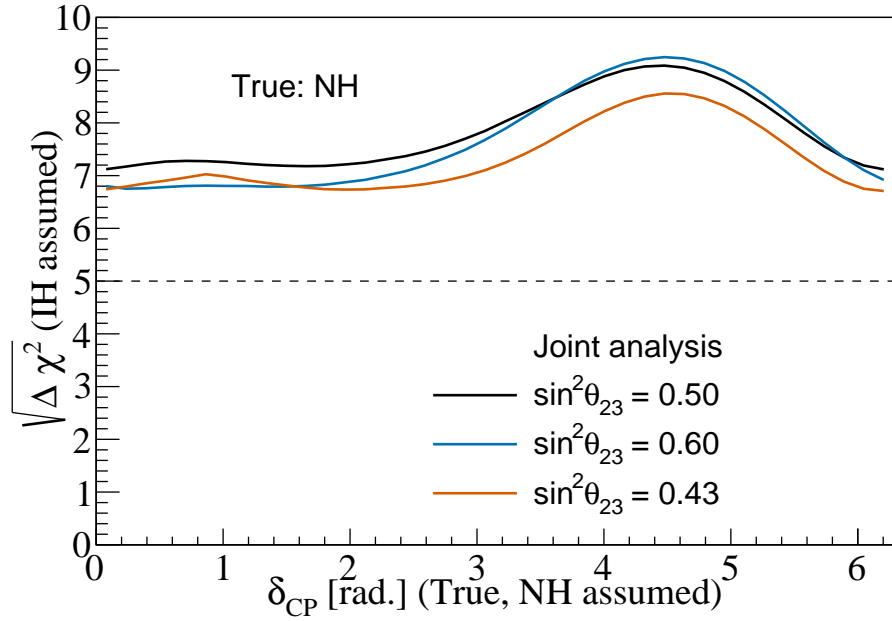


Figure 4-4: MH sensitivities as a function of *true* δ_{CP} calculated for the joint analyses of all considered experiments but at different $\sin^2 \theta_{23}$ values.

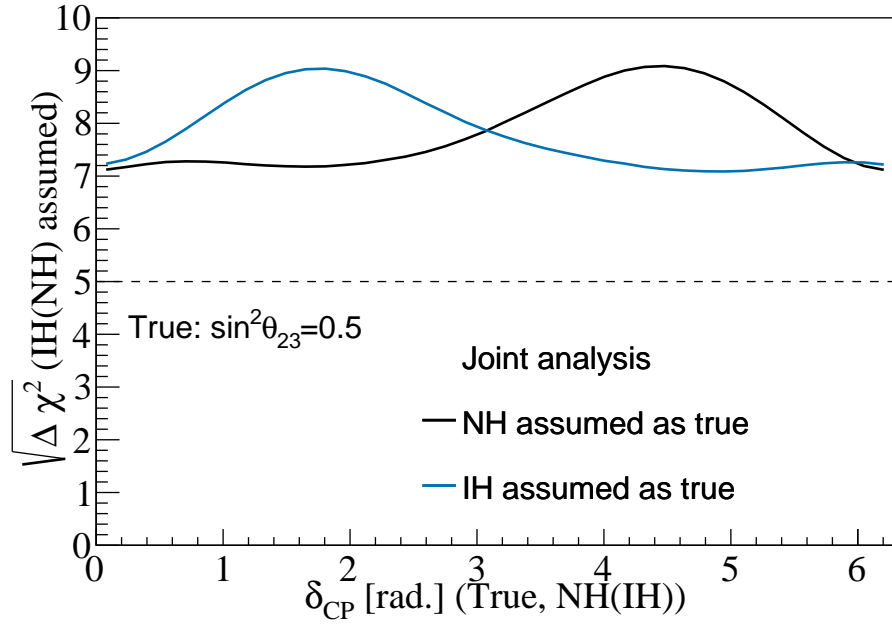


Figure 4-5: MH sensitivities as a function of *true* δ_{CP} calculated for all considered experiments for comparing two possible MH hypotheses. $\sin^2 \theta_{23} = 0.5$ is assumed to be true.

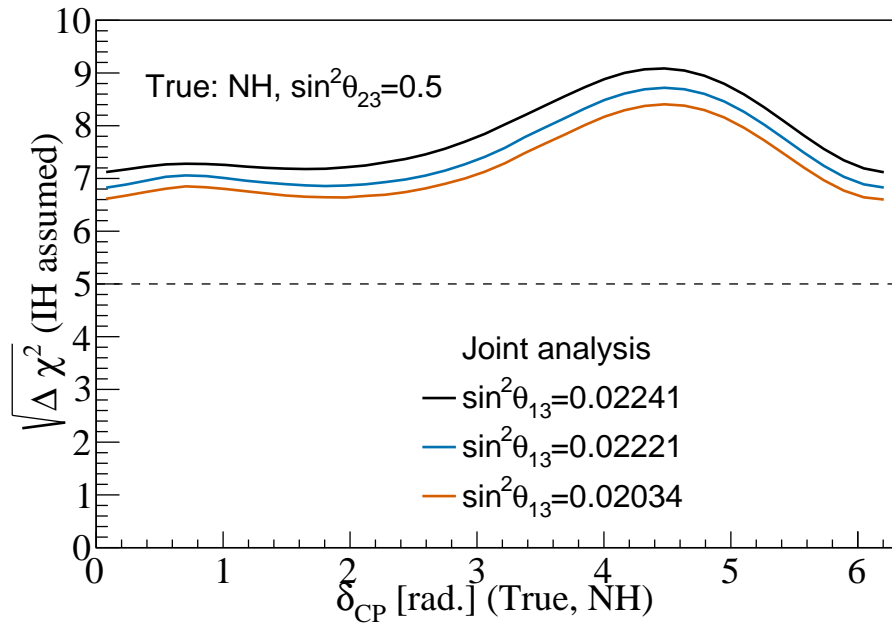


Figure 4-6: Dependence of the neutrino MH sensitivity on the θ_{13} true values: $\sin^2 \theta_{13} = 0.02241$ is the best fit obtained with NuFIT 4.1 [5], $\sin^2 \theta_{13} = 0.02221$ is with NuFIT 5.0 [6], and $\sin^2 \theta_{13} = 0.02034$ is 3σ C.L. lower limit. *Normal* MH and $\sin^2 \theta_{23} = 0.5$ are assumed to be true.

resolution is still well above 5σ C.L.

4.4 CP Violation

The statistical significance $\sqrt{\Delta\chi^2}$ to exclude the CP-conserving values ($\delta_{\text{CP}}=0,\pi$) or sensitivity to CPV is evaluated for any *true* value of δ_{CP} with the *normal* MH assumed.

$$\Delta\chi^2(\delta_{\text{true}}) \sim \text{Min}\left(\chi_{\text{total}}^2(\delta_{\text{true}}) - \chi_{\text{total}}^2(\delta_{\text{test}} = 0, \pm\pi)\right) \quad (4.8)$$

For the minimization of χ^2 over the MH options, we consider two cases: (i) MH is *known* and *normal*, same as the truth value or (ii) MH is *unknown*. Fig. 4-7 shows the CPV sensitivity as a function of the *true* value of δ_{CP} for both MH options obtained by different analyses: (i) T2K-II only; (ii) a joint T2K-II and R-SBL experiments; (iii) a joint of T2K-II, NO ν A-II and R-SBL experiments; and (iv) a joint of T2K-II, NO ν A-II, JUNO and R-SBL experiments. The result shows that whether the MH is *known* or *unknown* affects on the first three analyses, but not the fourth. This is because, as concluded in the above section, the MH can be determined conclusively with a joint analysis of all considered experiments.

It can be seen that the sensitivity to CP violation is driven by T2K-II and NO ν A-II. Contribution of the R-SBL neutrino experiment is significant only at the region where δ_{CP} is between 0 and π and when the MH is not determined conclusively. JUNO further enhances the CPV sensitivity by lifting up the overall MH sensitivity and consequently breaking the MH- δ_{CP} degeneracy. At δ_{CP} close to $-\pi/2$, which is indicated by recent T2K data [7], the sensitivity of the joint analysis with all considered experiments can reach approximately the 5σ C.L.. We also calculate the statistical significance of the CPV sensitivity as a function of *true* δ_{CP} at different values of θ_{23} , as shown in Fig. 4-8. When *inverted* MH is assumed, although A_{CP} amplitude fluctuates in the same range as when *normal* MH, that the probability and rate of ν_e appearance becomes smaller make the statistic error, $\sigma_{\nu_e}^{\text{stat.}}$, lower. In sum, sensitivity to CP violation, which is proportional to $A_{\text{CP}}/\sigma_{\nu_e}^{\text{stat.}}$, is slightly higher if the *inverted* MH is assumed to be *true* as shown in bottom of the Fig. 4-8.

Table 4.4 shows the fractional region of all possible *true* δ_{CP} values for which we can exclude CP conserving values of δ_{CP} to at least the 3σ C.L., obtained by the joint analysis of all considered experiments. Due to the fact

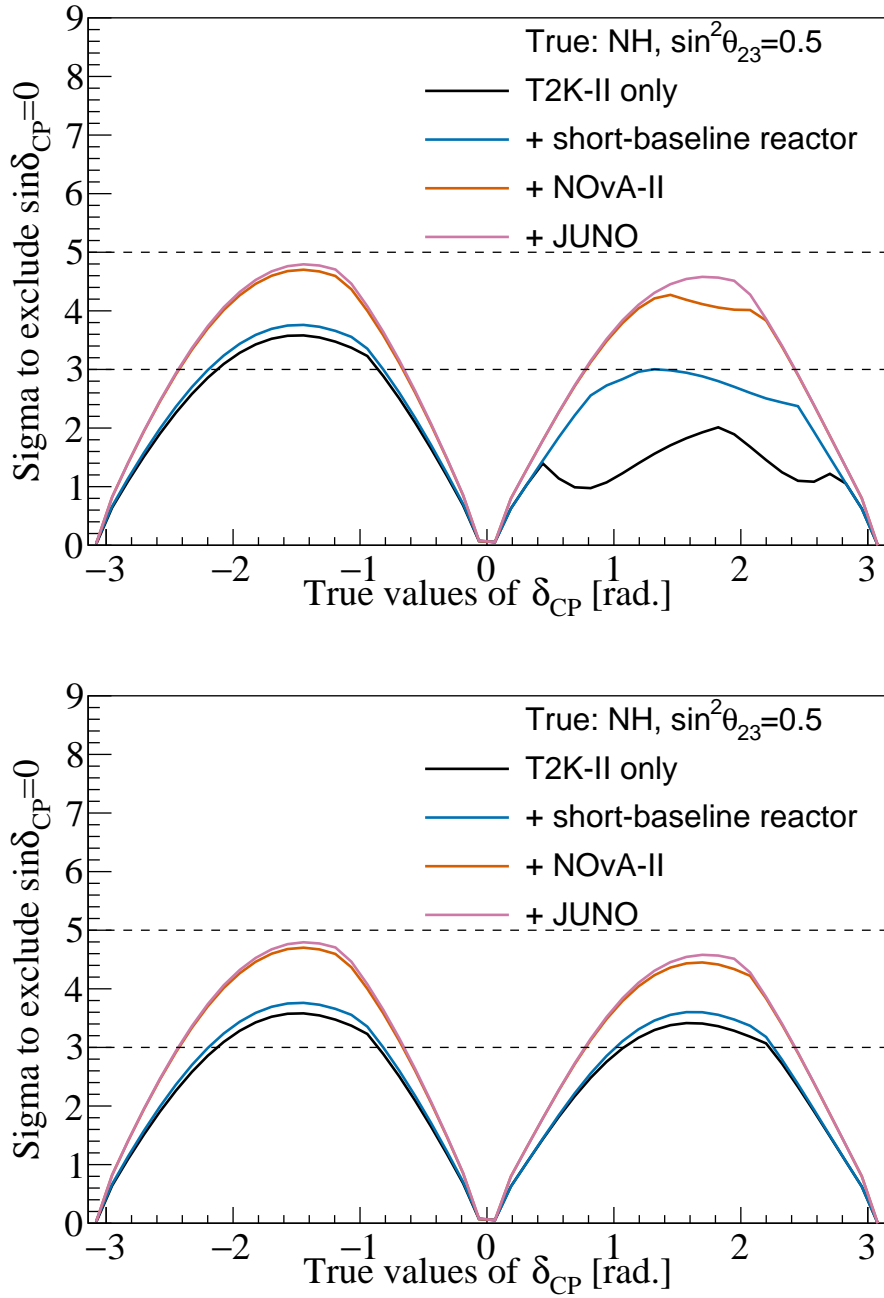


Figure 4-7: CPV sensitivity as a function of the *true* value of δ_{CP} obtained with different analyses. *Normal* MH and $\sin^2\theta_{23} = 0.5$ are assumed to be *true*. Top (bottom) plot is with the MH assumed to be *unknown* (*known*) in the analysis respectively.

that the MH is resolved completely with the joint analysis, the CPV sensitivities are quantitatively identical no matter whether the MH is assumed to be *known* or *unknown*.

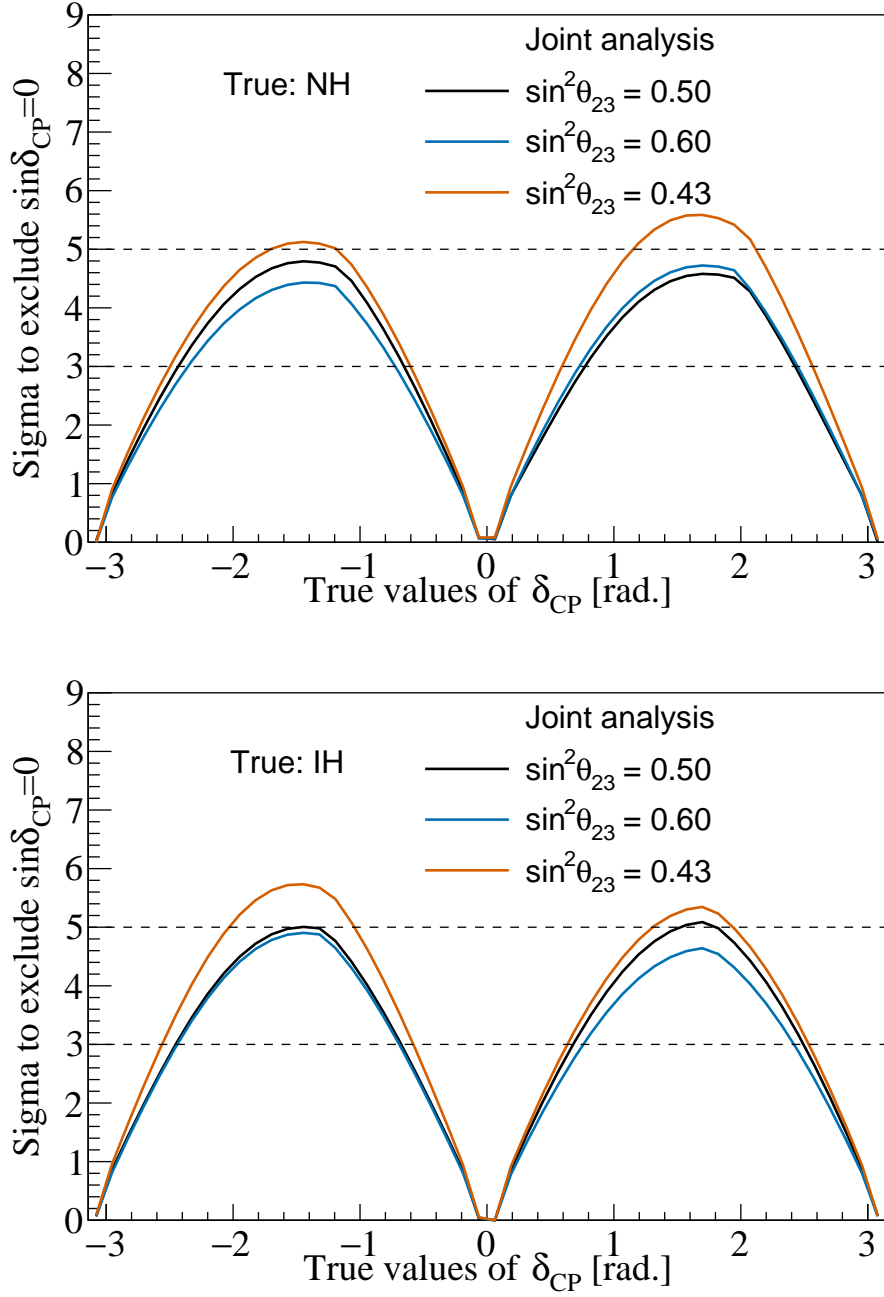


Figure 4-8: CPV sensitivity as a function of the *true* value of δ_{CP} obtained with a joint analysis of all considered experiments at different *true* $\sin^2 \theta_{23}$ values (0.43, 0.5, 0.6). Top (bottom) plot is with the *normal* (*inverted*) MH respectively assumed to be true.

4.5. Effect of varying exposure of T2K-II on mass hierarchy and CP Violation

Table 4.4: Fractional region of δ_{CP} , depending on $\sin^2 \theta_{23}$, can be explored with 3σ or higher significance

Value of $\sin^2 \theta_{23}$	0.43	0.50	0.60
Fraction of <i>true</i> δ_{CP} values (%), NH	61.6	54.6	53.3
Fraction of <i>true</i> δ_{CP} values (%), IH	61.7	57.2	54.2

4.5 Effect of varying exposure of T2K-II on mass hierarchy and CP Violation

Due to the budget issue, it is possible that T2K-II will take data less than the original proposal as discussed in ref. [8]. In this sense, we study three scenarios of the T2K-II POT exposure: 20×10^{21} , 15×10^{21} , and 10×10^{21} POT. While the MH resolving is still well-above 5σ C.L., the CPV sensitivity depends significantly on the POT exposure as shown in Fig. 4-9 and 4-10. However there is still a large fraction of δ_{CP} value excluded with 3σ C.L. The study emphasize the important to provide as many as possible the proton beam to T2K experiment for reaching the highest capability of CPV search.

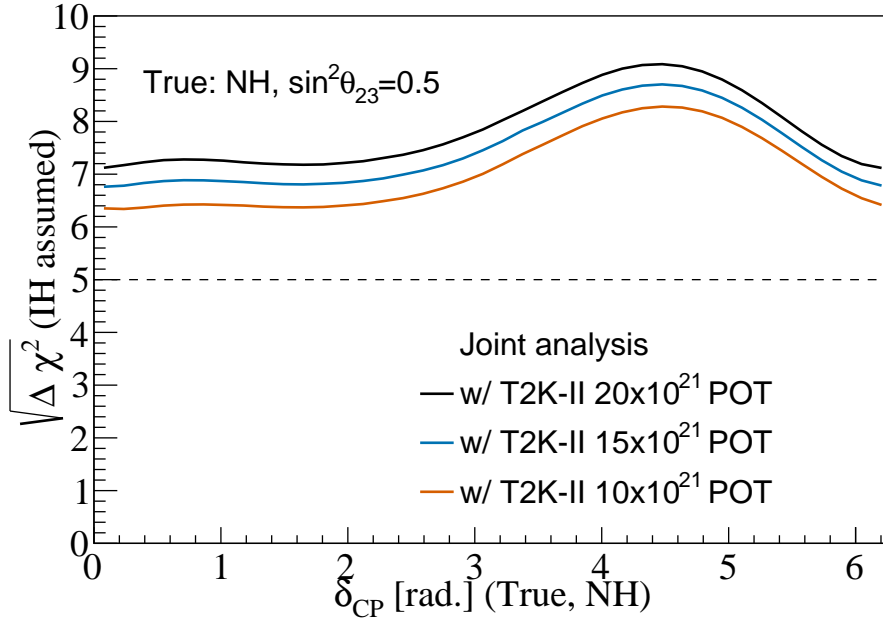


Figure 4-9: Dependence of the combined sensitivity on T2K-II POT exposure on MH sensitivities as a function of *true* δ_{CP} obtained with a joint analysis of all considered experiments. *Normal* MH and $\sin^2 \theta_{23} = 0.5$ are assumed to be true.

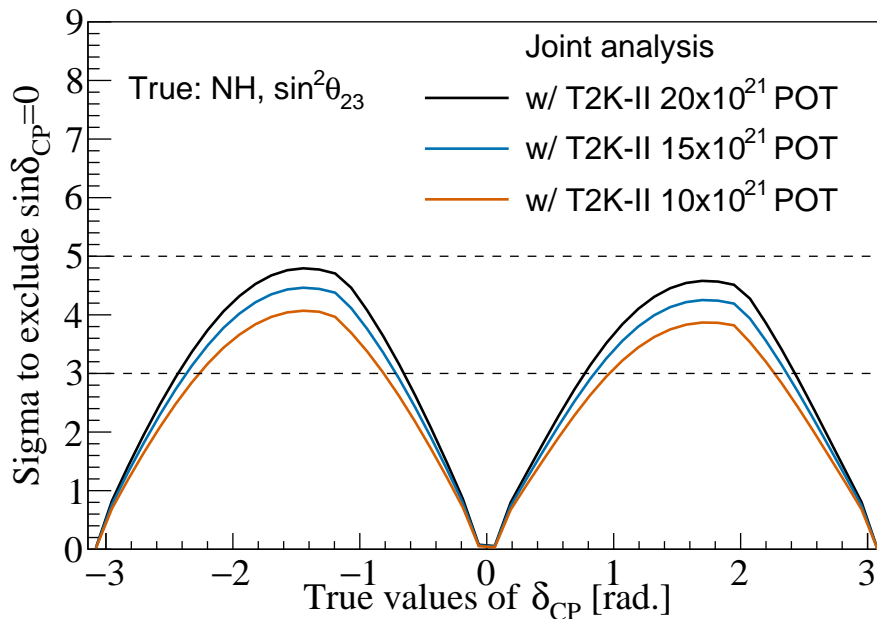


Figure 4-10: Dependence of the combined sensitivity on T2K-II POT exposure on CPV sensitivity as a function of the *true* value of δ_{CP} obtained with a joint analysis of all considered experiments. *Normal* MH and $\sin^2 \theta_{23} = 0.5$ are assumed to be true.

4.6 Discussion

We briefly discuss the implications arising from our results in light of the recent updated results from T2K [3], NO ν A [2], SK [9], IceCube DeepCore [10], and MINOS(+) [11] presented at Neutrino 2020 conference. T2K prefers the *normal* MH with a Bayes factor of 3.4; SK disfavors the *inverted* MH at 71.4-90.3% C.L.; both NO ν A and MINOS(+) disfavor the *inverted* MH at less than 1σ C.L. The prospect of resolving completely the MH by combining T2K-II, NO ν A-II and JUNO by 2027 thus is very encouraging. We find out that in Ref. [8] the authors address a similar objective and come to a quite similar conclusion even though a different calculation method and assumption of the experimental setup are used. On the leptonic CPV search, the leading measurement is from T2K where a 35% of δ_{CP} values are excluded at 3σ C.L. Comparing to Ref. [7], although the statistic significance to exclude CP conservation is reduced, from 95% C.L. to 90% C.L., the updated data looks more consistent with the PMNS prediction than before.

While SK also favors the maximum CP violation, NO ν A shows no indication of asymmetry of neutrino and antineutrino behaviours. With the combined analysis of T2K-II, NO ν A-II, and JUNO by 2027, it is expected that more than half of δ_{CP} values can be excluded with more than 3σ C.L.

Bibliography

- [1] Suekane, F. *Neutrino Oscillations: A Practical Guide to Basics and Applications*, vol. 898, 2015.
- [2] Himmel, A. New Oscillation Results from the NO ν A Experiment, 2020. URL <https://doi.org/10.5281/zenodo.4142045>.
- [3] Dunne, P. Latest Neutrino Oscillation Results from T2K, 2020. URL <https://doi.org/10.5281/zenodo.4154355>.
- [4] Zhan, L. *et al.* Determination of the Neutrino Mass Hierarchy at an Intermediate Baseline. *Phys. Rev. D* **78**, 111103, 2008. [0807.3203](https://arxiv.org/abs/0807.3203).
- [5] Esteban, I. *et al.* Global analysis of three-flavour neutrino oscillations: synergies and tensions in the determination of θ_{23} , δ_{CP} , and the mass ordering. *JHEP* **01**, 106, 2019. [1811.05487](https://arxiv.org/abs/1811.05487).
- [6] Esteban, I. *et al.* The fate of hints: updated global analysis of three-flavor neutrino oscillations. *JHEP* **09**, 178, 2020. [2007.14792](https://arxiv.org/abs/2007.14792).
- [7] **T2K Collaboration** *et al.* Constraint on the matter-antimatter symmetry-violating phase in neutrino oscillations. *Nature* **580** (7803), 339–344, 2020. [Erratum: *Nature* 583, E16 (2020)], [1910.03887](https://arxiv.org/abs/1910.03887).
- [8] Cabrera, A. *et al.* Synergies and prospects for early resolution of the neutrino mass ordering. *Sci. Rep.* **12** (1), 5393, 2022. [2008.11280](https://arxiv.org/abs/2008.11280).
- [9] Nakajima, Y. Recent results and future prospects from Super-Kamiokande, 2020. URL <https://doi.org/10.5281/zenodo.4134680>.

Bibliography

- [10] Blot, S. Neutrino oscillation measurements with IceCube, 2020. URL <https://doi.org/10.5281/zenodo.4156203>.
- [11] Carroll, T. Final Long-Baseline Results from MINOS and MINOS+, 2020. URL <https://doi.org/10.5281/zenodo.4156118>.

Chapter 5

Octant Degeneracy and Precision Measurements of Oscillation Parameters in T2K-II, NO ν A-II and JUNO

Besides the neutrino mass hierarchy and CP violation in the lepton sector, the other outstanding problem that demands attention is the true octant of θ_{23} mixing angle. In section 5.1, we present the importance and present status of the neutrino oscillation parameters. The allowed regions of $\sin^2 \theta_{13} - \delta_{CP}$ and $\sin^2 \theta_{23} - \Delta m_{31}^2$ constrained by T2K-II, NO ν A-II and JUNO, are present in sections 5.2 and 5.3. We conclude the chapter by presenting the results on octant resolving sensitivity in the section 5.4.

5.1 Introduction

Based on their predictions of various oscillation parameters, many BSM models can either be accepted or rejected. So, a precise measurement of the oscillation parameters can guide us towards a successful BSM theory. Determination of δ_{CP}

can also give clue in understanding the present matter-antimatter asymmetry of the universe. The matter-antimatter asymmetry of the universe can be explained by the process of baryogenesis. But the baryogenesis in SM is not sufficient to explain the observed baryon asymmetry of the universe. One option to create additional baryon asymmetry is via leptogenesis in which the decay of heavy right handed neutrinos (for instance, those belonging to the See-Saw models) can create lepton asymmetry, which can be converted to baryon asymmetry. Different studies show that under certain conditions, it may be possible to connect the leptonic CP phase δ_{CP} to leptogenesis.

As per the global analysis from experimental data available upto July 2020, for the allowed 3σ ranges of the oscillation parameters [1, 2], the present status of the magnitude of the elements of the PMNS matrix is given as,

$$|U|_{PMNS}^{3\sigma} = \begin{pmatrix} 0.801 \rightarrow 0.845 & 0.513 \rightarrow 0.579 & 0.143 \rightarrow 0.156 \\ 0.233 \rightarrow 0.507 & 0.461 \rightarrow 0.694 & 0.631 \rightarrow 0.778 \\ 0.261 \rightarrow 0.526 & 0.471 \rightarrow 0.701 & 0.611 \rightarrow 0.761 \end{pmatrix} \quad (5.1)$$

The θ_{13} mixing angle is well-measured by reactor-based neutrino experiments, dominated by Daya Bay. The solar mass-squared difference are independently well constrained by the Solar experiments and VLBL reactor experiment KamLAND data. T2K and NO ν A are the only ongoing LBL experiments, although in the global fits K2K and MINOS results besides them are also considered. The LBL experiments are sensitive to θ_{23} and Δm_{31}^2 through the disappearance sample $\nu_\mu \rightarrow \nu_\mu$ ($\bar{\nu}_\mu \rightarrow \bar{\nu}_\mu$), to θ_{13} and δ_{CP} through their appearance $\nu_e \rightarrow \nu_\mu$ ($\bar{\nu}_\mu \rightarrow \bar{\nu}_e$) samples and to mass-hierarchy resolution due to the matter effect potentials the neutrinos (anti-neutrinos) experience in their propagation to the detectors through Earth matter. However, MINOS/MINOS+ is sensitive to $|\Delta m_{31}^2|$ but not to θ_{13} and δ_{CP} due to its operation for muon neutrino disappearance search only.

θ_{23} octant degeneracy: In equation 2.77, the uncertainty in appearance measurement comes from θ_{23} , apart from $\sin \delta_{CP}$. In ν_μ disappearance measurement, given by Equation 2.74, the amplitude gives the measurement of $\sin^2 2\theta_{23}$ at the oscillation maxima $\Phi_{31} = \frac{\pi}{2}$. There are two possible values of

5.2. Allowed regions of θ_{13} mixing angle and δ_{CP}

$\sin^2 \theta_{23}$ for a given value of $\sin^2 2\theta_{23}$ from the disappearance measurement [3], given by

$$\sin^2 \theta_{23} = \frac{1 \pm \sqrt{1 - \sin^2 2\theta_{23}}}{2} \quad (5.2)$$

As the difference between the two solutions is $\sqrt{1 - \sin^2 2\theta_{23}}$, it can be large even if the term is small. For example, if $(1 - \sin^2 2\theta_{23})$ is measured to be $\sin^2 2\theta_{23} > 0.97$, the possible range of $\sin \theta_{23}$ is between 0.41 and 0.59, which allows both the octants. This is called the octant θ_{23} degeneracy problem. To solve this problem, it is necessary to show that $\sin^2 2\theta_{23}$ is ~ 1 or determine which solution/octant is correct by combining oscillation measurements from different experiments. As the disappearance sample is sensitive to $\sin^2 2\theta_{23}$, octant can't be resolved by this sample alone in LBL i.e. whether $\theta_{23} < \pi/4$ or $> \pi/4$ can't be answered. However, the octant degeneracy can be resolved by adding appearance sample as the term $\sin^2 \theta_{23}$ appears and also by considering SuperKamiokande and Ice Cube DeepCore data. The present best fit of θ_{23} lies in the upper octant (see Table 1.3). The lower octant is allowed at $\sim 2.4\sigma$ confidence level from the global data fits. Maximal mixing is now disfavoured with a significance of $\Delta\chi^2 = 3.9$, including Super-K data.

5.2 Allowed regions of θ_{13} mixing angle and δ_{CP}

The θ_{13} mixing angle can be constrained precisely by measuring the disappearance of $\bar{\nu}_e$ in the R-SBL neutrino experiment. The A-LBL experiments, on the other hand, can provide a constraint of θ_{13} mixing angle correlated to δ_{CP} , mainly thank to the measurements of the appearance of $\nu_e(\bar{\nu}_e)$ from the beam of $\nu_\mu(\bar{\nu}_\mu)$ respectively. The sensitivities are calculated at three different *true* values of δ_{CP} ($0, \pm \frac{\pi}{2}$). A 3σ C.L. range of $\sin^2 \theta_{13}$ [0.02046, 0.02440] is taken from Ref. [4]. Fig. 5-1 shows the 3σ C.L. allowed region of $\sin^2 \theta_{13}$ - δ_{CP} obtained with a joint analysis of the T2K-II and NO ν A-II. The precision of $\sin^2 \theta_{13}$ can be achieved between 6.5% and 10.7% depending on the *true* value of δ_{CP} . It will be interesting to compare the measurements of θ_{13} from R-SBL experiments and from the A-LBL experiments with such high precision.

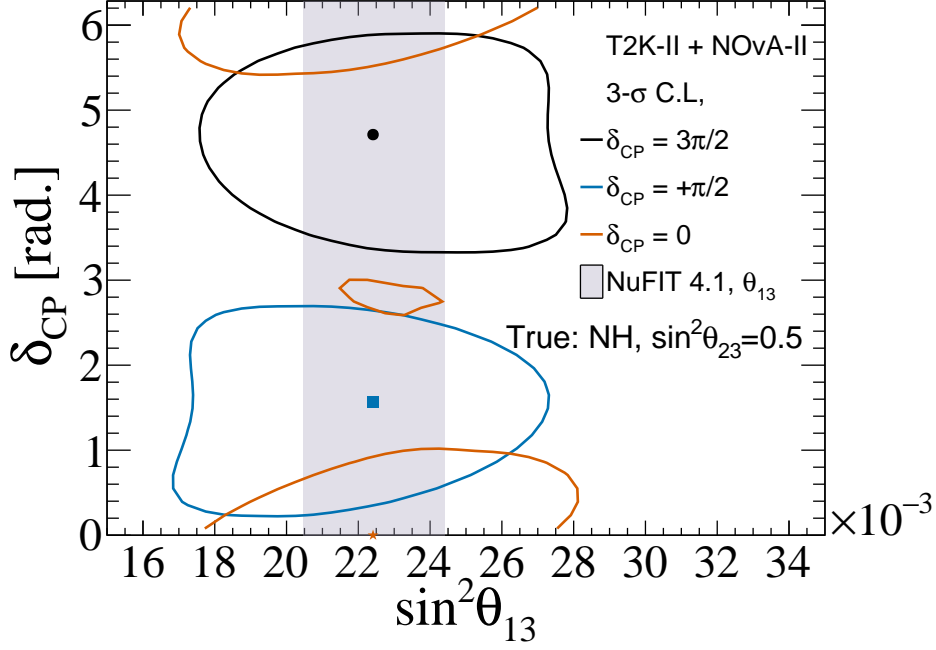


Figure 5-1: Allowed region of $\sin^2 \theta_{13}$ - δ_{CP} at the 3σ C.L. compared between a joint analysis of T2K-II and NO ν A-II and the present constraint from the global data [4].

5.3 Allowed regions of θ_{23} mixing angle and Δm_{31}^2

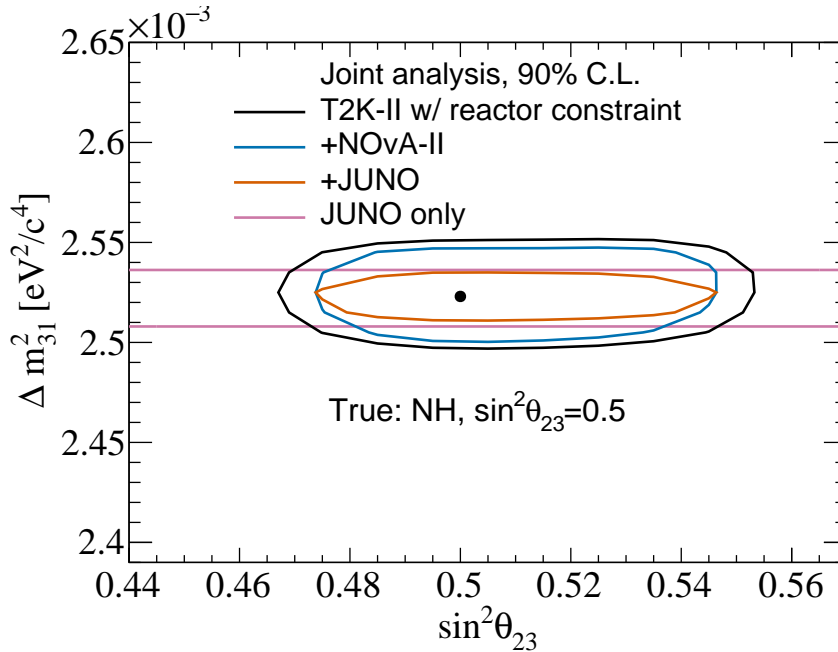


Figure 5-2: Allowed region in the $\sin^2 \theta_{23} - \Delta m_{31}^2$ space at 90% C.L. with various experimental setups. *Normal* MH and $\sin^2 \theta_{23} = 0.5$ are assumed to be true.

As shown in Fig. 5-2, both JUNO alone and a combined sensitivity of T2K-II and

5.4. Resolving the octant of the θ_{23} mixing angle:

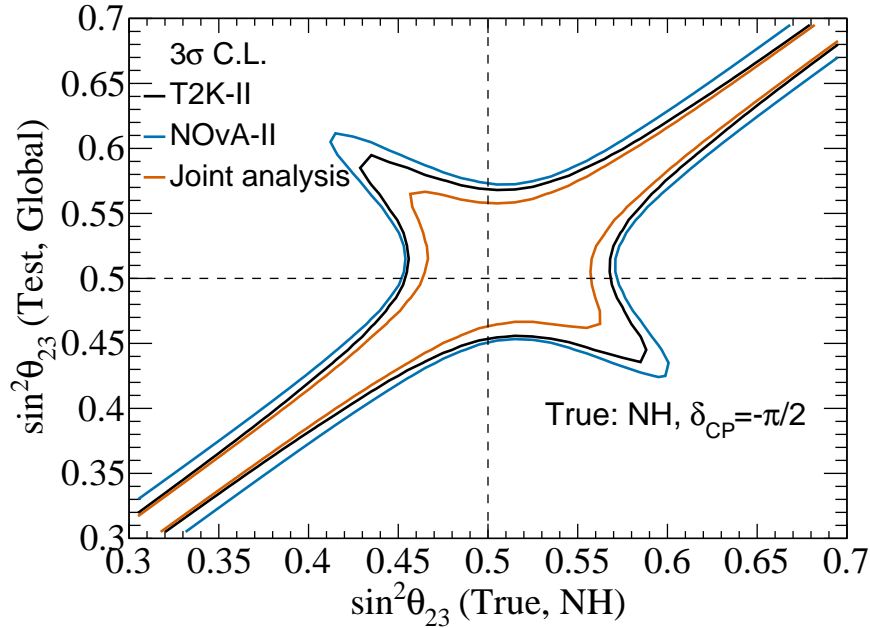


Figure 5-3: Allowed region of *test* $\sin^2 \theta_{23}$ at 3σ C.L. as a function of *true* $\sin^2 \theta_{23}$. *Normal* MH and $\delta_{\text{CP}} = -\frac{\pi}{2}$ are assumed to be true.

NO ν A-II experiments can reach a sub-percent-level precision on the atmospheric mass-squared splitting Δm_{31}^2 . A comparison at such precision may provide a very good test for the PMNS framework. Besides, assuming a maximal mixing $\sin^2 \theta_{23} = 0.5$, a combined sensitivity of T2K-II and NO ν A-II can achieve approximately 6% and 3% precision for the upper and lower limit on $\sin^2 \theta_{23}$ respectively. A capability to solve the θ_{23} octant in case the mixing angle θ_{23} is not maximal in the next section.

5.4 Resolving the octant of the θ_{23} mixing angle:

We consider a range $[0.3, 0.7]$ of possible *true* $\sin^2 \theta_{23}$ values and that the *true* MH is *normal*. For each *true* $\sin^2 \theta_{23}$ value, the marginalized χ^2 is calculated at various values of *test* value θ_{23} with both possibilities of the MH. The minimization over the MH options is firstly performed to obtain global minimum χ^2 for any combination of the *true* and *test* values of θ_{23} . The allowed regions of test $\sin^2 \theta_{23}$ as a function of true $\sin^2 \theta_{23}$ can be obtained, e.g. at the 3σ C.L., as shown in Fig. 5-3.

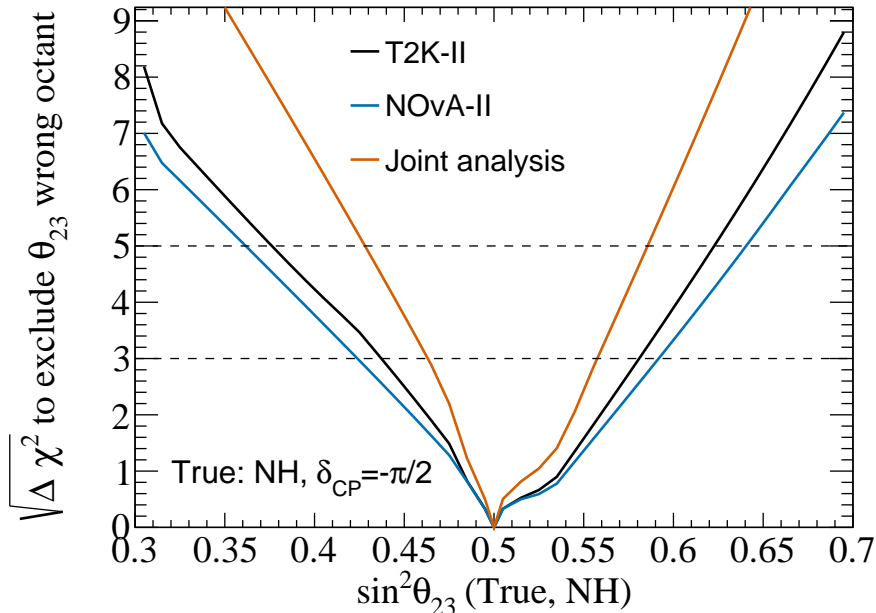


Figure 5-4: Statistical significance to exclude the *wrong* octant as a function of $\sin^2 \theta_{23}$. *Normal* MH and $\delta_{\text{CP}} = -\frac{\pi}{2}$ are assumed to be true.

The statistical significance to exclude the *wrong* octant given a *true* (non-maximal) value of θ_{23} is calculated by taking the difference between the minimal value of the global χ^2 in the *wrong* octant and the *true* octant of θ_{23} . The octant resolving sensitivities with T2K-II, NO ν A-II alone or with a combined analysis is shown in Fig. 5-4. The θ_{23} octant resolving power can be enhanced significantly when combining T2K-II and NO ν A-II data samples, particularly the θ_{23} octant can be determined at 3σ C.L or higher if $\sin^2 \theta_{23}$ is ≤ 0.46 or ≥ 0.56 .

5.5 Discussion

Regarding the octant of the θ_{23} mixing angles, T2K, NO ν A, SK, and MINOS(+) data prefer non-maximal mixing with statistical significance between 0.5σ to 1.5σ C.L. If the *true* value of θ_{23} is close to the best fit in the global data fit [2], $\theta_{23} = 0.57$, a combined analysis of T2K-II, NO ν A-II and JUNO can exclude the *wrong* octant with 3σ C.L. There is a room for improvement in the above-mentioned physic potentials, for example, by adding an atmospheric neutrino data sample from the SK experiment. There are on-going efforts to combine data from T2K

and SK along with a joint analysis of T2K and NO ν A. Such activities are vital to realizing a grand framework for combining the special-but-statistically-limited neutrino data in the future.

Bibliography

- [1] Gonzalez-Garcia, M. C. & Pena-Garay, C. Three neutrino mixing after the first results from K2K and KamLAND. *Phys. Rev. D* **68**, 093003, 2003. [hep-ph/0306001](#).
- [2] Esteban, I. *et al.* The fate of hints: updated global analysis of three-flavor neutrino oscillations. *JHEP* **09**, 178, 2020. [2007.14792](#).
- [3] Suekane, F. *Neutrino Oscillations: A Practical Guide to Basics and Applications*, vol. 898, 2015.
- [4] Esteban, I. *et al.* Global analysis of three-flavour neutrino oscillations: synergies and tensions in the determination of θ_{23} , δ_{CP} , and the mass ordering. *JHEP* **01**, 106, 2019. [1811.05487](#).

Chapter 6

Conclusion and Future Scopes

In this thesis, the prospects of determining the neutrino mass hierarchy, exploring leptonic CP violation, resolving of θ_{23} octant degeneracy and precision measurements of oscillation parameters θ_{13} , θ_{23} , δ_{CP} and Δm_{31}^2 are studied, in light of three terrestrial neutrino oscillation experiments: the extended run of Tokai-To-Kamioka (T2K-II) and NuMI Off-axis ν_e Appearance (NO ν A-II), as well as the reactor-based medium baseline (R-MBL) experiment Jiangmen Underground Neutrino Observatory (JUNO).

Firstly, we describe the specifications of the above three neutrino oscillation experiments. We describe the experiments using updated information on fluxes, signal and background efficiencies, and systematic errors. We discuss the simulation technique adopted to study the physics potential of the experiments. We present our results on the event spectra for the selected ν_e ($\bar{\nu}_e$) appearance and ν_μ ($\bar{\nu}_\mu$) disappearance channels for T2K-II and NO ν A-II, and $\bar{\nu}_e$ disappearance channel JUNO.

We present our neutrino oscillation analysis based on the simulated data. We present the results on the MH determination and the CPV sensitivity of the above experiments. A joint analysis of JUNO with the A-LBL experiments, NO ν A-II and T2K-II, shows a great boost in the MH determination. This is expected since a joint analysis will break the parameter degeneracy between δ_{CP} and the sign of

Δm_{31}^2 . Due to the parameter degeneracy among δ_{CP} , the sign of Δm_{31}^2 , θ_{13} , and θ_{23} in the measurement with the A-LBL experiments, we also expect that the MH determination depends on the value of θ_{23} . The results conclude that the *wrong* mass hierarchy can be excluded at greater than 5σ C.L. for all the *true* values of δ_{CP} and for any value of θ_{23} in the range constrained by experiments. We find out that in the paper *Scientific Reports volume 12, Article number: 5393 (2022)* by A. Cabrera *et. al.*, the authors address a similar objective. While their qualitative findings are consistent with our studies, there may still be numerical differences need to be understood. The CPV sensitivity is shown as a function of the *true* value of δ_{CP} for both MH options: (a) MH is *known*, or (b) MH is *unknown*. The result shows that whether the MH is *known* or *unknown* does not affect on the joint analysis of the three experiments because the MH- δ_{CP} degeneracy is uplifted. It can be seen that the sensitivity to CP violation is driven by T2K-II and NO ν A-II. Contribution of the R-SBL neutrino experiment is significant only at the region where δ_{CP} is between 0 and π and when the MH is not determined conclusively. At δ_{CP} close to $-\pi/2$, which is indicated by recent T2K data, the sensitivity of the joint analysis with all considered experiments can reach approximately the 5σ C.L..

We also studied the resolution of the θ_{23} octant and the precision measurement of the oscillation parameters in T2K-II, NO ν A-II and JUNO. The 3σ C.L. allowed region of $\sin^2 \theta_{13}$ - δ_{CP} obtained with a joint analysis of the T2K-II and NO ν A-II is compared to that of the present constraints as in NuFit 4.1. Both JUNO alone and a combined sensitivity of the T2K-II and NO ν A-II experiments can reach a sub-percent-level precision on the atmospheric mass-squared splitting Δm_{31}^2 . A comparison with such precision may provide a very good test for the PMNS framework. A capability to solve the θ_{23} octant in case the mixing angle θ_{23} is not maximal is also discussed. The θ_{23} octant resolving power can be enhanced significantly when combining T2K-II and NO ν A-II data samples, particularly the θ_{23} octant can be determined at 3σ C.L or higher if $\sin^2 \theta_{23}$ is ≤ 0.46 or ≥ 0.56 .

Finally, we would like to emphasize that the joint analysis in reality is expected to be more complicated than what we have done. Many systematic sources must be

taken into account for each experiment, and for a joint analysis, the correlation of systematic errors among experiments is important for extracting precisely the oscillation parameters. However, we affirm that the above conclusions are still valid since the measurement uncertainties, particularly for CP violation and the neutrino mass hierarchy, are still dominated by statistical errors.

Although the picture of neutrino oscillation is concrete, yet, far from complete and requires collaborative efforts. To resolve the octant degeneracy, combined sensitivity studies of data from ongoing and upcoming atmospheric neutrino experiments such as SuperKamiokande, IceCube, PINGU, HyperKamiokande and KM3NeT along with accelerator-based and reactor-based neutrino experiments, as well as exploiting second oscillation maxima at longer baselines like DUNE, P2O and ESS ν SB can be realised. It is imperative to consider the dependence and correlation of systematic errors while performing joint analysis of different neutrino oscillation experiments. Precisely measuring the six oscillation parameters gives us a window to directly test the unitarity of the PMNS matrix. To observe the effect on the presently unresolved issues which we have covered in this thesis, non-standard neutrino oscillation phenomena, such as NSI, the sterile hypothesis, and neutrino decay, if any, can be taken into consideration.

Publications

Journals

1. Nath, A., and Francis, Ng. K., “Detection techniques and investigation of different neutrino experiments”, *International Journal of Modern Physics A*, Vol. 36, No. 13, 2130008 (45 pages), 2021 [10.1142/S0217751X21300088](https://doi.org/10.1142/S0217751X21300088).
2. Cao, S., Nath, A., Ngoc, T. V., Francis, Ng. K., Hong Van, N. T., and Quyen, P. T., “Physics potential of the combined sensitivity of T2K-II, NO ν A extension, and JUNO”, *Physical Review D*, Vol. 103, Issue 11, pages 112010, 2021 <https://link.aps.org/doi/10.1103/PhysRevD.103.112010>.

Book Chapters

1. Nath, A., “Detection methods and neutrino oscillation experiments”, *Advances in Physics and Application-2020, Duliajan College*, ISBN: 978-93-91953-06-5, 2021.
2. Nath, A., and Francis, Ng. K., “Precision measurements of atmospheric mixing parameters and octant resolving”, *Advances in Physics and Application-2020, Duliajan College*, ISBN: 978-93-91953-06-5, 2021.

Conferences Proceedings

1. Francis, Ng. K., and Nath, A., “The Effects of Majorana Phases in Estimating the Masses of Neutrinos”, *International Journal of Modern Physics: Conference Series*, Vol. 47, 1860100, 2018 <https://doi.org/10.1142/S201019451860100X>.

POSTERS/ORAL PRESENTATION/PAPERS PRESENTED IN CONFERENCES

1. Nath, A., and Francis, Ng. K., International Conference on Recent Issues in Nuclear and Particle Physics, Visva-Bharati, West Bengal, India, Feb 3-5, 2019.
2. Nath, A., Cao, S., Ngoc, T. V., Van, N. T., Quyen, P. T., and Francis, Ng. K., XXIX International Conference on Neutrino Physics and Astrophysics, Fermilab, USA, Jun 22-Jul 2, 2020.
3. Nath, A., and Francis, Ng. K., International E-Conference on New Frontiers in Science and Technology, Research Institute of Science and Technology, Manipur University Campus, India, Jul 9-11, 2020.
4. Nath, A., and Francis, Ng. K., International e-Poster Conference on “Advances in Physics and Applications”, Duliajan College, Dibrugarh University, Assam, India, Nov 23-28, 2020. (*presented two papers*)
5. Nath, A., and Francis, Ng. K., XXIV DAE-BRNS Symposium on High Energy Physics, NISER, Jatni, Odisha, India, Dec 14-18, 2020.

WORKSHOPS/SCHOOLS ATTENDED

1. *Electroweak Symmetry Breaking, Flavour Physics and BSM*, Indian Institute of Technology, Guwahati, December 18-22, 2017.
2. *Vietnam School on Neutrinos*, ICISE, Quy Nhon, Vietnam, July 7-19, 2019.
3. *SERB Preparatory School on Theoretical High Energy Physics*, Department of Physics, Tezpur University, October 14 - November 9, 2019.
4. *Workshop on Particle Physics*, Department of Physics, Assam Don Bosco University, August 17-31, 2020.
5. *Neutrinos: Here, There & Everywhere - International Summer School 2021*, PhD School of SCIENCE, Niels Bohr Institute, University of Copenhagen, July 26-30, 2021 (*Course no.: 5915-21-11-31, Credits earned: 2.50*).

About

Ankur Nath was born in the state of Assam, India. He obtained his schooling and higher secondary education in Assam. Later, he moved to Shillong, Meghalaya and completed his B.Sc. in Physics at St. Anthony's College. He received his masters degree in Physics in the year 2016 from North Eastern Hill University, Meghalaya, India. He enrolled into the Ph.D. course in 2017 under Dr. Ng. K. Francis, Associate Professor, Department of Physics, Tezpur University. He also visited the Institute For Interdisciplinary Research in Science and Education (IFIRSE) in mid-2019 and conducted his doctoral research in collaboration with Dr. Son Cao.